BULLETIN OF THE ASTRONOMICAL INSTITUTES OF THE NETHERLANDS

1958 DECEMBER 31 VOLUME XIV NUMBER 488

COMMUNICATIONS FROM THE NETHERLANDS FOUNDATION FOR RADIO ASTRONOMY AND THE OBSERVATORY AT LEIDEN

A SURVEY OF THE CONTINUOUS RADIATION FROM THE GALACTIC SYSTEM AT A FREQUENCY OF 1390 Mc/s

BY GART WESTERHOUT

This paper describes the results of a survey of the radiation along the galactic ridge and a search for discrete sources. The observations were the first to be made with the 25-m radio telescope at Dwingeloo, which has a beamwidth of 0°.57 at this frequency. The first calibration of the radio telescope, which was made in the months before the survey started, showed that the pilot which mechanically converts right-ascension and declination into azimuth and altitude is accurate to about ± 0°.01. The telescope itself was calibrated optically by observing bright stars with a small optical telescope attached to the reflector. The setting and guiding accuracy was found to be ± 0°.03. The alignment of the radio axis was checked by observing bright radio sources. The refraction at 1390 Mc/s is of the same order as the optical refraction (Figure 2a). The standard positions of the four bright sources appeared to be correct to within 0°.02. The total-power receiver had an excellent gain stability. A determination of the extinction failed through lack of data. The intensity ratios of the four bright sources are determined with an accuracy of the order of 1% and are given in Table 3. The absolute brightness temperatures and flux densities are estimated to be correct to within 20%.

A rapid survey was made of the whole sky in search of bright sources; a total of 36 was found, 10 of which were not situated in the region of the main survey. The limit of detection was about 20 °K. The main survey covered a region approximately 40° wide along the galactic equator, from $l = 320°$ to $l = 56°$, and a region of 30° × 50° around the Orion nebula. In the latter region no radiation above 2 °K was detected with the exception of three discrete sources. Maps in equatorial and galactic co-ordinates are given for the region $l = 320°$-$56°$. The position in latitude and the top intensity of the galactic ridge are given in Table 5. Table 6 contains the positions, intensities and identifications of 82 discrete sources, 56 of which are thermal. Of these 35 are identified with optical emission nebulae in a comparison with the Palomar-Schmidt atlas and several catalogues. Their emission measure, density and mass are also given in Table 6. It appears that only the more massive nebulae among the optically observed emission regions are detected. Two thirds of the sources have $M > 1000\ M_{\odot}$.

A comparison with MILLS' high-resolution survey at 85 Mc/s enabled us to separate the background radiation of the galactic ridge into a thermal and a nonthermal component (Figures 13 and 14). The brightness temperature of the nonthermal radiation was assumed to be proportional to $\nu^{-2.70}$. The space distribution of ionized hydrogen in the Galactic System was derived from the distribution of the thermal component. The radio and optical data for the region around the sun agree if we assume that the majority of emission regions have emission measures between 400 and 800, densities between 5 and 10 cm^{-3} and diameters between 5 and 30 pc. We find that between 0.6 and 0.15% of space is filled with ionized hydrogen. The density ratio of ionized and neutral hydrogen near the sun is between 0.06 and 0.03. The average space density of ionized hydrogen increases to a value of 7 times that near the sun at $R = 3.5$ kpc, and is zero for $R < 2$ kpc. The total mass of the ionized hydrogen is $6.3 \times 10^7\ M_{\odot} \pm 40\%$. Some suggestions are given which relate the expanding neutral hydrogen in the region $R < 3$ kpc and the expanding spiral arm at $R = 3$ kpc with the density maximum of ionized hydrogen at $R = 3.5$ kpc. A model for the source in the galactic centre, which fits the observations at 85 and 1390 Mc/s, consists of a thermal source with halfwidths of 0°.55 × 0°.25 and a 1390 Mc/s top temperature of 500 °K, and a nonthermal source with halfwidths of approximately 2° × 1° and a 1390 Mc/s top temperature of 25 °K.

A table of contents is given on page 260 at the end of the paper.

Introduction

Most of the surveys of the continuous radiation at radio frequencies made so far were obtained with wide-beam antenna systems. They all show a strong concentration of the radiation intensity towards the galactic plane and the galactic centre. An analysis of a number of such surveys by HANBURY BROWN and HAZARD (1953) showed that at the lower frequencies the absorption by ionized interstellar hydrogen must cause important changes in the distribution of the radiation. According to WESTERHOUT and OORT (1951) the contribution of ionized hydrogen to the total radiation at 100 Mc/s is negligible. Since the surface brightness of this radiation remains almost constant at frequencies higher than 100 Mc/s, whilst the surface brightness of the nonthermal sources of radiation decreases with increasing frequency, the

CONTENTS

major component of the radiation near the galactic plane at high frequencies must be the ionized interstellar gas.

As is known from optical data and 21-cm line observations (WESTERHOUT 1957, SCHMIDT 1957), the interstellar gas is strongly concentrated towards the galactic plane. Therefore, to obtain quantitative data on the distribution of radio radiation at high frequencies, surveys made with high angular resolution are needed. From the data presented hereafter it is clear that the surveys at 600 Mc/s (PIDDINGTON and TRENT 1956) and 900 Mc/s (DENISSE *et al.* 1955, 1957), which were made with beams having a halfwidth of about 3°.0, give a resolution which is still insufficient to obtain a true picture of the distribution of the radiation in the vicinity of the galactic plane.

A determination of the flux density of some discrete sources with beam widths of 0°.9 at 1420 Mc/s (HAGEN *et al.* 1954) and 0°.4 at 3200 Mc/s (HADDOCK *et al.* 1954) showed that the well-known emission nebulae are strong radio sources at the high frequencies.

The present investigation is the first survey of the radio emission from a large part of the galactic ridge at high frequencies made with a narrow beam (0°.57). Almost simultaneously the first narrow-beam (0°.9) survey at a low frequency was made by MILLS *et al.* (1958). In the region of the sky common to both surveys, a detailed comparison yielded a separation of the radiation in the galactic plane into two components. We are greatly indebted to Dr B. Y. MILLS for putting his observations at our disposal prior to publication.

A programme of calibrations of the radio telescope preceded the observations. The calibration procedure and its results are described in Chapter 1. The receiver and data used in the reductions of the observations are described in Chapters 2 and 3, whilst Chapters 4 and 5 give the observations and their reduction including a series of contour maps. In Chapter 6 the formulae for thermal emission are given, and the individual sources listed in table 6 are discussed, comparing them if possible with optical observations. Chapter 7 contains a comparison of the observations of the general background radiation and the source Sgr A with the results of the low-frequency survey by MILLS *et al.*

1. *Calibration of the radio telescope*

The instrument used in the present investigation was the azimuthally mounted paraboloidal mirror at Dwingeloo. It has a diameter of 25 m and a focal distance of 12 m. The telescope is operated by the Netherlands Foundation for Radio Astronomy, and is financed by the Netherlands Organization for Pure Research (Z.W.O.). A brief description of the telescope and the problems involved in its erection was given by VAN DE HULST *et al.* (1957).

A more complete description of the telescope, pilot and calibration will be given by HOOGHOUDT (1959), who supervised the entire construction.

Before the telescope could be put into use, a large programme of calibrations had to be made. These calibrations consisted of mechanical, optical and radio-astronomical measurements, and were made in July and August, 1956. The radio-astronomical measurements were made at a frequency of 1390 Mc/s. A natural extension of the calibration programme was an investigation of the continuous radiation from the Galactic System and from localized sources at that frequency. The observations were made in September, 1956.

a. *Calibration of the pilot*

Setting of the telescope can be done in either azimuthal or equatorial co-ordinates. A mechanical co-ordinate transformer hereafter called "pilot", is used to convert from equatorial to azimuthal co-ordinates. The position in hour angle t, declination δ, azimuth A and altitude h can be read off on scales coupled to the pilot by means of an electrical servo system. Setting and reading in right-ascension α is also possible through a differential gear on the t-scale, subtracting the hour angle from the sidereal time provided by a synchronous motor. The pilot may be moved in t and δ with synchronous motors at a number of fixed speeds ranging from the sidereal rate of 0°.25 per minute (daily motion) to 72°/min. It is coupled to the azimuth and elevation drives of the telescope by an electrical servo system. Since the telescope is mainly used for observations in equatorial co-ordinates, the first step in the calibration procedure is the calibration of the pilot and its scales. In the factory it was carefully adjusted so as to give the correct conversion. The calibration was intended to determine the zero points of the equatorial and azimuthal co-ordinate systems, as well as to investigate the proper working of the pilot as a whole. All measurements were made by feeding hour angle t and declination δ into the pilot and reading off azimuth A and altitude h. Zero points were adjusted by measurements at a number of points with simple relations between azimuthal and equatorial co-ordinates, i.e. the horizon, the equator, the meridian, the zenith and the pole. The performance of the pilot over the whole sky was checked by computing the values of A and h for about 200 points at 30 different values of t and 7 values of δ and comparing those with the readings of the pilot.

The deviations were between 0° and 0°.02 with an average of about ± 0°.01 except for a few points where deviations up to 0°.04 were found. Such cases were probably due to the accumulation of errors in the various gears of the reading mechanism.

In the work which followed it was always assumed that the pilot gave azimuth and altitude with an accuracy of ± 0°.01 (estimated uncertainty).

b. *Optical calibration of the telescope*

The second step was the determination of the zero point of the azimuth and altitude scales of the telescope itself, and of the servo system connecting the pilot output with the telescope drive. These measurements were made entirely by means of optical observations of fundamental stars. For this purpose a small optical telescope with a 50 mm lens and a focal distance of 500 mm was mounted exactly parallel to the geometrical axis of the paraboloidal mirror.

In the course of construction the shape of the paraboloid had been adjusted with respect to a plane, perpendicular to this axis; the deviations from a true paraboloidal shape were not permitted to be more than 10 mm at all elevation angles. The accuracy of the alignment of the optical telescope and the geometrical axis of the paraboloid was of the order of 0°.005. We are indebted to Ir SCHEEPMAKERS for his assistance in this operation.

The setting errors of the radio telescope are due to play in the driving gears, electronic errors in the servo system and deformation of the telescope. They were expected to be of the order of 0°.05. The easiest way therefore to measure star positions is to use the pilot for setting; the errors introduced by the pilot are much smaller than those of the system as a whole. The positions of 50 stars were taken from the *American Ephemeris*. While one observer made the setting in α and δ a second observer determined the deviations ΔA and Δh in azimuth and altitude of a star with a set of calibrated cross wires in the optical telescope. The accuracy of one determination was of the order of 0°.01. During a measurement the pilot moved in hour angle with the sidereal rate, causing the telescope to follow the daily motion. After each series of about 50 measurements, which took 2 to 3 hours, the zero points of the azimuth and elevation servo systems were readjusted and the measurements were repeated with the improved zero. In the determination of Δh optical refraction corrections were applied.

The final series, consisting of about 100 position determinations over the whole sky, showed a mean error per point of ± 0°.02. The values of ΔA showed in addition a sinusoidal variation with A, having an amplitude of ± 0°.02. Since the deviations of ΔA with h, Δh with A and Δh with h showed no variation, it must be inferred that the variation in ΔA originates in the driving system of the telescope, possibly in one of the gears. The horizontal and vertical axes of the telescope are thus found to be correctly mounted to well within 0°.03, while the mean error of one setting of the whole system in equatorial co-ordinates is ± 0°.03.

c. *Determination of the radio axis*

The radio axis is defined as the direction of maximum gain, and is intended to be identical with the optical axis of the paraboloid. It may differ from it through a wrong position of the antenna in the focus or through deformation of the mirror. The position of the radio axis with respect to the optical axis was determined by finding the right-ascension α and declination δ of four of the brightest radio sources, and comparing the values found with the best known radio or optical data (PAWSEY 1955). The data used are given in Table 1. To find α and δ, sweeps were made through a source in α and δ, using the pilot, at a speed of 0°.25 per minute. Thus in about four minutes the major part of the antenna pattern, which has a width between half-power points of 0°.57, has swept across the source. From two sweeps in opposite sense, the values of α and δ could be determined with a mean error of ± 0°.01 for the three brightest sources. From the differences $\Delta\alpha$ and $\Delta\delta$ between

TABLE 1

Positions of four bright radio sources, used in the calibration

Source	α_{1950}	δ_{1950}	$\alpha_{1956.7}$	$\delta_{1956.7}$
	°	°	°	°
Cas A	350.297	58.531	350.376	58.567
Cyg A	299.435	40.596	299.496	40.615
Tau A	82.881	21.982	82.987	21.987
Vir A	187.075	12.668	187.163	12.630

measured and true co-ordinates the differences ΔA and Δh may be determined from

$$\begin{aligned} \Delta A \cos h &= \Delta\delta \sin \psi - \Delta\alpha \cos \delta \cos \psi, \\ \Delta h &= \Delta\delta \cos \psi + \Delta\alpha \cos \delta \sin \psi. \end{aligned} \quad (1)$$

In the present investigation the transformation to ΔA and Δh was made graphically, determining the parallactic angle ψ from a star map with a movable altazimuth co-ordinate system.

An average value of ΔA and Δh was found from a number of measurements, and the position of the antenna was altered accordingly by changing the length of the guy wires which hold the supporting mast. At the same time the focal distance was varied to obtain maximum gain. In this manner the antenna was brought exactly to the focus of the paraboloid.

The differences Δh are not constant with h. This is due partly to refraction and partly to a number of mechanical effects, of which the stretching of the guy wires holding the antenna mast and the bending of the mast are the most important. The mechanical effects are zero at $h=90°$, but each of itself becomes important at low altitudes. They more or less cancel out by a suitable selection of elasticity of the guy

FIGURE 1

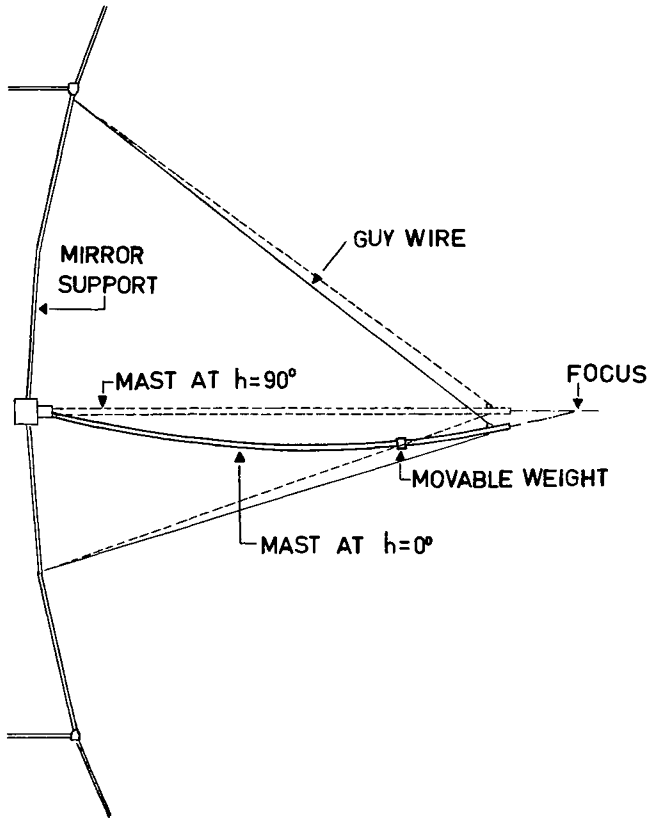

Suspending and bending of the antenna mast.

wires and stiffness and weight of the mast (Figure 1). The position of the centre of gravity of the mast and therefore the amount of cancelation, may be changed by moving a weight along the mast. A rough measurement indicated that the change in position of the top of the mast with altitude resulted in a change Δh of the order of 0°.02. It is clear that most of this change must happen at altitudes above 20°. Inspection of Figure 2, where Δh is plotted versus h, shows that the difference between the optical refraction and the value of Δh increases more steeply between $h=90°$ and 20° than below $h = 20°$. We may draw the conclusion that refraction at 22 cm is of the same order as optical refraction.

To find the misalignment of the mast it is of course most convenient to measure the positions of the radio sources in the neighbourhood of the meridian, where $\Delta h = \Delta\delta$ and $\Delta A \cos h = \Delta\alpha \cos \delta$, and where h is a maximum, so that refraction effects are small. To arrive at the curve of Δh versus h however, measurements had to be made at low elevations. For that purpose the sources Cyg A, Tau A and Vir A were used, since Cas A reaches a minimum altitude of 21°. The points for Cyg A, which culminates at $h = 3°$ in the North, and Tau A, which sets in the Northwest, have a lower weight because the curves were slightly deformed by strong scintillation (intensity fluctuations up to 20%) on most of the observing nights. The effect is not too great however, because the scintillation period in most cases was of the order of 5 minutes, while the essential part of a measurement took only 1 minute.

FIGURE 2a

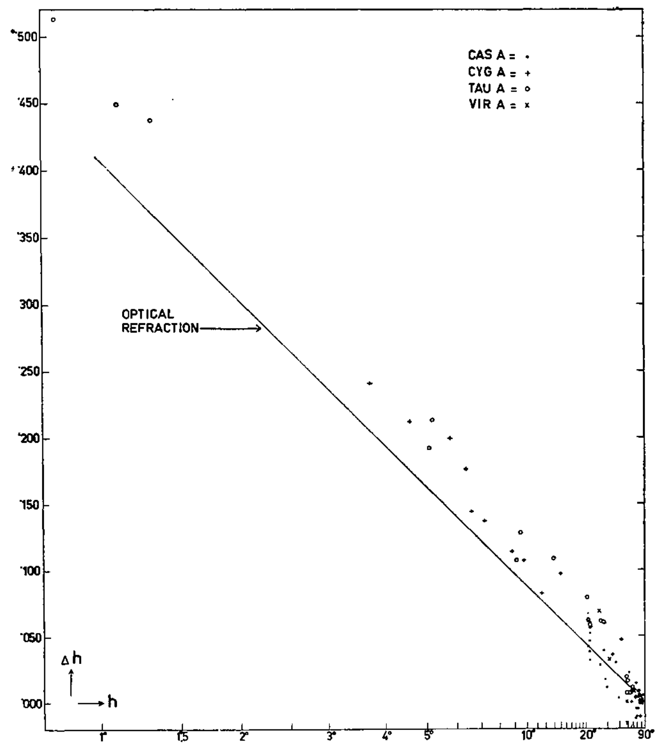

Deviation Δh from the standard position of radio stars. The scale of abscissae is chosen so as to make the optical refraction curve a straight line.

FIGURE 2b

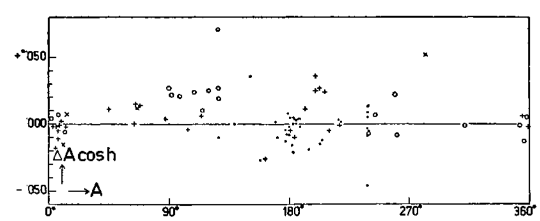

Deviation ΔA cos h from the standard position of radio stars.

The plot of ΔA versus A (Figure 2b) shows maximum deviations from zero of $\pm$ 0°.03, whilst there is an indication of the same sinusoidal variation with an amplitude of $\pm$ 0°.02 as found in the optical measurements of star positions. The maximum deviations from a smooth curve in the plot of Δh versus h are likewise of the order of $\pm$ 0°.03. This figure is the same as that given by the optical measurements. This indicates that the accuracy with which the position of a bright radio source can be measured is determined entirely by the mechanical setting accuracy of the telescope.

One interesting point arising from the radio-axis measurements should be mentioned. As is apparent from Figure 2, no systematic deviations larger than $0^\circ.02$ exist between the positions of the four bright sources. It may therefore be concluded that at 1390 Mc/s the positions of these sources are the same as the positions found at the lower frequencies to within $0^\circ.02$.

d. *The antenna pattern*

During this series of measurements an accurate determination of the shape of the antenna pattern in the horizontal and vertical plane was obtained. This was done by sweeping back and forth in α and δ through Cas A while it was almost exactly in lower culmination. The curves obtained give the antenna pattern in the horizontal and vertical direction. Another set of sweeps was made at the instant when the daily motion of Cas A was vertically downward. A sweep in δ then is similar to a sweep in A, and an α sweep is the same as a sweep in h. All sweeps gave the same result to well within 1% in intensity. The antenna pattern both in vertical and horizontal direction resembles a gaussian curve with a halfwidth of $0^\circ.57$ to about 1%, down to 1/3 of the top intensity. Below this the width of the pattern is on the average $0^\circ.03$ smaller than the corresponding gaussian curve. The near side lobes in the vertical and horizontal planes are below 1/2% of the top intensity. No attempt was made to determine the full antenna pattern, so that nothing is known about the 45° side lobes or the far side and back lobes. In the reduction of the survey no indications were found of any near side lobes; thus it may safely be assumed that these are also below 1/2%. A correction for the angular size of Cas A would reduce the halfwidth of the antenna pattern by $0^\circ.01$ to $0^\circ.56$. In the reductions the value $0^\circ.57$ has been used throughout.

e. *General remarks on the calibrations*

It seems useful to reconsider the various calibrations in the light of the 25 months' experience since the first calibration was made.

The calibration of the pilot will have to be done at least once a year. The pilot is mounted in the rotating laboratory in the base of the telescope, where there is a continuous traffic of observers and technicians, and where it is subject to very slight but continuous vibrations due to the telescope motion. Also, temperature differences may be considerable. Since the reliability of position determinations and setting depend to a great extent on the pilot, its maintenance is of the utmost importance. The same obviously applies to the reading scales and to the servo mechanism which couples them with the pilot. In particular the α scale must be readjusted every time the sidereal time clock is reset. Power failures, which occur several times a year, stop the standard frequency generator which supplies the frequency to drive the sidereal time motors.

In principle the optical calibration need only be made once. After the first calibration scratch marks may be made on the telescope to give the position of $A = 0$ and $h = 0$, and these may be used for all further zero settings. It was decided to make the final marks only after the telescope had been in full use for some time, when all mechanical readjustments which were still necessary after the end of the building period were finished. It is planned to do this in the near future. The new optical calibration will have to be preceded by a check on the alignment of the optical telescope and the geometrical axis of the mirror, since strains in the beams of the mirror and in the mounting of the optical telescope may have changed its position. The optical telescope is mounted in the open air. It may have been used as a grip, or knocked in one way or another. It seems advisable to recheck optically the performance of the whole telescope every few years, to ensure that no outside influences—e.g. sinking of the foundations, earthquakes, very strong winds—have changed the position of its axes.

If no readjustments are necessary a total of 200 position measurements of stars over the whole sky is enough to obtain ample accuracy. The measurements should preferably be divided over a few nights with different wind directions. In certain positions of the telescope the wind will cause the play in the gears to work in one direction. A series of 30 or 50 star measurements is sufficient to determine the zero point with enough accuracy to enable a readjustment to be made. After some practice, one position measurement, including the setting of the pilot and telescope, takes about 3 minutes.

Each time the antenna has been removed from the top of the mast a redetermination of the radio axis is necessary. If the same antenna is remounted this can be confined to a number of measurements at high elevations in order to determine the new radio axis. If an antenna with different weight is mounted a complete redetermination of the change of Δh with h must be made, since the bending of the mast and the stretching of the top guy wire will be different. Readjustment of the movable weight may be necessary. Since a full determination of one position, including setting of the telescope and a few sweeps through the source in both α and δ, takes about

20 minutes, this work is rather time-consuming. Once the radio axis is made parallel to the geometrical axis at high altitudes, however, the further measurements of Δh may be made as a part of the normal observing programme until enough are available.

The mast can be lowered by increasing the length of the top guy wire, whereby it pivots around its base. A stop on that guy wire makes it possible to bring the mast back to its old position. The position of the radio axis was found to be exactly the same each time the mast had been lowered.

2. *Antenna and receiver*

The electronic equipment was built and maintained by Ir C. A. MULLER and his staff at the Radio Observatory, Dwingeloo. The excellent performance of the receiver was due entirely to their special efforts. Many thanks are due to Ir MULLER for making this receiver available, and for his continuous interest in the measurements. Parts of the receiver were the same as those used previously in the 7.5 m Würzburg aerial in Kootwijk, described by MULLER (1956) and MULLER and WESTERHOUT (1957), and later used for the 21-cm line measurements in Dwingeloo.

The antenna was a half-wave dipole mounted on a conical termination of the supporting mast which ended in a coaxial line. A reflector plate of dimensions 26 × 17 cm was mounted half a wavelength above the dipole. It was bent in the H plane such that the antenna pattern was the same in both principal planes.

A rigid coaxial line made of brass tubing connected the antenna with the crystal mixer, which was mounted in a box just behind the surface of the paraboloid mirror. The local oscillator frequency of 1390 Mc/s was obtained by 216 × multiplication of a 6.4 Mc/s crystal oscillator signal. A servo system operating on the power supply of the frequency multiplier kept the d.c. crystal current of the crystal mixer constant to about 0.1%.

The 35 Mc/s intermediate frequency amplifier was a cascode with a bandwidth of 5 Mc/s.

No image suppression was used and the antenna was carefully matched at both 1355 and 1425 Mc/s, so that the signal received was an average of the signal at these two frequencies. Assuming that the spectrum of the radiation received is flat, the average reception frequency is 1390 Mc/s, corresponding to a wave length of 21.6 cm.

The first stages of the i.f. amplifier and the last stages of the frequency multiplier were mounted in the box behind the mirror. The detector used was a thermionic vacuum diode operated as a quasi-linear detector. We have to know the relation between the reading of the output meter and the incoming energy. Let the incoming energy be $W = W_\circ + P$, where $W_\circ$ is the energy when the antenna is pointing to an empty sky and P the energy from a radio source. This will give rise to a deflection of the recorder of $E = E_\circ + r$, where $E_\circ$ is the deflection for an energy input $W_\circ$ and r is the reading obtained when the aerial is pointed to a radio source. Assuming that in the measuring range, $E^\alpha = W$, and taking $P = r$ for small values of r, then (SEEGER *et al.* 1956)

$$P = r\left\{1 + \frac{\alpha - 1}{2E_\circ} r + \frac{(\alpha-1)(\alpha-2)}{6E_\circ^2} r^2 + \ldots\right\}. \qquad (2)$$

To obtain the value of α, the relation between E and W was measured by replacing the antenna by a matched resistor and inserting attenuations, by steps of 1 db, in the i.f. amplifier. The attenuator, which had a range of 20 db, was described by SEEGER (1956) and thanks are due to him for putting it at our disposal.

In the measuring range, which extends from $E_\circ = 6100$ units to $E_{\text{Cas A}} = 6781$ units, we found $\alpha = 2.05 \pm .03$. The units in which $E_\circ$ is given are used throughout this investigation. The intensity of the source Cas A is the highest measured. With these values, the formula relating incoming energy to meter reading is

$$P = r(1 + \underset{\pm .000003}{0.000086}\, r). \qquad (3)$$

This relation, as well as the value of the noise figure derived below, is independent of the relation between E and W outside the measuring range. In particular, the value of E for $W = 0$ does not enter into the derivation.

It is shown in Chapter 3d that for small increments 1 unit = 0.45 °K ± 30% in antenna temperature. A 300 °K increase in antenna temperature then gives, by equation (3), a reading $r' = 630$ units ± 30%. The noise figure, determined from the relation

$$N - 1 = \frac{W_\circ}{W' - W_\circ} = \frac{E_\circ^{\alpha}}{(E_\circ + r')^{\alpha} - E_\circ^{\alpha}} \qquad (4)$$

is found to be $N = 5.5$ (7.4 db) ± 30%. A constant amount was subtracted from the large signal from the detector by means of a series of back-off voltages. The sensitivity of the d.c. amplifier could be changed by a factor of 100 in steps of about a factor of 2.5.

The ratio between the various sensitivities was measured very carefully so that intensities of the strong radio sources, which were measured with a sensitivity 5 times smaller than that of the survey, could be reduced to the same intensity scale. The time constant of the d.c. amplifier was variable between 0.1 and 32 seconds. The recording meter was a Honeywell Brown pen recorder.

3. *Reduction data*

a. *Receiver gain*

Throughout the observing period, the total receiver gain was checked by measuring the intensity of the source Cas A. A measurement consisted of a number of α- and δ-sweeps through the source, extending the sweep over a few degrees. Since Cas A is situated in a region where the top intensity of the galactic ridge was just at the limit of measurement, i.e. more than a factor 100 smaller than the intensity of the source itself, a straight zero line could be drawn between the regions on either side. It was very convenient that this could be done with the four bright sources. Even the background intensity around Cyg A was the same in all directions, notwithstanding the nearness of the bright extended complex source Cyg X. Therefore, the uncertainty in the intensity of these sources does not depend on the uncertainty of the background level underlying the source, as is usually the case at lower frequencies or with the sources superposed on the galactic ridge.

With the exception of three sudden jumps the receiver gain remained constant to within 4% over periods of a week. One jump was due to change of tubes in the receiver, the others were of unknown origin. Most of the measurements of Cas A were made at $h > 30°$; the change of extinction between $h = 30°$ and $h = 90°$ is smaller than 0.5%.

b. *Extinction*

An attempt was made to measure the extinction in the earth's atmosphere. If the extinction factor in the zenith is p and the equivalent air mass traversed at zenith distance z is $F(z)$, we have

$$I(z) = I(0)\, p^{F(z)-1}, \qquad (5)$$

where $I(z)$ is the intensity of the source at zenith distance z and $F(0) = 1$. For $z < 80°$, $F(z)$ does not differ appreciably from sec z. The values of $F(z)$ were taken from the *Handbuch der Astrophysik* (SCHOENBERG 1929). A series of measurements of $I(z)$ at different z, permits us to determine p from

$$\log p = \frac{d \log I(z)}{d\, F(z)}. \qquad (6)$$

Since $F(z)$ is 3 at $h = 20°$ and 12 at $h = 4°.2$, it is clear that only measurements at very low altitudes can provide a reasonable estimate of p. Measurements were made of the intensity of Cyg A, Tau A and Sgr A. One measurement consisted of three or four sweeps through the source; in a few instances, at low elevations, the telescope was made to follow the source for five to ten minutes to obtain a better average. Most of the intensities of Cyg A and Tau A at small h were rather inaccurate due to scintillation. The scintillation periods were mostly of the order of 5 minutes, and in one case the amplitude reached a value of 20%. Short-period scintillation (5 sec) was at the most 3%. No scintillation was visible in Sgr A. Immediately before or after each measurement the intensity of Cas A was determined, which made an accurate correction for gain changes possible. The values of log I are plotted in Figure 3 as a function of $F(z)$. Constant amounts were added to the values for Tau A and Sgr A to make them comparable to those for Cyg A. Log p was determined from Figure 3, for different ranges of $F(z)$, and is given in Table 2.

FIGURE 3

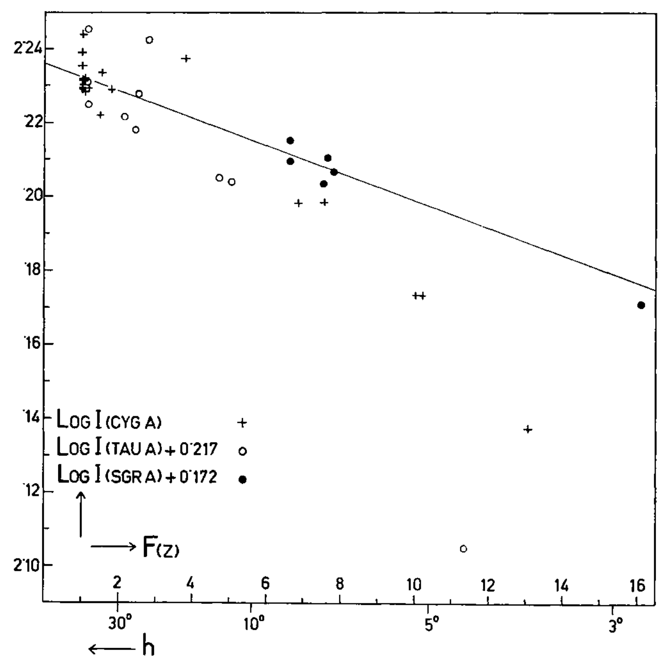

Intensities of three bright sources as a function of equivalent air mass, for determination of extinction.

TABLE 2

Determination of the extinction

	z h $F(z)$	70°-82° 20°- 8° 3 - 7	82°-86° 8°- 4° 7 -12	82°-87°.2 8°- 2°.8 7 -16	60°-87° 30°- 3° 2 -15
log p (continuum)	Cyg A	−.006	−.010	—	—
	Tau A	−.008	−.016	—	—
	Sgr A	—	—	−.004	—
log p (21-cm line)	Kootwijk	—	—	—	−.0037
	Dwingeloo	—	—	—	−.0035

The value of log p determined from 21-cm line measurements in Kootwijk (MULLER and WESTERHOUT 1957) is represented by a straight line in Figure 3 and is given in Table 2. The provisional result of similar 21-cm line extinction measurements made in Dwingeloo is also tabulated. Both the continuum method and the line method of determining the extinction have their disadvantages. The line method would be somewhat better, in principle, because the sources of 21-cm line radiation are usually extended in comparison with the small sources used for the continuum measurements, and are therefore much less influenced by scintillation. However, in the case of the Kootwijk and Dwingeloo receivers it is complicated by the automatic gain control, which is influenced by changes in radiation from the air and the ground in the main lobe and in the side and back lobes. Obviously, much better continuum results could have been reached if many measurements had been made. Due to lack of time, this was not possible. The results given in Table 2 and Figure 3 show a large discrepancy between the values derived from Cyg A and Tau A, measured in northerly directions, and the values derived from Sgr A and the 21-cm line, measured between the Southeast and the Southwest.

Although the measurements are too scarce and too inaccurate to permit any definite conclusions, the extinction in the North seems to be considerably higher than in the South, while it also increases towards the horizon in the North. It would be very interesting to verify whether there is a connection between scintillation, extinction and ionospheric effects. The latter tend to be strongest in northerly directions.

The agreement of the better-quality 21-cm line extinction and that derived from Sgr A, and the fact that most of the survey measurements at low altitudes were made in the South, led us to adopt the Kootwijk 21-cm line value for the reductions. Thus, all measurements were corrected for extinction, taking $\log p = -0.0037$.

TABLE 3

Intensities and intensity ratios of four bright sources

	Cas A		Cyg A		Tau A		Vir A		
		m.e.		m.e.		m.e.		m.e.	
Intensity 1)	681.0	±.4	427.0	±.7	254.8	±1.5	59.4	±1.2	units
Intensity 2)	681.0	±.4	425.2	±.9	254.6	±2.1	58.3	± .8	units
Average intensity	681.0	±.4	426	± 1	255	±2	59	±1	units
Intensity, corrected for alinearity	721	±2	442	±2	261	±2	59	±1	units
Ratio	1.000		0.613	±.004	0.362	±.004	0.082	±.002	
Antenna temperature	324	±100	199	±60	117	±35	26.5	±8	°K (±30%)
Flux density	3100	±600	1900	±400	1120	±220	250	±50	10^{-26} Watt/m² (c/s) (±20%)

c. *Intensity ratios of four bright sources*

The series of measurements made for the determination of extinction also included a number of measurements of the source Vir A. Accurate intensity ratios of the four sources Cas A, Cyg A, Tau A and Vir A were determined from it in two ways.

1) 14 Measurements were made of the intensity of Cyg A, between $h = 67°$ and $h = 78°$; the intensity of Tau A was measured six times, between $h = 20°$ and $h = 59°$, and five measurements were made of Vir A, between $h = 26°$ and $h = 49°$. They were corrected for extinction with $\log p = -0.0037$ and compared with the intensity of Cas A, which was determined before or after each measurement and also corrected for extinction. The intensities found, together with their mean errors, are given in units in the first line of Table 3.

2) Only those intensities were used which were obtained when the source was at approximately the same altitude as that at which the comparison measurement of Cas A was made. Therefore, no extinction corrections had to be applied. The comparison is based on nine measurements of Cyg A, three of Tau A and three of Vir A. The intensities are given in the second line of Table 3. Since Cas A was used as the comparison source, its mean error should be zero. However, the uncertainties of the ratios between the various sensitivities of the d.c. amplifier also enter into the comparison, because the sources had to be measured at different sensitivities. The m.e. of 0.4 quoted for Cas A is due to this. The second determination, into which the uncertainty in the extinction does not enter, should have a higher weight than the first. It depends however on a smaller number of measurements. Since the same measurements were used for both determinations, the differences in the results and the similarity of the mean errors give an impression of the uncertainty. A straight average of the two values is given in the third line of Table 3. The intensities, which are in fact meter readings, were then corrected for the alinear relation between meter reading and incoming energy (equation (3)) and the ratios were determined (fourth and fifth lines). With the correction factors determined in Chapter 3d, we also find the antenna temperatures and the flux densities of these sources. These absolute intensities have much greater errors than the ratios.

d. *Absolute intensity scale*

The definition and derivation of the terms and equations used in this section are given by SEEGER, WESTERHOUT and VAN DE HULST (1956). No direct determination of the directivity and the antenna efficiency was made. The method used in Kootwijk to determine the relation between meter reading and brightness temperature by pointing the antenna to a nearby pinewood (MULLER and WESTERHOUT 1957) was not possible, since the paraboloid could not reach negative altitudes. Two methods were used to derive the absolute intensity scale.

1. The flux density of Cas A, found in Kootwijk by means of the pinewood method (WESTERHOUT 1956), was compared with the intensity in units given in Table 3. Thus, $S = 3100 \times 10^{-26}$ Watt/m^2 (c/s) ($\pm$ 30%) corresponds to 721 units, and 1 unit $= 4.3 \times 10^{-26}$ Watt/m^2(c/s) $\pm$ 30%. The beam directivity

$$D' = 4\pi \Big/ \iint\limits_{\text{full beam}} f(\theta, \varphi) d\Omega = 4\pi/\Omega', \qquad (7)$$

where Ω' is the effective solid angle of the beam, may be computed from the measured shape of the antenna pattern. Since this is almost gaussian with halfwidths $s_a = s_b = 0°.57$, it follows that
$\Omega' = 1.134\, s_a\, s_b = 0.369$ square degrees, and
$D' = 112000$.

Equal increase in the recorded intensity is obtained by an increase of 1 °K in T_b over the full beam or an increase of flux density

$$S_u = 8\,\pi\, k/\lambda^2 D' \qquad (8)$$

at the centre of the beam. With $S_u = 6.6 \times 10^{-26}$, we have 1 unit = 0.65 °K $\pm$ 30% in brightness temperature T_b.

On the assumption that the spectrum of Cas A for frequencies higher than 40 Mc/s is a straight line (WHITFIELD 1957, SEEGER 1957), we find from the spectrum fitting all observations a flux density at 1390 Mc/s which is about 25% lower than the Kootwijk value. A measurement by HAGEN *et al.* (1954) at 1420 Mc/s gives a flux density which is 14% lower than the Kootwijk value. Our flux density and brightness temperature per unit should be 25% and 14% lower, respectively, if one of these values were the correct one.

2. In a region of the sky far removed from the galactic plane, four sweeps in altitude have been made between $h = 2°$ and $h = 20°$, in the South. The change of intensity with altitude must be due to stray radiation from the ground and to radiation of the air. Assuming that the stray radiation is sufficiently constant over an altitude range between 4° and 8°, whilst no radiation from the ground enters into the main lobe and near side lobes for $h > 4°$, the change of intensity should be entirely due to air radiation. If the extinction factor in the zenith is p, the brightness temperature due to air radiation is

$$\Delta T = (1 - p^{F(z)})\; T_o. \qquad (9)$$

Assuming the average air temperature along the line of sight to be 280 °K, and using $\log p = -0.0037$ (Chapter 3b), we find the expected change of ΔT with h. Equating this to the observed change, measured in units, we find 1 unit = 0.67 °K in T_b. The mean error of p, determined from the Kootwijk 21-cm line measurements, is 10%; since only provisional results of the determination of p in Dwingeloo are known, and taking into account the assumptions made, we adopt an error of 30% in the above value. This is only a guess.

Since the determination of the directivity of the Kootwijk antenna, which caused the large uncertainty in the Kootwijk flux density of Cas A, only partially entered into the determination of p, the results of methods 1) and 2) are largely independent. In view of the striking agreement of the results of the two determinations we adopt a mean error in the absolute intensity scale of $\pm$ 20%. The absolute intensities are then still in accordance with HAGEN's value for Cas A, but not with the assumption of a straight line for the total spectrum.

Since no determination of the antenna directivity could be made, no values can be given for the antenna temperatures. Assuming, however, a stray factor $\beta = 0.30$, we find 1 unit = 0.45 °K in T_a. The uncertainty in this value is at least 30%. In the further reductions, the following factors were adopted:

1 unit = 4.3×10^{-26} Watt/m^2(c/s) $\pm$ 20% m.e.
1 unit = 0.65 °K in T_b $\pm$ 20% m.e.
1 unit = 0.45 °K in T_a $\pm$ 30% m.e.

4. *The measurements*

a. *A search for discrete sources*

Before the main survey was started, and when adjustments to the telescope and drive mechanism were still in progress, a search was made for discrete sources over the whole visible sky. Since the pilot could not yet be used, the only possible motions were in azimuth and altitude. In order to be able to use the telescope even when a great pointing accuracy was not possible, sweeps were made in azimuth, with the speed of 72°/min provided by the azimuth setting motor, between $A = 330°$ and 30°, at altitude intervals of 0°.3. With this sweep speed and a receiver time constant of 0.2 sec, every discrete source with an intensity greater than 30 units ($T_b = 20$ °K, $S = 130 \times 10^{-26}$ Watt/m^2(c/s)) was found as a sharp spike well in excess of the noise peaks. Some weaker sources were also detected. The lowest intensity

FIGURE 4

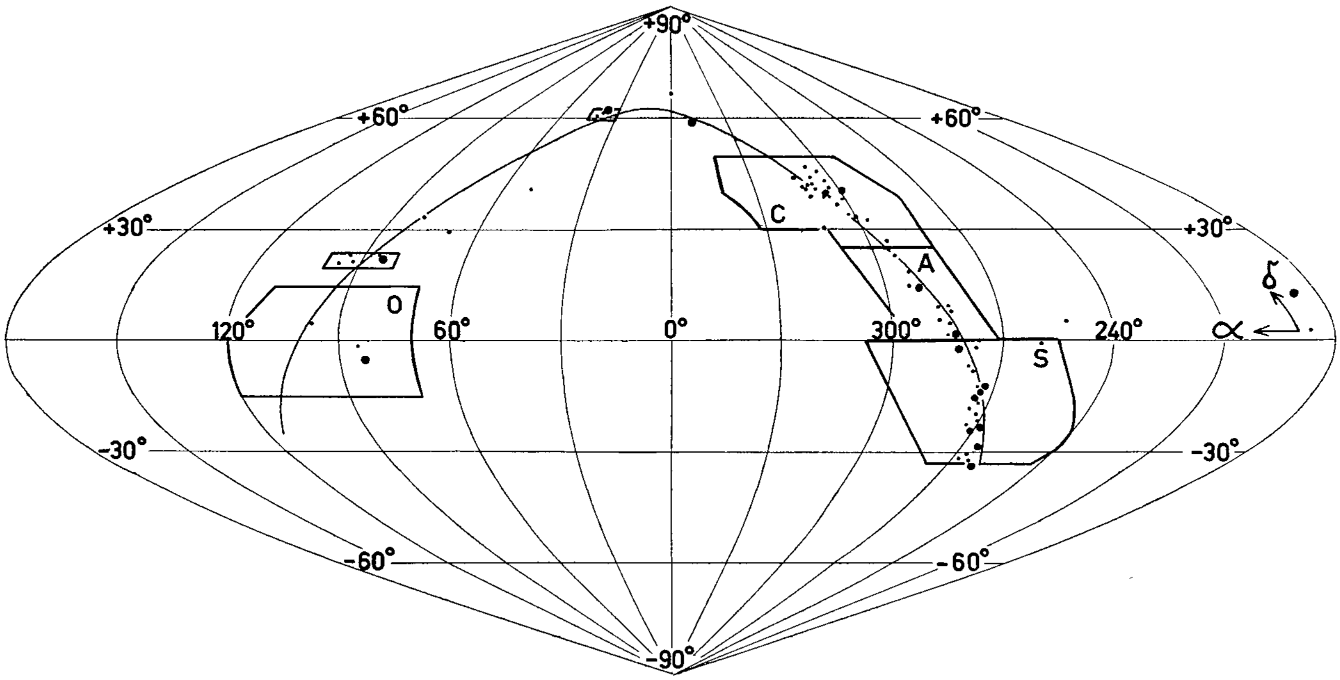

Equal-area chart of the whole sky, with the boundaries of the main survey and the two source maps, and the positions of the discrete sources. Big dots are sources with $I > 30$ units.

TABLE 4

Approximate boundaries of the survey

Region	α	δ	l	b
S(agittarius)	$245^\circ - 295^\circ$	$-35^\circ - 0^\circ$	$320^\circ - 360^\circ$	$-20^\circ - +20^\circ$
A(quila)	$275 - 300$	$0 - +25$	$0 - 30$	$-10 - +10$
C(ygnus)	$280 - 340$	$+25 - +50$	$30 - 55$	$-20 - +15$
O(rion)	$70 - 120$	$-15 - +15$	$165 - 195$	$-30 - +15$

measured was 15 units. For the sources with intensities between 15 and 30 units, the survey was incomplete. The region around the Sun, i.e. roughly between $\alpha = 120^\circ$ and 160°, $\delta = 0^\circ$ and $+30^\circ$, had to be excluded because of solar radiation in near side lobes. The accuracy of a position determination was about 2° in α and $0^\circ.5$ in δ. A total of 61 spikes on the records was suspected of being due to discrete sources. They were studied more closely by making slow α-sweeps (2 or 4° per minute) at intervals of $0^\circ.1$ or $0^\circ.2$ in δ around the estimated positions, after the telescope calibration was finished. Out of these, 36 were confirmed, 10 of which were not situated in the regions included in the main survey. They are included in Table 6, and contour maps of the surroundings of two of them are given in Figure 10. Their position is indicated in Figure 4. No trace of any source could be found in the neighbourhood of the positions of the other 25, so that the spikes on the records must have been spurious. This search for discrete sources, including the confirming measurements, took approximately 400 hours. As a result, all sources of which the brightness surpasses the limit mentioned above have been found in the region $\delta > -35^\circ$, excluding the small region around the Sun. They are given as big dots in Figure 4. A rapid survey like this one seems to be well worthwhile as a suitable compromise between the time-consuming work of accurately surveying an essentially empty region of the sky and the looking at interesting regions only.

b. *The main survey*

The measurements for the main survey and all detailed investigations consisted of sweeps in right-ascension, with speeds of 2 °/min in regions where the intensity gradient is steep, and 4 °/min in other regions. At most declinations, two sweeps were made in opposite directions. Markers were automatically placed on the record by means of a micro-switch mounted on the α-scale of the pilot, which short-circuited the recorder every degree in α for a very

FIGURE 5

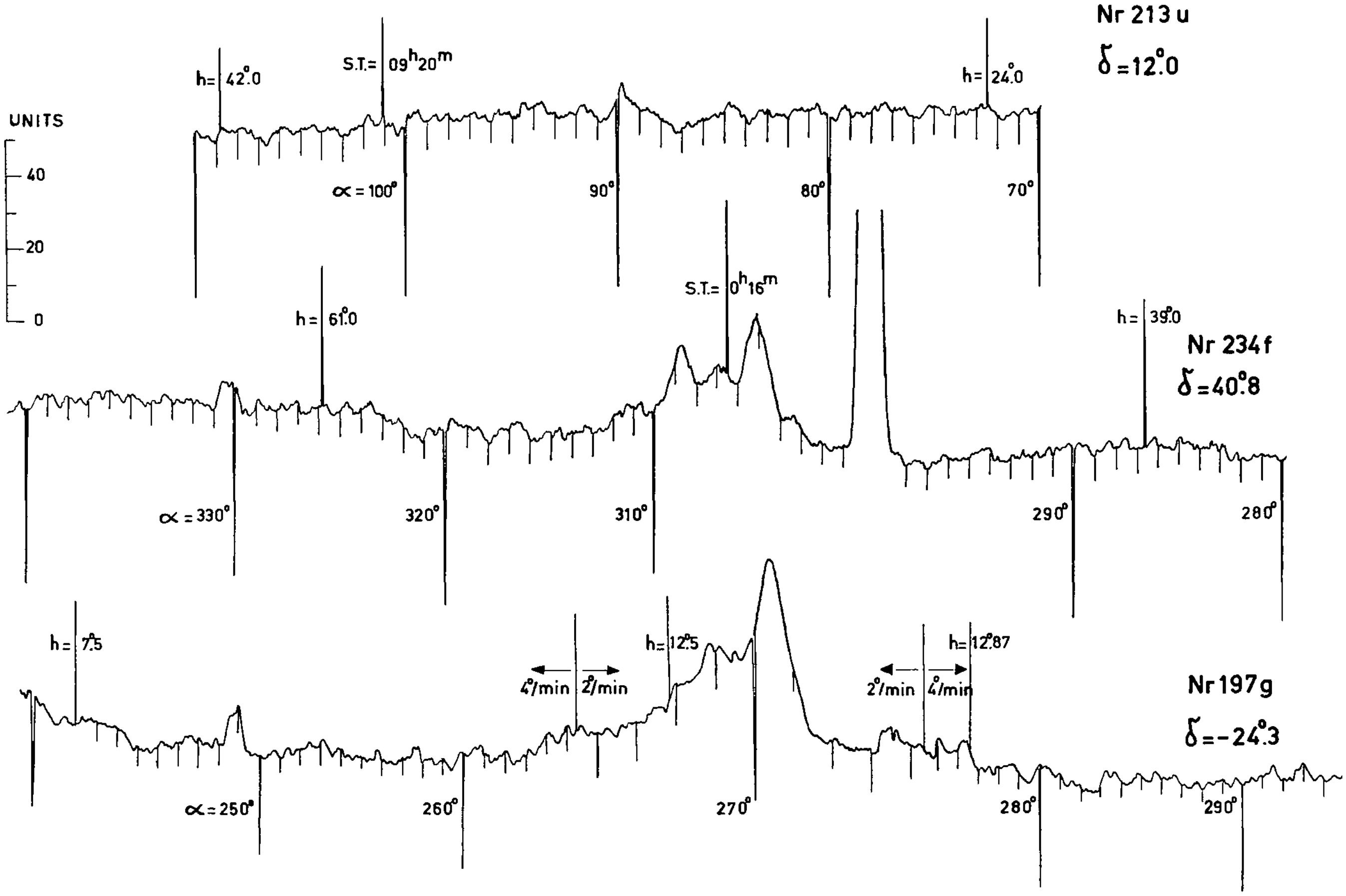

Sample recorder tracings of sweeps in α, at constant δ, for regions O, C and S.

FIGURE 6

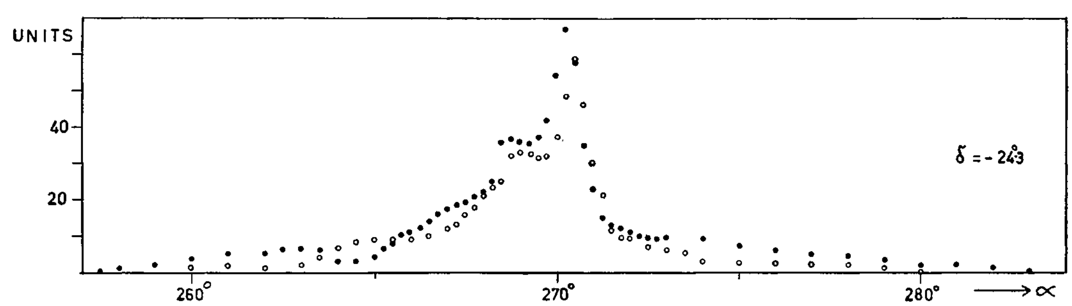

Example of a reduced cross-section.

short time; the position of these degree markers was accurate to within a few hundredths of a degree. The length of the markers was determined by the time constant of the recorder and by the length of time the recorder was short-circuited. At every multiple of 10 degrees this length of time was automatically increased, so that the 10-degree markers were easily distinguishable. The time constant of the d.c. amplifier used was 1.6 sec. In Table 4 and Figure 4 the approximate boundaries of the regions investigated are given. The total observing time was approximately 300 hours. Two sweeps in opposite directions were made at declination intervals of 0°.3 in regions S and O. In region C, the declination intervals were also 0°.3, but between $\delta = 38°.7$ and 44°.1, the interval was decreased to 0°.15. In region A, which was added to the survey in the last days, when some extra time became available, about one third of the declinations was covered only once, and the declination intervals varied between 0°.1 and 0°.3. Only half of the sweeps between $\delta = 0°$ and 10° were extended to $b = \pm 10°$, the other half to $b = \pm 5°$.

In addition to these regular programmes, extra series of sweeps at 2 °/min were made between $\delta = -26°$ and $-32°$ through the source Sgr A. Some sweeps at slow speed (0°.25/min) both in α and δ were made through Sgr A and the Orion nebula.

Outside the main survey, some sweeps were made through the galactic plane at irregular intervals to obtain some idea regarding its intensity, and series of sweeps were made through and around the sources found in the search programme. Sample tracings in regions O, C and S are shown in Figure 5. The quality of the measurements was best in region S. A number of measurements in A, C and O were of very poor quality, the reason for which is unknown. It could hardly be due to low-level outside interference, because the region S sweeps were made between approximately 17 and 20 hours local time, and the A, C and O sweeps between approximately 20 and 24 hours, 0 and 4 hours and 5 and 9 hours local time, respectively. During the night hours, outside interference was expected to be low. One possible reason, which was not investigated at the time of the observations, but was suggested later, was the influence of discharges through oil leakage in the elevation motors of the telescope. The possibility of such discharges was discovered some months later, when the motors were taken apart. The region S sweeps were all made very close to the meridian, where the change in altitude during an α sweep is small. A large part of the region O and A sweeps and all the region C sweeps were made well after culmination, when this change is considerable. The higher speed of the elevation motors may have caused a stronger discharge phenomenon and therefore more interference.

Peak-to-peak values of the noise on the region S tracings were of the order of 3 units (= 2 °K). On the tracings through regions A, C and O the peak-to-peak noise value was about the same, but sharp peaks and humps up to 6 units (4 °K) were very frequent. Furthermore, in some of the region C and many of the region O tracings, sudden jumps in the zero level occurred of up to 6 units (4 °K).

5. *The reductions*

a. *Zero lines*

No absolute intensity determinations were made, and therefore the zero intensity is unknown. Extrapolation from measurements at much lower frequencies (85, 100 and 242 Mc/s for example) shows that at 1390 Mc/s the brightness temperature for $|b| > 15°$ fluctuates between absolute values of the order of 1 to 2 °K (Chapter 7). From some α sweeps which were extended well beyond $|b| = 20°$ it was found that no fluctuations greater than about 1 °K occur. It seems therefore safe to assume that somewhere between $|b| = 10°$ and $|b| = 20°$ the intensities are the same to within 1 °K. Hence the average intensity at those values of $|b|$ was used as the zero level of the survey. Thus, the zero levels were drawn as straight lines through those parts of the tracings where $|b| > 10°$ or 15°. Parts of some tracings at $\delta < -20°$ were made at such low altitudes that corrections to the zero line had to be applied for the change of the air radiation with h, which was non-linear in the sweeping direction, α (Chapter 3d).

In region A no sweeps were extended to $b = \pm 20°$. The greater part was extended to $b = \pm 10°$, the remainder to $b = \pm 5°$. The zero lines were drawn between the more or less flat extremities of the tracings. It must therefore be realized that in this region the zero level is probably higher than in the other regions. This can clearly be seen from the run of contour 1 in the map in Figure 9.

In Chapter 7 it is estimated that the zero level in region A is 2 units (1.4 °K) higher than in the other regions.

b. *Mean curves*

A smooth pencil line was drawn through each tracing. The intensity above the zero level was read off at every degree in α, and in places with a steep intensity gradient at every 1/2 or 1/4 degree, while a second person plotted it on graph paper. Measurements made at the same declination were plotted in the same graph. Corrections were applied for extinction, and the intensities were reduced to the same sensitivity by multiplying the ordinates by a previously tabulated correction factor. Since two sweeps at the same declination were always made in opposite directions, the shift of the curves due to the effect of the receiver time constant could easily be seen and corrected for. With a sweep speed of 2 °/min and a time constant of 1.6 sec, it is expected to be about 0°.05. Its observed value varied between this and 0°.1, the larger value being probably due to the effect of the time constant of the recorder pen. The corrected curves were averaged by drawing a mean curve in the same graph. Thus, a series of average cross-sections at constant δ through the galactic plane, in general at δ-intervals of 0°.3, was obtained. An example of such a cross-section is given in Figure 6. The values of δ were corrected for refraction and bending (Figure 2).

c. *Maps*

The values of α at which the intensity is a multiple of 5 units were read from these cross-sections, tabulated and then plotted as points on equal-area charts. Points of equal intensity were connected and the resulting contour lines were smoothed (Figure 8). This was in particular necessary with contours 1 and

2, giving intensities of 5 and 10 units respectively, which in places showed a waviness with an amplitude of up to 5° in α over distances of the order of 1°, due to the fact that at these intensities the gradient with α is very small (see Figure 6). Therefore, a small uncertainty in the zero level corresponds to a large uncertainty in the position of the points with intensity 5 or 10.

A bulge in the lowest contours, derived from several measurements at different declinations, was not smoothed away. The exact shape of such a bulge, however, is still largely dependent on the zero level. A bulge in contour 1, and to a lesser degree in contour 2, should therefore be taken only as an indication of the existence of a region of somewhat higher intensity, without giving its exact outline. It is clear that the direction in which the sweeps were made, i.e. at constant δ, should be visible in these contours. This is particularly noticeable in the region between $l = 24°$ and 45°, where the intensities are low. No attempt was made to smooth the contours further in this region or to readjust the zero levels of the measurements.

From a careful study of measurements at the same δ, and of neighbouring cross-sections, it was concluded that the error in the contours was everywhere smaller than 1/2 contour interval, i.e. 2.5 units or 1.6 °K, with the exception of contours above 10, where the error is smaller than 5% of the contour value.

No correction was applied for the smoothing effect of the antenna pattern. The set of circular contours for the source Cyg A (Figure 8a) give the shape of the antenna pattern, because its halfwidth (contour 44) is far in excess of the angular size of the source.

No map is presented for the Orion region (region O). The intensities in this region are everywhere below 5 units, except at the position of the sources No 10 (Orion nebula), No 16 (Rosette nebula) and No 12 (NGC 2024).

A very careful examination of the cross-sections was made at the points where they cross the galactic equator. In order to minimize the irregularities, those parts of the measurements which showed no jumps in the zero level were averaged over regions a few degrees wide in δ. The existence of a galactic ridge in this region could not be established. The intensity above the general background of such a ridge must be below 4 units (2.5 °K). A small map is given of the Rosette nebula (No 16).

Maps of the surroundings of the sources IC 1795 (No 3) and Tau A (No 9) are also presented. The observations were made during the checking of the sources found in the search programme. They have the same accuracy as the other maps.

All maps in equatorial co-ordinates are for epoch 1957. The map in galactic co-ordinates, given in Figure 9, at the end of this paper, was obtained in the following manner. With the aid of the new Lund Tables (OHLSSON *et al.* 1956), which give the conversion $(l, b) \rightarrow (\alpha, \delta)$ for 1958, based on the standard galactic pole ($\alpha = 12^h40^m$, $\delta = +28°$, 1900.0), a galactic co-ordinate grid was drawn in the equatorial maps. A sheet of transparent paper on which a rectangular grid was already drawn was then placed on top of the equatorial maps, and squares of $2° \times 2°$ were made to coincide as well as possible. The contour lines inside such a square were then copied, and the next square was treated in the same way. Thus, the distorted galactic co-ordinate system on the equatorial maps was linearized. The positional errors made in this procedure are estimated to be below 0°.1, and the accuracy of the galactic map is therefore of the same order as that of the other maps. The difference of one year between the epoch of the measurements and that of the Lund Tables is too small to have any influence on the accuracy.

The contour intervals of all maps are 5 units (3.25 °K in T_b). The numbers in the contours are multiples of 5 units.

d. *Galactic ridge*

The position in α and δ of the top of the galactic ridge was determined as well as possible from each cross-section. Corrections were applied for refraction and bending, and the equatorial co-ordinates were converted into galactic co-ordinates, which are given in Table 5. At places where a strong source distorts the cross-sections, the values of b_{max} are omitted; in Figure 7, which presents the same data as Table 5, no points are given at those longitudes. Instead, a cross indicates the position of the source. The accuracy in latitude for each point is of the order of 0°.1 for $l < 15°$. These data may be used in a determination of the galactic plane (*I.A.U.* 1958). The top intensities are also given. These include the intensities of sources on or very near the ridge. The lower envelope of this curve may be considered as representing the integrated intensity of distant sources, and is used in Chapter 7 to determine the distribution of thermal and nonthermal sources.

e. *Discrete sources*

The positions, intensities and sizes of the discrete sources, found in the main survey and in the search programme, were determined independently of the contour maps in the following manner. The intensity and the position in α and δ of a top in the α-sweeps was tabulated, corrected for refraction and bending, and for extinction. The top intensities were then plotted as a function of δ, the top of this curve giving the δ of the source. The average of α at this and the surrounding declinations is the α of the source. This

TABLE 5

Position and intensity of the top of the galactic ridge. In the neighbourhood of bright sources the values of b_{max} are omitted.

l	b_{max}	I	T_b	l	b_{max}	I	T_b	l	b_{max}	I	T_b	l	b_{max}	I	T_b
		units	°K			units	°K			units	°K			units	°K
°	°			°	°			°	°			°	°		
320.09	−1.38	28	18	339.26	−1.58	32	20	358.47		89	58	13.06	−1.35	16	10
320.33	−1.18	33	21	339.66	−1.67	29	19	358.74		62	40	13.28	−1.29	15	10
320.53		65	42	340.03	−1.68	29	19	359.03	−1.38	35	23	13.59	−1.46	13	9
320.78		134	87	340.33	−1.63	42	27	359.39	−1.40	30	20	13.85	−1.49	13	9
320.83		139	90	340.62	−1.50	44	28	359.69	−1.32	25	16	13.91	−1.41	13	9
321.05		114	74	341.08	−1.55	43	28	0.10	−1.50	21	14	14.07	−1.49	15	10
321.87	−1.20	25	16	341.41	−1.52	41	26	0.37	−1.36	22	14	14.27	−1.42	17	11
322.21	−1.17	32	21	341.74	−1.73	46	30	0.68	−1.53	23	15	14.51	−1.47	14	9
322.81	−1.49	32	21	342.01	−1.62	45	30	0.83	−1.57	20	13	14.50	−1.24	12	8
323.04	−1.29	40	26	342.32	−1.51	41	27	0.93	−1.53	19	12	14.66	−1.32	15	10
323.33	−1.17	38	24	342.57	−1.32	34	22	1.04	−1.52	19	12	14.85	−1.25	12	8
323.73	−1.21	35	23	343.18	−1.84	40	26	1.09	−1.43	21	14	15.27	−1.61	10	6
324.13	−1.30	36	23	343.41	−1.62	27	18	1.28	−1.55	22	14	15.77	−1.71	13	8
324.44	−1.20	40	26	343.80	−1.71	29	19	1.37	−1.46	20	13	16.22	−1.91	23	15
324.76	−1.13	34	22	344.13	−1.73	32	21	1.41	−1.37	21	13	16.47		38	25
325.32	−1.49	41	26	344.40	−1.59	28	18	1.44	−1.24	18	12	16.54		49	32
325.58	−1.30	43	28	344.70	−1.50	29	19	1.64	−1.38	22	14	16.64		65	42
326.12	−1.57	47	31	345.20	−1.79	31	20	1.79	−1.46	18	11	16.81		82	53
326.37		61	40	345.50	−1.77	28	18	1.66	−1.00	22	14	17.03		75	49
326.77		82	53	345.94	−1.88	29	19	2.27		56	36	17.17		64	42
327.08		117	75	346.18	−1.71	39	25	2.35		62	40	17.22		60	39
327.32		167	108	346.56	−1.75	41	27	2.45		60	39	17.38		36	23
327.52		241	157	346.83	−1.63	40	26	2.50		51	33	17.54		19	12
327.73		287	187	347.15	−1.60	29	19	2.60		41	26	17.74	−0.93	13	8
328.01		205	133	347.55	−1.72	31	20	2.67		38	24	18.25	−1.22	9	6
328.40		107	69	347.79	−1.50	30	20	2.76	−1.62	29	19	18.59	−1.22	12	8
328.69		83	54	348.21	−1.68	33	22	2.99	−1.42	22	14	18.97	−1.30	15	9
329.03		62	40	348.49	−1.56	32	20	3.38	−1.38	20	13	19.19	−1.08	12	8
329.58	−1.60	45	29	349.11	−2.09	27	18	3.74	−1.50	17	11	19.66	−1.26	8	5
329.92	−1.59	40	26	349.43	−2.06	39	25	4.06	−1.50	18	12	20.06	−1.38	8	5
330.22	−1.53	40	26	349.55	−1.85	45	29	4.43	−1.54	19	12	20.50	−1.55	8	5
330.49	−1.57	39	25	349.95	−1.75	37	24	4.81	−1.63	19	12	20.75	−1.40	8	5
330.89	−1.46	41	26	350.27	−1.70	40	26	5.10	−1.55	23	15	20.99	−1.21	12	8
331.09	−1.60	43	28	350.63	−1.74	49	32	5.43	−1.50	29	19	21.21	−0.98	11	7
331.25	−1.48	34	22	350.96	−1.71	55	36	5.74	−1.45	23	15	21.60	−1.04	13	8
331.49	−1.27	30	20	351.20	−1.54	45	30	6.02	−1.36	21	14	22.05	−1.23	9	6
331.94	−1.47	34	22	351.53	−1.54	42	28	6.50	−1.60	17	11	22.27	−1.03	8	5
332.29	−1.46	32	21	351.69	−1.62	47	31	6.92	−1.74	18	12	22.54	−0.88	7	4
332.59	−1.37	32	21	351.94	−1.68	39	26	7.14	−1.53	21	13	23.16	−1.33	6	4
333.02	−1.53	35	23	352.23	−1.57	47	31	7.48	−1.51	15	10	23.03	−0.65	5	3
333.51	−1.79	38	25	352.53	−1.52	43	28	7.78	−1.45	12	8	23.71	−0.68	3	2
333.76		49	32	352.87	−1.51	37	24	8.24	−1.70	12	8	23.90	−0.41	8	5
333.96		60	39	353.16	−1.43	41	26	8.56	−1.65	17	11	24.79	−0.16	5	4
334.24		74	48	353.52	−1.45	39	25	8.94	−1.72	18	12	25.47	−0.73	4	3
334.54		63	41	353.89	−1.53	36	24	9.09	−1.39	14	9	26.51	−1.52	3	2
334.86		43	28	354.27	−1.60	39	25	9.50	−1.48	14	9	27.13	−2.33	7	4
335.04	−1.45	35	23	354.67	−1.69	39	25	9.82	−1.44	11	7	26.60	−1.25	5	3
335.52	−1.64	32	21	354.72	−1.60	35	23	10.21	−1.55	14	9	27.02	−1.56	8	5
335.88		44	29	354.92	−1.29	31	20	10.57		17	11	26.99	−1.13	8	5
336.23		52	34	355.35	−1.45	31	20	10.87		28	18	27.27	−1.39	5	4
336.49		49	32	355.61	−1.32	21	13	11.13		22	14	27.13	−0.99	8	5
336.82		41	27	356.07	−1.56	32	21	11.31	−1.01	14	9	27.30	−0.88	8	5
337.14		27	18	356.33	−1.39	37	24	11.71	−1.14	12	8	27.73	−1.21	6	4
337.72	−1.91	42	28	356.71	−1.49	37	24	12.20	−1.40	13	9	28.11	−1.42	5	3
337.93	−1.67	47	31	357.09	−1.55	32	21	12.13	−1.20	11	7	28.27	−1.31	4	3
338.14	−1.41	42	27	357.46	−1.62	38	25	12.44	−1.24	9	6	28.40	−0.93	7	5
338.60	−1.60	35	23	357.85		47	31	12.60	−1.27	11	7	28.64	−0.76	8	5
338.95	−1.62	35	23	358.21		63	41	12.95	−1.57	13	9				

FIGURE 7

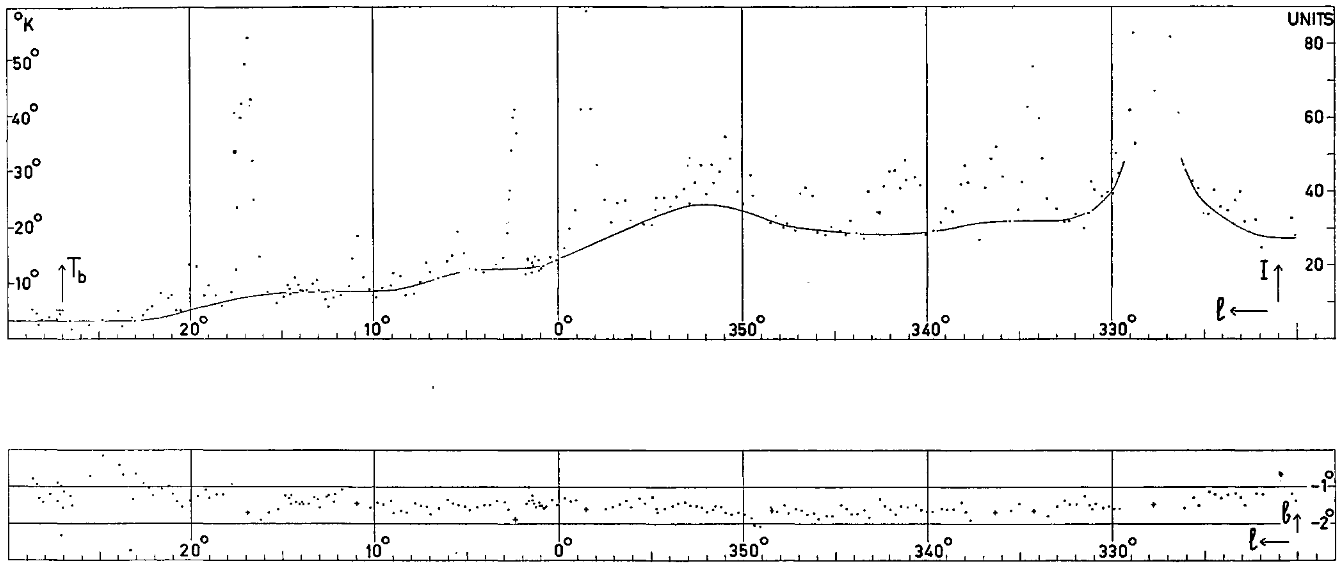

Intensity and latitude of the galactic ridge. Latitudes in the neighbourhood of bright sources (+) have been omitted.

method proved very satisfactory; from a comparison of independent position determinations of the same source, based on two sets of measurements, it was found that the accuracy for a not too faint source was better than half the positioning accuracy of the telescope. The positions derived in this manner are given by points in the contour maps. Most of the cross-sections, both in α and δ, could be fairly well represented by gaussian curves. The widths at half the top intensity are used to indicate the source-size.

Through a few bright sources, α- and δ-sweeps were made at 0.25 °/min; the positions and halfwidths determined from these curves were in excellent agreement with those determined from the 2 °/min cross-sections. The positions and intensities of all sources found in this investigation are given in Table 6, and optical identifications are discussed in Chapter 6c. The numbers and identifications of the sources along the galactic ridge are given along with the map in Figure 9 at the end of this paper.

6. *Discussion and identification of discrete sources*

a. *Thermal emission*

The classical absorption coefficient for free-free transitions within an ionized gas with electron temperature T_e and equal number of electrons and protons n per cm³ is

$$\varkappa(\nu) = \frac{4e^6 n^2 L}{3\sqrt{2\pi}\,(m_e k T_e)^{3/2}\, c\nu^2}, \qquad (10)$$

where L is a logarithmic factor which is variously defined by different authors (e.g., SMERD and WESTFOLD 1949; PIDDINGTON 1950) and which changes slightly with density and frequency. For all practical purposes, we may put $L = 24$ in this investigation. Gathering the constants in one factor, we have

$$\varkappa(\nu) = 0.12\, n^2\, T_e^{-3/2}\, \nu^{-2}. \qquad (11)$$

The brightness temperature of a part of a nebula where the optical depth is τ, is

$$T_b = T_e(1 - e^{-\tau}), \qquad (12)$$

with

$$\tau = \int \varkappa(\nu) ds = 0.12\, T_e^{-3/2}\, \nu^{-2} \int n^2 ds. \qquad (13)$$

The integral $E = \int n^2 ds$, where ds is the length of the column of gas in the line of sight, is called the emission measure (STRÖMGREN 1948, 1949). The conventional units of E are cm^{-6}pc; with ν in Mc/s we then get

$$\tau = 3.6 \times 10^5\, T_e^{-3/2}\, \nu^{-2}\, E. \qquad (14)$$

At the frequency of 1390 Mc/s, used in this investigation, and assuming that the average ionized hydrogen nebula has an electron temperature $T_e = 10^4$ °K, we have

$$\tau = 1.88 \times 10^{-7}\, E. \qquad (15)$$

We see that for $E < 10^6$, $\tau < 0.2$ and we may approximate

$$T_b = \tau \,.\, T_e. \qquad (16)$$

According to STRÖMGREN, such a high value of E has been observed only in the densest parts of the Orion nebula. The instrument may smooth out peaks in the distribution of E because of its limited resolving power. It is therefore not certain that higher values do not occur. OSTERBROCK (1955, 1957), who

FIGURE 8a

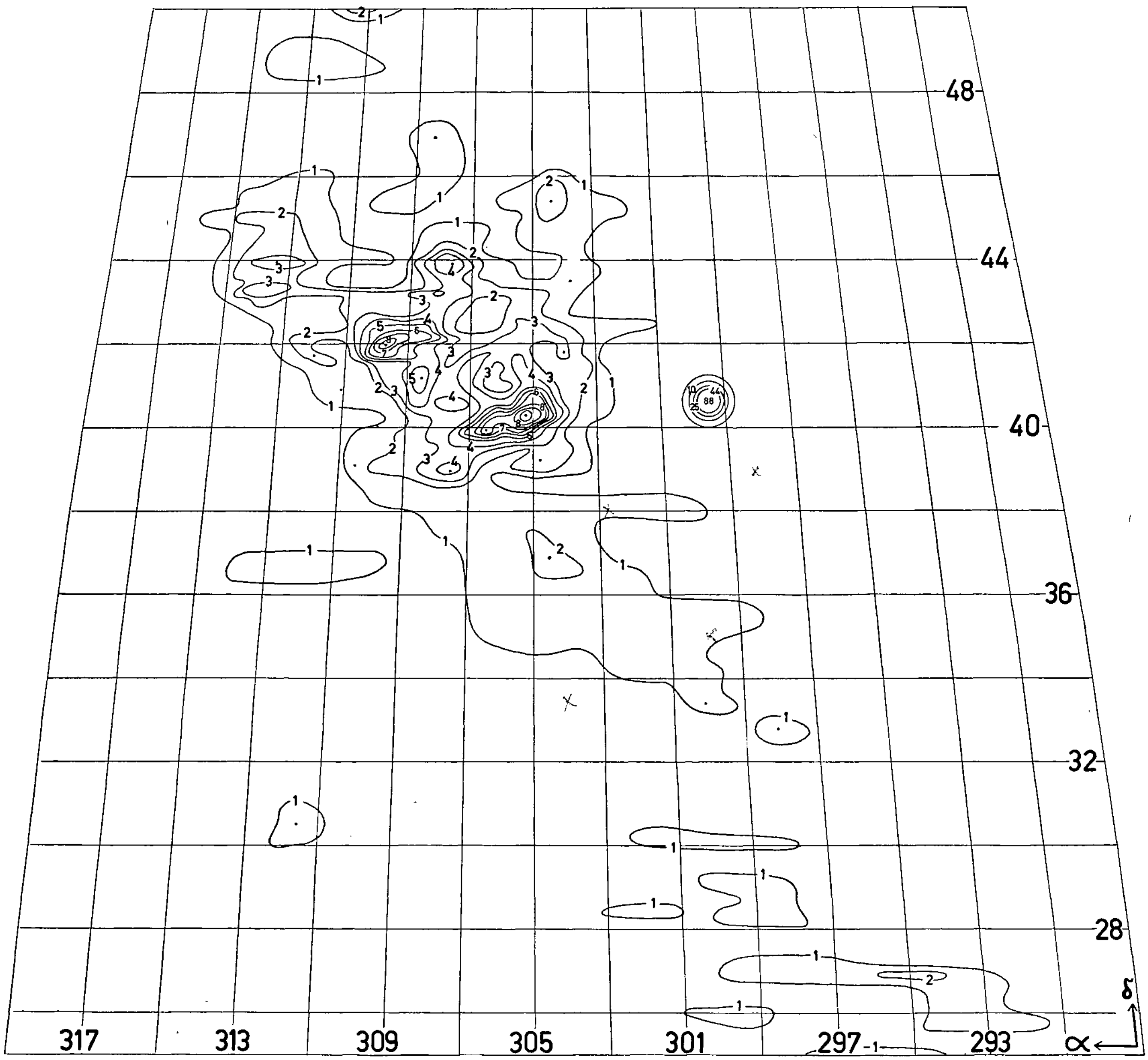

Map of region C in equatorial co-ordinates. Contour intervals are 5 units (3.25 °K in T_b).

measured the intensity ratio of the components of the [O II] λ 3727 emission line in several nebulae, found electron densities in the Orion nebula leading to values of E not far different from STRÖMGREN's values. Cases where $E > 10^6$ are so exceptional that we will use the approximation for small τ throughout.

The flux density of the total radiation from a discrete source is

$$S = 2k\nu^2 c^{-2} \int T_b \, d\Omega \,, \qquad (17)$$

where the integral is extended over the whole source, which subtends a solid angle Ω radians.

If we approximate an emission nebula, projected on the sky, by a circular area with diameter φ degrees and a constant emission measure, i.e. taking for E the average over the whole nebula, then with (13) and with E in cm^{-6}pc, we have

$$S = 2.6 \times 10^{-26} \, \varphi^2 \, T_e^{-1/2} \, E \,. \qquad (18)$$

It should be noted that, apart from the small change in L, the value of S is independent of frequency as long as the nebula is optically thin. With $T_e = 10^4$ °K, we find

$$E = 38 \times S \times 10^{26} \, \varphi^{-2} \,. \qquad (19)$$

This formula enables us to find E, averaged over the

FIGURE 8b

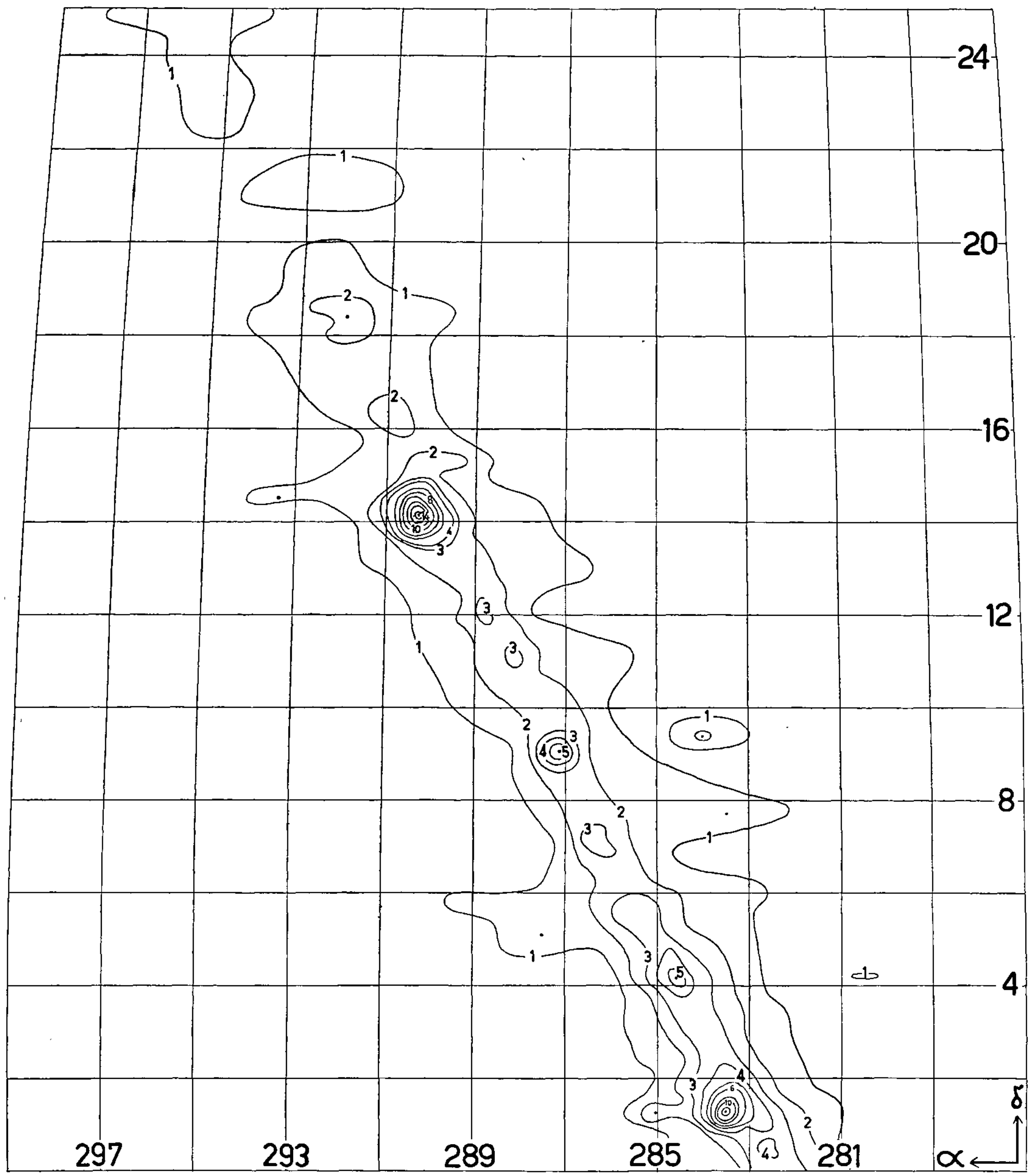

Map of region A in equatorial co-ordinates. Contour intervals are 5 units (3.25 °K in T_b).

nebula, if the flux density S and the angular diameter of the nebula can be determined from radio observations, or if the diameter is known from optical data. It is clear that a determination of E in this manner can compete very favourably with optical determinations, since the only uncertainties are in the value of S (20 to 40%, depending on the brightness of the source) and in the determination of the equivalent diameter φ (estimated at 30%).

Not many optical determinations of E have yet been made, so that a comparison of the results is hardly possible.

As in the optical case, a model has to be assumed for the nebula if we wish to determine its density n and mass M from E, or S and φ. One of the most important assumptions is the variation of n through the nebula, since the determination of n from $\int n^2 ds$ depends to a great extent on the distribution of n along the line of sight. On photographs of emission nebulae many nebulae appear to have a rather constant brightness over a large part of their surface. Usually their intensity decreases fairly rapidly near the edges and many have only a few rather small

FIGURE 8c

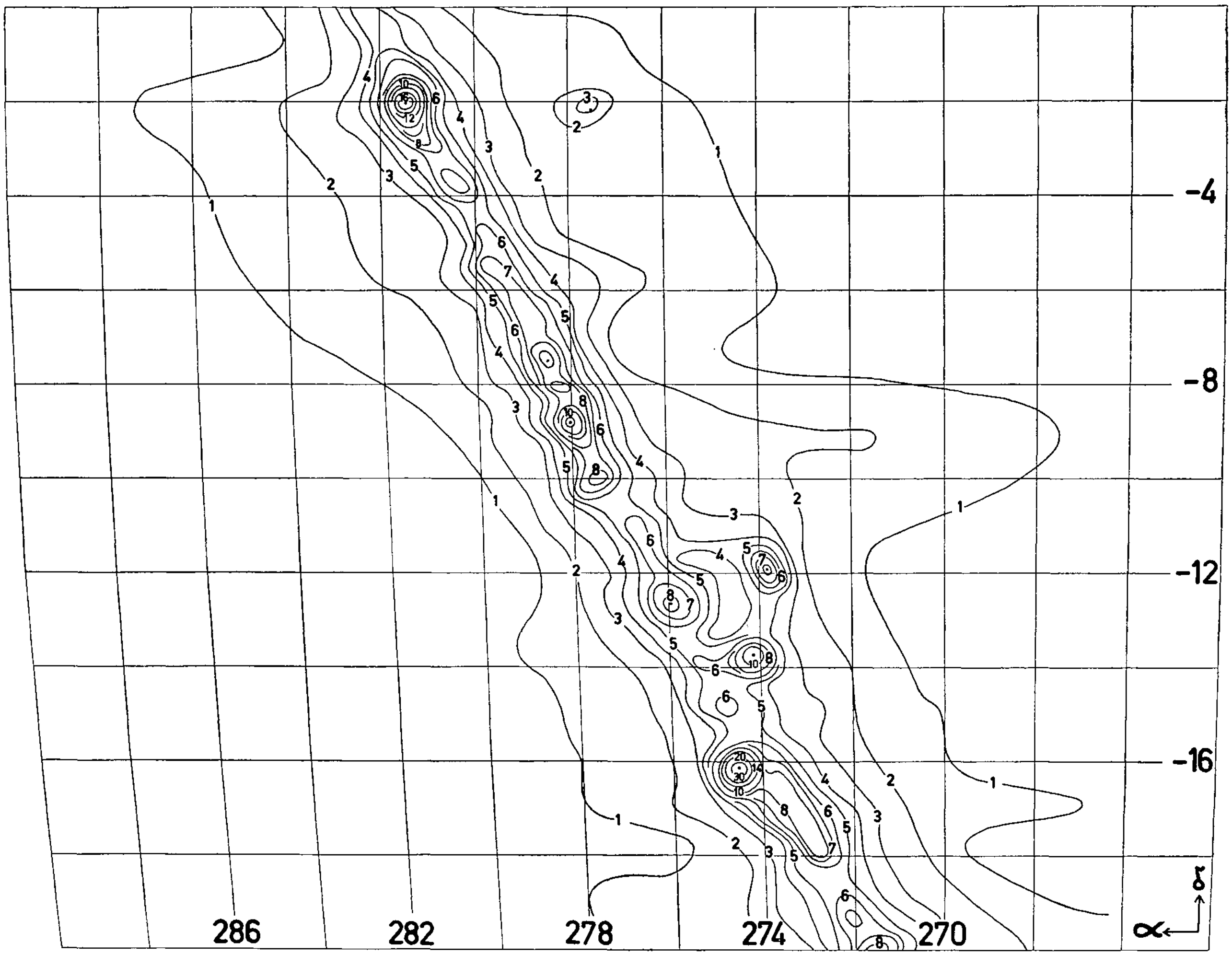

Map of region S (1) in equatorial co-ordinates. Contour intervals are 5 units (3.25 °K in T_b).

cores of strong brightness, while others have none. For lack of better information, and to obtain at least a very rough estimate of densities and masses, we assume that the density is constant throughout the nebula. We further assume that the nebula is cylindrical, with a circular cross-section of diameter φ degrees, and a length l, equal to the linear diameter; $l = r \, . \, \varphi/57.3$, where r is the distance of the nebula in parsecs. In this model, the density is

$$n = 4.8 \times 10^{13} \times S^{1/2} T_e^{1/4} \varphi^{-3/2} \, r^{-1/2} \,, \qquad (20)$$

and the total mass

$$M/M_\odot = 4.8 \times 10^6 \times S^{1/2} \, T_e^{1/4} \, \varphi^{3/2} \, r^{5/2} \,. \qquad (21)$$

Had we assumed a model consisting of a homogeneously filled sphere, we would have had to use a diameter 1.13 times smaller than that of the cylinder to obtain the same mass. Because of the other uncertainties it is clear that the exact shape of the model is not important.

The value of T_e cannot be determined from our data. Theoretically and from optical observations it is shown that this value must be of the order of 10 000 °K. Recent observations of absorption at low frequencies (MILLS 1956; SHAJN 1957) seem to be consistent with this figure. We will thus assume $T_e = 10\,000$ °K throughout this investigation. The formulae then are

$$n = \frac{48}{\varphi} \sqrt{\frac{S \times 10^{26}}{r\varphi}} \qquad (22)$$

and

$$M/M_\odot = 4.8 \times 10^{-6} \, \varphi r^2 \sqrt{\varphi r S \times 10^{26}} \,. \qquad (23)$$

Similar formulae were derived by MILLS (1956).

The value of E was determined for all thermal sources. Criteria used to decide whether a source was thermal or nonthermal were: a) identification with an optical emission nebula; b) its spectrum. It may be shown that all sources observed in the present survey would be well above the sensitivity limit of various surveys at much lower frequencies, if their spectrum

FIGURE 8d

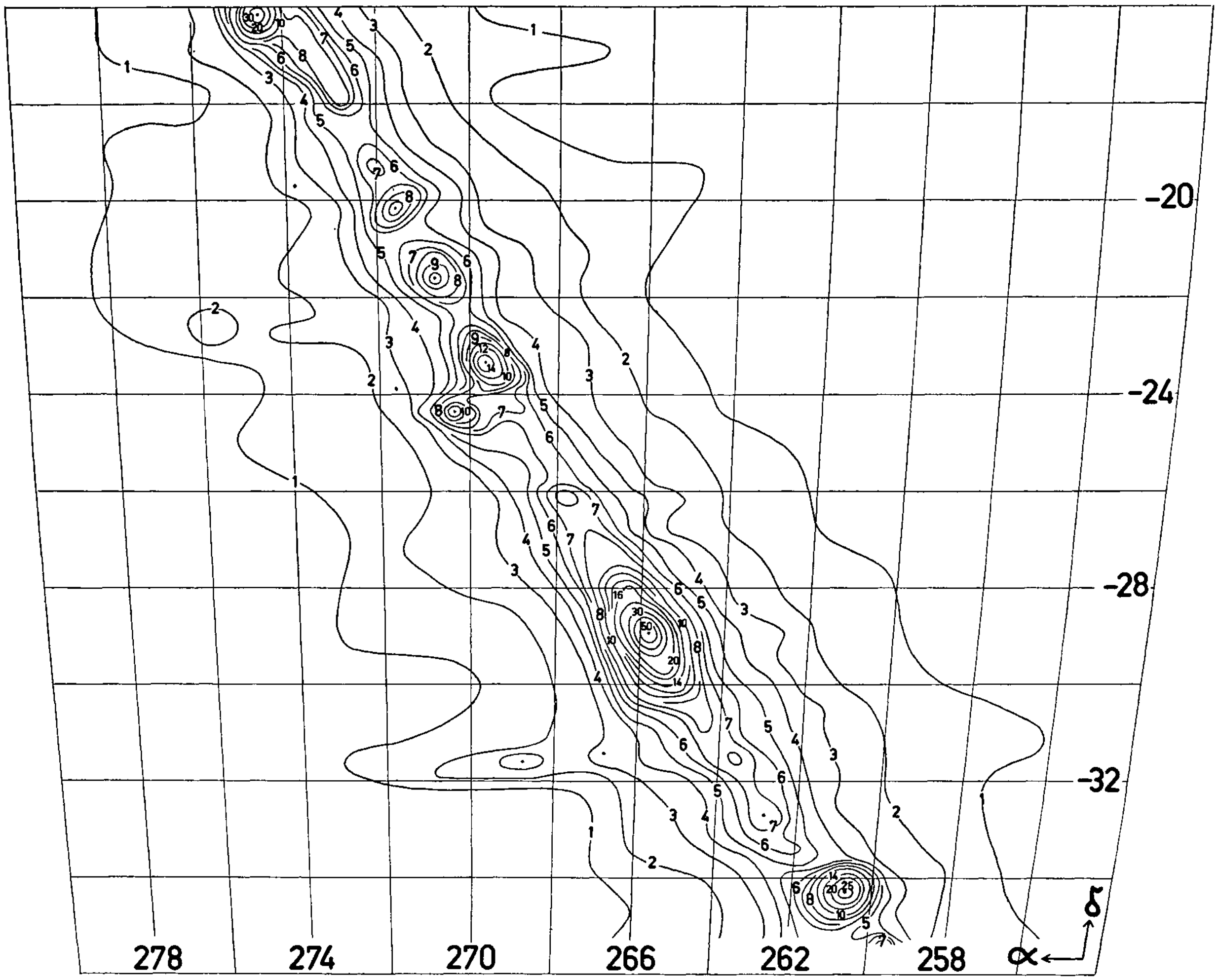

Map of region S (2) in equatorial co-ordinates. Contour intervals are 5 units (3.25 °K in T_b).

were nonthermal, i.e. if their flux density increased with decreasing frequency. The flux density of a thermal source on the other hand, is almost independent of frequency at the high frequencies, when it is optically thin, and decreases with decreasing frequency at the low frequencies, where it becomes optically thick. Therefore, if one of the sources in Table 6 was not found at lower frequencies, it was classified as thermal, and if possible, E was computed. It is tabulated in Table 6, column 16. If it could not be identified with an emission nebula, a question mark was put in this column.

b. *Individual sources*

The maps were compared with the photographs of the *Palomar Sky Survey* by drawing them on transparent paper on the same scale (53.6 mm per degree) and placing them on top of the photographs. In the neighbourhood of each source, a few stars from the BD or CD catalogues were plotted to allow an accurate comparison of the positions of nebulae and sources. Furthermore, the positions of the emission nebulae from the catalogues of SHAJN and GAZE (1955), SHARPLESS (1953) and GUM (1955) were plotted on the maps and compared both with the photographs and the positions and shape of the sources. This kind of comparison was very useful, for instance when a nebula was evidently partly covered by a dark cloud. Then the optical position of the nebula is the position of the visible part, while the radio position is not influenced by the presence of the dark cloud, and therefore differs from the optical value. In cases where there might be some doubt as to whether the boundaries of the visible part of a nebula are its real boundaries, or whether they are determined by dark clouds in the foreground, the radio position makes a decision possible. The observed radio positions are given in Table 6, column 2, with their estimated mean errors in column 3. To enable an easy comparison with various optical and radio catalogues, the co-ordinates for

FIGURE 10

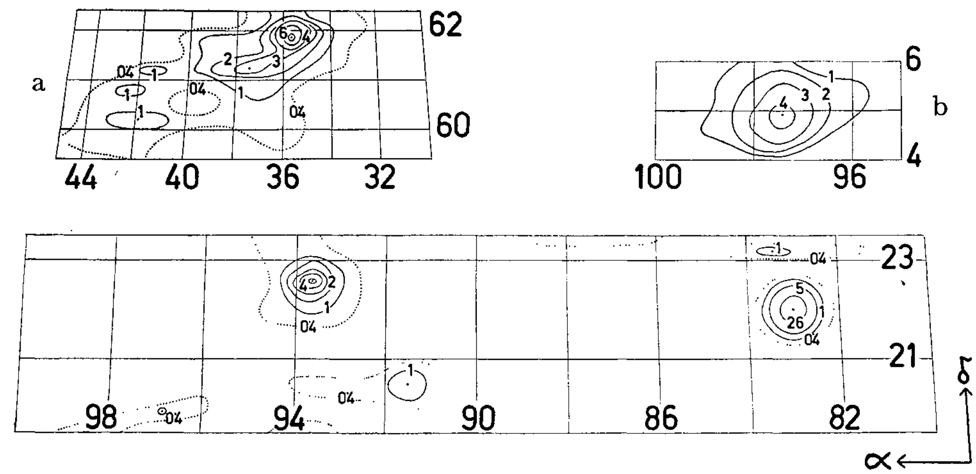

Maps of the surroundings of three discrete sources. Contour intervals are 5 units (3.25 °K in T_b).
a: IC 1795 (Nos 3, 4 and 5). b: Rosette nebula (No. 16). c: Crab nebula (Nos 9, 11, 13, 14 and 15).

1950 and 1900, as well as the galactic co-ordinates, are given in columns 4, 5 and 6.

No mean errors are given for the sources Nos 9, 18, 57 and 81, which were used for the calibration of the radio telescope; it was pointed out in Chapter 1e that the positions found at the lower frequencies are probably correct to within 0°.02. The sources Nos 2, 6 and 19 were observed by setting the telescope on or sweeping through the tabulated position, and therefore no mean errors can be given.

The numbers of the emission nebulae from the catalogues of SHARPLESS (E) and SHAJN and GAZE (SG) which are identified with sources, are given in columns 21 and 22 of Table 6. The SG-numbers are those from the revised summary of their four previous lists, and do not correspond to the S-numbers used by other authors. Identification of S- with SG-numbers may be made from their (1955) catalogue. The numbers from the catalogue of GUM are given in brackets in colum 23. I.A.U. numbers, as given by PAWSEY (1955) in his catalogue of reliably known discrete sources, are to be found in the same column. NGC or IC numbers of the nebulae or associated clusters are given in column 20. The top intensity above the background level, I, is given in column 12.

After subtraction of the background, the widths W_r of the observed cross-sections and/or contours at half intensity were determined. They are tabulated in column 7. For a source which was not circularly symmetric, two values of W were obtained. For all identified sources, the optical dimensions W_o were determined from the photographs and are given in column 8. In general, the very faint extremities of a nebula were not included in W_o. In most instances where the diameter of a nebula could be determined both from the photographs and from the radio measurements the two values agreed to within 30%.

The flux density S of a point source, i.e. a source of which all cross-sections have the same halfwidth as the antenna pattern, may be computed by multiplying the top intensity I in units by 4.3×10^{-26} Watt/m²(c/s) as derived in Chapter 3d. It is tabulated in column 13. If the source cross-section was wider than the antenna pattern (halfwidth s), i.e. if the source was extended, a correction factor for size, g, was applied to the value S', determined from the maximum intensity as if it were a point source, so that $S = g. S'$. For a source of which the true shape is gaussian, with halfwidth φ, we have

$$g = 1 + \frac{\varphi^2}{s^2} = \frac{W^2}{s^2},$$

whilst for a small cylindrical source (true cross-section rectangular) with diameter φ, the value of g is

$$g = 1 + 0.35 \frac{\varphi^2}{s^2}.$$

When two values of W are given, we have taken $W = \sqrt{W'W''}$. We may determine g either from the observed radio cross-sections (g_r, column 9) or from the size of the optical nebula (g_o, column 10). When both determinations were possible, the values agreed reasonably well.

For some sources, g_r was obtained by integration over the source. To those values, given in column 9, the letter i was added. The choice between the various possibilities of determining g was based on a study of the shape of the contours and of the Palomar Schmidt photographs. Where both g_r and g_o are given, the value in brackets was not used.

Similar considerations determined the value of and the choice between φ_r and $\varphi_o = \sqrt{W'_o W''_o}$. They are tabulated in columns 14 and 15. The emission measure E, computed by means of equation (19), is given in column 16. For nonthermal sources, a dash is placed in this column.

To obtain at least a very rough estimate of the distance r of the nebulae, the catalogues and other publications of CEDERBLAD (1946), MORGAN *et al.* (1952), SHARPLESS and OSTERBROCK (1952), MORGAN *et al.* (1953), JOHNSON (1953, 1955, 1956), SHARPLESS (1954), JOHNSON and MORGAN (1954) and GUM (1955), were consulted. Because of great difficulties in finding the exciting stars and determining their absorption, the distances are not known with any certainty. No attempt was made to evaluate the accuracy of the data, but it must be assumed that in many cases r may well be incorrect by 50%. In several instances, in particular in the region of Cygnus, we assumed the value of r from presumed connections of the nebulae in question with nebulae or associations of which the distance is given in the literature. This is indicated by a question mark with the value of r, column 17, and also with the values of n and M, columns 18 and 19.

As may be seen from equations (20) and (21) the influence of the uncertainty in r on the value of n is small, but the influence on M is very great. Consequently, the errors in M may well be more than a factor of 2. Of course, the assumption of a constant-density model may also introduce considerable errors. Nevertheless, it seemed worth while to compute n and M from the available data, since a knowledge of the order of magnitude of the densities and masses of average emission nebulae is already of great value. For sources Nos 1, 22, 24, 29 and 38 an attempt was made to distinguish between the rather bright central core of the nebula, and the whole nebula with the faint outer parts included. It is clear that a determination of the flux density for the central part is somewhat arbitrary due to the limited resolving power of the radio telescope. It was thought worth while, however, to obtain some idea of the differences between the values of E, n and M averaged over the central part, and those averaged over the whole nebula.

For sources Nos 33, 68 and 74, two or three values of the co-ordinates are given. They are ridges, running roughly between those positions. Sources 26 and 36 are regions, a few degrees wide, which were so conspicuous that we felt justified in including them in the table as separate sources.

c. *Notes to Table 6*

1. The main source is apparently the nebula surrounding BD + 66° 1676/79. Medium brightness, dark lanes, in particular on N side. Radio source extended to N; this is probably due to the big arc which is a bright part of the ring-shaped nebula SG 285. Main source is central part of this nebula. It is not clear which part has been classified NGC 7822.
2. A search for the Andromeda nebula had negative results.

3, 4, 5. Contour map in Figure 10a.

3. Bright irregular nebula on NW side of IC 1805. Dark lanes across it look somewhat like M 20.
4. Irregular nebula, medium brightness; bright central part, diameter 0°.2, coincides with centre of contours. The extension to the NE (SG 18) is somewhat visible in the contours.
5. Elliptical nebula, fairly uniform, medium brightness; bright patches on N side, with dark matter. The radio contours suggest an extension to the NNW over about 3/4 degree. Dark matter may indeed obscure this part of the nebula.

6, 7. Nonthermal sources.

8. Circular nebula with elephant trunk structure, medium brightness. No observations were made of the faint extensions to the N or of IC 405, which is 1°.7 NW of IC 410.

9, 11, 13, 14, 15. Contour map in Figure 10c.

10. HADDOCK *et al.* (1954) and MILLS *et al.* (1956) find $\varphi_r = 0°.25$. This would have given $W_r = 0°.62$ with our antenna. Slow sweeps in α and δ gave $W_r = 0°.58 \pm °.02$, which is not compatible with the above value. The optical diameter of the brightest part, $\varphi_o = 0°.17$, gives $W_r = 0°.59$. We therefore used the optical value of φ_o in the computations. The average value of E, generally quoted, is 100×10^3. Our value is in between this and 8000×10^3, the value in the centre. MILLS *et al.* (1956) find a mass of 20 $M_\odot$.
11. Very faint nebulosity, diameter 0°.08, at 0°.04 S of BD + 23°982, has dark lanes across it. Radio source is 0°.8 W of this nebula, but may also be zero-line error.
12. Bright nebula, 0°.25 ENE of ζ Ori. Dark band across it. S boundary is formed by right-angled cloud containing horsehead.
13. Concentrated, symmetrical nebula, medium brightness. No Palomar Schmidt plate available for comparison.
14. Nonthermal source. Our position is 0°.15 further E than that found by BALDWIN and DEWHIRST (1954) at 81.5 Mc/s. It is not in the centre of the nebula, as theirs is, but displaced towards the bright arc. Possibly the arc is the main source of thermal emission, while the nonthermal radiation originates in the entire source. The relatively stronger intensity of the thermal radiation at our high frequency would then explain the displacement.

Table 6

Positions, intensities, physical data and identification of discrete sources

	Observed position										Size and			
1	2		3		4		5		6		7	8	9	10
No	α	δ	α	δ	α	δ	α	δ	l	b	W_r	W_o	g_r	g_o
	1957		est. m.e.		1950		1900							
1	00.17°	+67.00°	±.15°	±.08°	00h 00.3m	+66° 58′	23h 57.8m	+66° 41′	85.83°	+ 5.02°	2° × 2°	2.3°	2 i	
												0.5	1	
2	10.09	+41.04	—	—	00 40	+41 00	00 37.3	+40 43	89.43	−21.27				
3	35.80	+61.87	.05	.05	02 22.7	+61 51	02 18.8	+61 37	101.47	+ 1.82	P?	0.3		1.3
4	37.50	+61.25	.4	.2	02 29.5	+61 13	02 25.6	+61 00	102.5	+ 1.6	1.2 × 1.5	1.5	1.5 i	
5	41.9	+60.2	.4	.2	02 47.0	+60 10	02 43.2	+59 58	104.8	+ 1.6	1.7 × 1.6	1.7 × 0.7	4 i	
6	49.24	+41.34	—	—	03 16.5	+41 19	03 13.2	+41 08	118.54	−12.30	P		1	
7	68.57	+29.54	.07	.10	04 33.8	+29 32	04 30.7	+29 26	138.43	−10.40	P		1	
8	79.97	+33.34	.10	.10	05 19.4	+33 20	05 16.1	+33 17	141.31	− 0.37	0.8 × 0.8	0.35	2	(1.4)
9	82.99	+21.99	—	—	05 31.5	+21 59	05 28.5	+21 57	152.29	− 4.35	P		1	
10	83.30	− 5.44	.03	.03	05 32.8	− 5 27	05 30.4	− 5 29	176.66	−17.92	P?	0.17		1.1
11	83.4	+23.2	.3	.10	05 33.2	+23 12	05 30.1	+23 10	151.46	− 3.38	2 × 0.4	0.08?		1
12	84.7	− 1.9	.10	.10	05 38.4	− 1 54	05 35.9	− 1 56	174.07	−15.04	P?	0.35		1.4
13	91.60	+20.50	.10	.10	06 06.0	+20 30	06 03.0	+20 30	157.65	+ 1.82	0.7 × 0.8	0.5	(1.8)	1.8
14	93.64	+22.57	.05	.05	06 14.1	+22 34	06 11.1	+22 35	156.74	+ 4.46	0.7 × 0.9	0.8	2	(3)
15	96.8	+19.9	.2	.10	06 26.8	+19 54	06 23.8	+19 56	160.5	+ 5.8	?			
16	97.42	+ 4.94	.05	.05	06 29.3	+ 4 57	06 26.6	+ 4 59	174.04	− 0.60	1.4 × 1.6	1.33	4 i	
17	186.76	+ 2.32	.10	.10	12 26.7	+ 2 22	12 24.1	+ 2 38	260.80	+64.34	P		1	
18	187.16	+12.63	—	—	12 28.3	+12 40	12 25.8	+12 57	256.85	+74.57	P		1	
19	194.5	+28.3	—	—	12 57.7	+28 20	12 55.1	+28 37	11.2	+86.6				
20	252.28	+ 5.07	.05	.05	16 48.8	+05 05	16 46.3	+ 5 10	350.73	+27.44	P		1	
21	260.40	− 0.96	.10	.10	17 21.2	+00 57	17 18.6	− 0 54	349.30	+17.43	P		1	
22	260.68	−34.29	.05	.05	17 22.2	−34 17	17 18.9	−34 14	320.85	− 0.65	0.6 × 0.6	1.1 × 0.7	1.45 i	
												0.4	1	
23	262.8	−32.7	.2	.2	17 30.8	−32 42	17 27.5	−32 40	323.16	− 1.26	1.5 × 1.5	2		6
24	265.79	−28.94	.03	.03	17 42.7	−28 56	17 39.5	−28 55	327.71	− 1.47	0.83 × 0.64		3.2 i	
													1.43	
25	266.8	−31.4	.5	.3	17 46.8	−31 24	17 43.5	−31 23	326.0	− 3.5		0.35		1.4
26	268	−11	—	—	17 52	−11	17 49	−11	345	+ 2				
	274	− 8			18 16	− 8	18 13	− 8	349	+ 6				
27	268.8	−31.6	1.0	.3	17 54.7	−31 36	17 51.5	−31 35	326.7	− 5.1	2 × 1		4?	
28	269.65	−23.37	.06	.05	17 58.2	−23 22	17 55.1	−23 22	334.26	− 1.64	0.68 × 0.94		2.0	
29	270.35	−24.36	.10	.07	18 01.0	−24 22	17 57.9	−24 22	333.72	− 2.68	0.67 × 0.68	1.0 × 0.6	1.4	
												0.21 × 0.15		1
30	270.75	−21.61	.08	.06	18 02.6	−21 37	17 59.6	−21 37	336.30	− 1.66	0.8 × 1.0	(2 × 0.5)	2.5	
31	271.60	−20.18	.1	.08	18 06.0	−20 11	18 03.0	−20 11	337.93	− 1.66	P		1	
32	271.7	−23.9	.5	.5	18 06.4	−23 54	18 03.3	−23 55	334.7	− 3.5		0.28 × 0.45		1.3
33	272.7	−18	—	—	18 10.4	−18 00	18 07.2	−18 00	340.3	− 1.6	2 × 0.8	1.0		3
	273.7	−16.4			18 14.4	−16 24	18 11.2	−16 25	342.3	− 1.6				
34	273.8	−19.7	.2	.2	18 14.8	−19 42	18 11.8	−19 43	339.34	− 3.25		0.2		1
35	273.84	−11.92	.08	.1	18 15.0	−11 55	18 12.2	−11 56	346.21	+ 0.44	0.8 × 0.8	0.75 × 0.45	(2.4 i)	2
36	274	−23	—	—	18 16	−23	18 12	−23	336	− 4				
	277	−18.5			18 28	−18 30	18 25	−18 30	341.5	− 7				
37	274.17	−13.75	.05	.05	18 16.3	−13 45	18 13.4	−13 46	344.76	− 0.72	0.62 × 0.80	0.47 × 0.37	1.5	(1.5)
38	274.55	−16.15	.06	.05	18 17.8	−16 09	18 14.9	−16 11	342.81	− 2.19	P?	0.4 × 0.5	1.5 i	
												0.07 × 0.1		1
39	275.95	−12.66	.15	.2	18 23.4	−12 40	18 20.6	−12 41	346.54	− 1.73	0.8 × 0.9		2.2	
40	277.5	− 2.2	.1	.2	18 29.6	−02 12	18 27.0	−02 14	356.50	+ 1.81	P	0.3	(1)	1.3

TABLE 6 (*continued*)

Intensity			Physical data						Identification			
11	12	13	14	15	16	17	18	19	20	21	22	23
No	I	10^{26} S	φ_r	φ_o	10^{-3} E	r	n	$M/M_\odot$	NGC/IC	E	SG	Remarks
	units	Watt/m²(c/s)			cm⁻⁶pc	pc	cm⁻³		No	No	No	
1	19 ±2	160		2.3°	1	2500?	3?	66000?	(NGC 7822)		285	Total
	10 ±3	40		0.5	6	2500?	17?	3300?			286	Central part
2	<4				—				NGC 224			Andromeda nebula, not visible
3	30 ±4	170		0.3	72	2000	85	1850	IC 1795	136	15	
4	14 ±4	90		1.5	2	2000	5	15000	IC 1805	136	16	
5	7 ±3	120		1.1	4	2000	10	10800	IC 1848		25	
6	5 ±1	22			—				NGC 1275			I.A.U. 03N4A
7	18 ±2	77			—							I.A.U. 04N3A
8	9 ±2	77		0.35	24	2000	45	1540	IC 410		55	
9	261 ±2	1120			—				NGC 1952			Tau A, Crab nebula,
												I.A.U. 05N2A
10	111 ±2	520		0.17	660	500	700	43	NGC 1976		66	Orion nebula, I.A.U. 05S0A
11	7 ±3	30		0.08	180?							Probably o-line error
12	16 ±2	95		0.35	30	500	100	55	NGC 2024		(80)	Part of IC 434, E of ζ Ori
13	9 ±2	70		0.5	11	1700	27	1700	NGC 2175		87	
14	25 ±2	215			—				IC 443		95	I.A.U. 06N2A
15	5 ±2				?							Probably o-line error
16	15 ±2	260		1.33	6	1400	13	8600	NGC 2244		97	Rosette nebula
17	15 ±2	65			?							
18	59 ±1	254			—				NGC 4486			Vir A, M 87, I.A.U. 12N1A
19	<4				—							Coma Cluster, not visible
20	17 ±3	73			—							I.A.U. 16N0A
21	15 ±3	65			—							
22	113 ±4	700		0.86	35	1000	50	3200	NGC 6357	8	120	Total } (G 66)
	113	480	0.38	(0.4)	120	1000	140	780				Central part }
23	10 ±5	260		2	2	800	10	4000	NGC 6383	11	121	(G 67)
24	265 ±5	3650										Total } I.A.U. 17S2A,
	215	1300	0.37		360	8200	85	2.5×10^5				Central part } Sgr A
25	4 ±2	24		0.35	8	1000	35	150		17		(G 69)
26	10 max				—							Extended region
												("Flare"?)
27	8 ±3	140			?							Possibly o-line error
28	42 ±4	360			—				(NGC 6514)	21?	124?	Nonthermal + M 20, (G 74a?)
29	43 ±3	260		0.8	15	1200	32	2750	NGC 6523	23	126	Total } (G 72), M 8,
	43	185		0.17	235	1200	270	230				Central part } Lagoon nebula
30	22 ±3	240	0.48		20					(24)	(129)	Identif. uncertain, (G 77a)
31	16 ±3	70			?							
32	4 ±2	22		0.36	6	1200	30	240	NGC 6559	27	130	Uncertain, (G 75)
33	15 ±5	190		1.0	7	1700	16	7900	IC 4701	35	137	Ridge, of which IC 4701
												is part, (G 79)
34	5 ±2	22		0.2	20	1800	59	275	IC 1284	39	140	(G 78)
35	30 ±5	260	0.57	(0.58)	30	1400	46	2500	NGC 6604	41	141	(G 84)
36	9 ±3				?							Extended region
37	40 ±3	260	0.41	(0.41)	60	2000?	66?	3600?	NGC 6611	42	142	(G 83), M 16
38	165 ±10	1060		0.45	200	1700	125	5600	NGC 6618	43	145	Total } I.A.U. 18S1A, M 17,
	165	710		0.08	4000	1700	1230	370				Centr. part } Ω nebula, (G 81)
39	12 ±3	110	0.63		10?					(45)	(147)	Identif. probably incorrect
40	9 ±2	50		0.3	20						152	

TABLE 6 (*continued*)

1	2		3		4		5		6		7	8	9	10
	Observed position										Size and			
No	α	δ	α	δ	α	δ	α	δ	l	b	W_r	W_o	g_r	g_o
	1957		est. m.e.		1950		1900							
	°	°	°	°	h m	° ′	h m	° ′	°	°				
41	278.04	− 8.81	±.1	±.1	18 31.8	−08 49	18 29.0	−08 51	350.90	− 1.75	P		1	
42	278.50	− 7.49	.1	.1	18 33.6	−07 30	18 30.9	−07 32	352.28	− 1.54	P	0.3°	(1)	1.3
43	281.45	− 2.03	.07	.07	18 45.4	−02 02	18 42.8	−02 05	358.48	− 1.60	0.6° × 0.7°		1.3	
44	283.49	+ 1.28	.03	.05	18 53.6	+01 16	18 51.1	+01 13	2.36	− 1.88	P		1	
45	283.5	+ 7.8	.3	.2	18 53.7	+07 47	18 51.2	+07 44	8.11	+ 1.16	2 × 0.8			
46	284.0	+ 9.36	.15	.1	18 55.7	+09 21	18 53.3	+09 17	9.75	+ 1.44	1.5 × 0.7		3	
47	284.59	+ 4.16	.1	.07	18 58.0	+04 09	18 55.6	+04 05	5.43	− 1.50	P		1	
48	285.05	+ 1.25	.1	.7	18 59.8	+01 14	18 57.3	+01 10	3.06	− 3.27	P		1	
49	287.14	+ 9.05	.07	.05	19 08.2	+09 02	19 05.8	+08 58	10.94	− 1.44	P		1	
50	287.50	+ 5.1	.15	.3	19 09.6	+05 05	19 07.2	+05 00	7.63	− 3.62	0.8 × 0.8		2	
51	290.29	+14.14	.04	.07	19 20.8	+14 08	19 18.5	+14 02	16.89	− 1.72	0.8 × 0.9	(0.6)	2.3	(2.1)
52	292.0	+18.4	.2	.2	19 27.7	+18 23	19 25.5	+18 17	21.42	− 1.03	1.4 × 1.4			
53	293.4	+14.5	.2	.05	19 33.3	+14 29	19 31.0	+14 22	18.69	− 4.14	1.5 × 0.6			
54	295.0	+26.9	.5	.3	19 39.7	+26 53	19 37.7	+26 46	30.1	+ 0.9	3 × 0.6			
55	295.1	+23.1	.3	.3	19 40.1	+23 05	19 38.0	+22 58	26.93	− 1.18	1.0 × 1.0	0.30 × 0.45		1.4
56	298.1	+32.8	.3	.2	19 52.1	+32 47	19 50.2	+32 39	36.6	+ 1.7	1.0 × 0.8		2.5	
57	299.50	+40.61	—	—	19 57.8	+40 35	19 56.0	+40 28	43.78	+ 4.91	P		1	
58	300.1	+33.4	.3	.2	20 00.1	+33 23	19 58.2	+33 14	38.0	+ 0.6	1.0 × 0.8		2.5	
59	301.4	+34.0	.5	.2	20 05.3	+33 59	20 03.4	+33 50	39.1	0.0	2 × 0.6	1.8 × 0.4	(2.9)	3.3
60	301.5	+38.0	1.0	.2	20 05.8	+37 59	20 03.9	+37 50	42.4	+ 2.2		0.3 × 0.2		1.2
61	303.8	+43.5	.2	.3	20 15.0	+43 29	20 13.3	+43 19	48.0	+ 3.9	1.5 × 1	0.25 × 0.35	(2.5)	1.3
62	304.0	+41.8	.1	.2	20 15.8	+41 47	20 14.0	+41 37	46.67	+ 2.78	P?	0.35 × 0.45		1.5
63	304.4	+45.4	.2	.3	20 17.4	+45 23	20 15.8	+45 13	49.7	+ 4.6	1.5 × 1.5		4	
64	304.5	+36.9	.5	.3	20 17.7	+36 53	20 15.9	+36 43	42.9	− 0.4	2.5 × 1.5	0.2		1.1
65	304.8	+39.2	.2	.1	20 19.0	+39 11	20 17.1	+39 01	44.91	+ 0.77	0.8 × 0.6	0.65 × 0.50	1.5	(2)
66	305.26	+40.23	.05	.05	20 20.8	+40 13	20 19.0	+40 03	45.95	+ 1.09	1.2 × 1.0		3.7	
67	306.45	+39.9	.2	.1	20 25.6	+39 53	20 23.7	+39 43	46.23	+ 0.16	P?	0.9		2
68	306.5	+39.6	—	—	20 26	+39 35	20 24	+39 25	46.0	0.0				
	307.0	+41.0			20 28	+41 00	20 26	+40 50	47.4	+ 0.5				
	306.0	+42.5			20 24	+42 30	20 22	+42 20	48.1	+ 2.0				
69	307.54	+38.96	.07	.05	20 29.9	+38 56	20 28.0	+38 46	46.00	− 1.07	1.2 × 0.7		2.6	
70	307.67	+43.88	.07	.08	20 30.4	+43 52	20 28.7	+43 41	49.94	+ 1.87	0.8 × 0.7	0.6 × 0.6	1.6	(2.1)
71	308.4	+46.9	.1	.1	20 33.4	+46 52	20 31.8	+46 42	52.63	+ 3.31	1.0 × 0.9	0.7	2.8	(2.5)
72	308.5	+42.5	.1	.2	20 33.8	+42 28	20 32.0	+42 18	49.22	+ 0.54	0.8 × 0.7		1.7	
73	308.59	+41.2	.06	.3	20 34.1	+41 10	20 32.4	+41 00	48.26	− 0.34	0.8 × 1.5		3.7	
74	308.8	+38.7	—	—	20 34.9	+38 40	20 33.2	+38 30	46.4	− 2.0	6 × 1.5			
	307.8	+44.7			20 30.9	+44 40	20 29.3	+44 30	50.6	+ 2.3				
75	309.72	+41.97	.05	.05	20 38.6	+41 57	20 36.8	+41 46	49.38	− 0.49	1.0 × 0.8		2.5	
76	310.5	+39.1	.3	.2	20 41.7	+39 04	20 39.9	+38 53	47.5	− 2.8	P?	0.25 × 0.40		1.3
77	311.1	+40.9	.2	.1	20 44.2	+40 52	20 42.3	+40 41	49.21	− 1.98	P?	0.55 × 0.40		1.7
78	311.6	+30.5	.5	.3	20 46.1	+30 28	20 44.0	+30 17	41.5	− 9.0	1.5 × 1.5		4	
79	312.0	+41.7	.2	.1	20 47.8	+41 40	20 45.9	+41 29	50.27	− 1.97	P?	0.2	1	
80	313.4	+43.9	.1	.1	20 53.4	+43 52	20 51.6	+43 40	52.6	− 1.3	2.5 × 2.5	2.5	8.5 *i*	
81	350.38	+58.57	—	—	23 21.2	+58 32	23 18.9	+58 15	79.50	− 2.09	P		1	
82	6	7	—	—								0.508		1.30

TABLE 6 (*continued*)

Intensity			Physical data						Identification			
11	12	13	14	15	16	17	18	19	20	21	22	23
No	I	10^{26} S	φ_r	φ_o	10^{-3} E	r	n	$M/M_{\odot}$	NGC/IC	E	SG	Remarks
	units	Watt/m²(c/s)			cm⁻⁶pc	pc	cm⁻³		No	No	No	
41	18 ±4	75			(—)							
42	9 ±3	50		0°.3	20					(53)	(155)	Identif. uncertain
43	59 ±5	330	0°.3		125?					(56)	(158)	Identif. probably incorrect
44	44 ±4	190			—							
45	5 ±3				?					(58)		Ext. region. Identif. probably incorrect
46	8 ±2	105	0.85		5?							
47	10 ±3	45			?							
48	9 ±2	40			?							
49	17 ±3	75			?							
50	5 ±2	45	0.57		5?							
51	72 ±3	710	0.63		67?					(63)		Identif. probably incorrect
52	7 ±3				?							Uncertain maximum
53	4 ±2				?							Possibly o-line error
54	6 ±3				?							Uncertain maximum
55	4 ±2	25		0.36	7	1800	25	700	NGC 6823	65	166	
56	8 ±2	85			?							
57	442 ±2	1900			—							Cyg A, I.A.U. 19N4A
58	8 ±2	85	0.7		7						176	
59	6 ±2	85		0.85	4						177	
60	5 ±3	25		0.24	16	1500	55	250	NGC 6888	76	185	
61	5 ±2	30		0.3	12	1500?	40?	360?			191	
62	8 ±2	50		0.4	12	1500?	35?	770?	IC 1318a		193	
63	6 ±2	100	1.4		2	1500?	7?	7000?				
64	5 ±2	25		0.2	22	1500?	68?	180?		77	197	
65	7 ±3	45	0.4		11	900?	42?	200?			196	
66	37 ±5	590	0.94		25	6000?	16?	3×10^5?				Brightest component of Cyg X
67	20 ±5	170		0.9	8	900?	24?	1300?	IC 1318b	78	201	
68	17 max				?							Ridge
69	17 ±3	190	0.7		15						204	Identif. uncertain
70	16 ±3	110	0.5		18	1500?	39?	1500?		79	207	
71	7 ±2	85	0.76		6					82	215	
72	14 ±3	100	0.5		16							
73	15 ±4	240	0.94		10	1500?	21?	6000?				
74	10 ±6				?							Ridge
75	25 ±5	270	0.7		20	1500?	35?	3900?		(83)	(218)	Identif. uncertain
76	5 ±2	30		0.32	11					84	220	
77	4 ±2	30		0.47	5	900	26	200		85		
78	5 ±1	90	1.4		2	400?	14?	240?	(NGC 6990)		224	Part of Network nebula
79	5 ±2	20		0.2	21	900	84	50				
80	15 ±3	550	(2.5)	2.5	3	900	9	11000	NGC 7000 IC 5068 IC 5070	86	234 223 229	North America and Pelican nebulae
81	721 ±2	3100			—							Cas A, I.A.U. 23N5A
82	179 ±3	1000										Moon, age $16^{d}.7$; $T_{disk} = 270$ °K

15. No Palomar Schmidt plate available.
16. A bright ring-like nebula, described in detail by MINKOWSKI (1949, 1955). He gives $\varphi_o = 1^\circ.33$ and $n = 13.5$ cm^{-3}, in excellent agreement with our data, in which a homogeneous brightness is assumed. A ring would give larger n and smaller M. Contours in Figure 10b.
17. No Palomar Schmidt plate available.
19. A search for the Coma cluster of galaxies had negative results.
20. Nonthermal source.
21. Nonthermal source, 2C 1473 (SHAKESHAFT *et al.* 1955), Oph C (KRAUS *et al.* 1954).
22. Irregular nebula, divided into many parts by dark bands. Situated in heavily obscured region. Radio nebula far brighter than No 29 (M 8) but much less bright optically. Optical diameter of brightest parts is equal to radio diameter. The extension of the radio source towards the east corresponds with the optical extension. MILLS *et al.* (1956) observe the source in absorption. They find $T_e = 6700$ °K, $n = 37$ cm^{-3} and $M/M_\odot = 1500$. Our values, when reduced to $T_e = 6700$ °K, are $E = 29 \times 10^3$, $n = 45$ and $M/M_\odot = 2900$ for the total nebula, and $E = 100 \times 10^3$, $n = 127$ and $M/M_\odot = 710$ for the central part, in reasonable agreement with theirs.
23. A large ring-like nebula, rather irregular structure. On top of the galactic ridge, difficult to separate from the background. I and W_r very uncertain.
24. Believed to be galactic nucleus. Several small, faint, heavily obscured emission regions within the contours, probably foreground nebulae. Detailed discussion in Chapter 7f.
25. Rather bright emission region of roughly circular shape, visible as a bulge in contour 3.
26. Clearly the base of the "flare" at right-angles to the galactic plane, observed at low frequencies.
28. A ring quadrant of 0°.12 radius, very faint, just N of E 21, is exactly at the position of the source. Contours seem to be extended towards M 20, which is 0°.4 NE. Erroneously identified with M 20 by various authors. The faint ring would have to be a nonthermal emitter, since the spectrum is between that of a thermal and an average nonthermal source. High-frequency observations with a beam much narrower than ours are needed to separate the nonthermal source from M 20. Additional evidence for the existence of two sources comes from the positions:

M 20, $l = 334^\circ.73$, $b = -1^\circ.71$,

Our position (1390 Mc/s), $l = 334^\circ.26$, $b = -1^\circ.64$,

MILLS *et al.* (1958) (85 Mc/s), $l = 334^\circ.15$, $b = -1^\circ.48$.

At MILLS' low frequency, the nonthermal source is the major component, at our frequency the intensity of the nonthermal source and M 20 are comparable, resulting in a shift of the position towards M 20.

HADDOCK *et al.* (1954) find a rather low flux density, $S = 110$. They may have looked specifically at M 20, in which case we would have $E = 245 \times 10^3$, $n = 290$ cm^{-3}, $M = 170$ $M_\odot$, taking $\varphi_o = 0^\circ.13$. The width of the combined source, perpendicular to the line connecting the two sources, is well in excess of that of a point source; reason to believe that the nonthermal source is extended, with $\varphi_r = 0^\circ.35$.

29. A very bright, well-known nebula, irregular. The extent of the contours towards the E is due to faint extensions. In the computation for the total nebula the faint extensions were included in φ_o.
30. Elongated strip of faint emission (2° × 0°.5) with centre close to source position. Identification very unlikely: source seems too small, and elongated in direction perpendicular to nebulosity.
31. Highly obscured region, with some very faint emission.
32. Slight widening of contours 2 and 3. Possibly due to irregular patch of nebulosity, associated with M 8. Medium brightness, with bright patches.
33. Intense ridge, connected to the contours of No 38 (Omega nebula), probably caused by IC 4701, which is a roundish, irregular nebula of medium brightness.

Southern part of ridge runs into obscured region. Some emission at S end.

34. Slight widening of contours 2 and 3. Elliptical nebula, medium brightness, embedded in very conspicuous right-angled dark cloud. Some faint emission around it. See No. 36.
35. Irregular nebula, medium brightness. Main part contained in contour 6, but faint extensions over about 1°.5 to the E and SE, forming the ridge in the contour between this source and No. 37. In the N half of the empty region within contour 4, also much faint emission, which does not show in the contours.
36. At SW part of this region, around $\alpha = 274^\circ$, $\delta = -20^\circ$, a right-angled dark cloud; it forms the N boundary of a faint emission region (G 77b, E 32) which might well continue behind it. Nothing conspicuous in the rest of the region.
37. Bright irregular nebula, classic example of elephant-trunk structure. Contour 9 encloses the whole nebula, brightest part well within contour 10. Dark band over N half, which displaces optical centre to the S. Extension of contour 6 to the E does not show on the photographs.
38. Well-known very bright nebula, rather irregular,

associated dark matter. Brightest part on 200″ photograph only 0°.03 W of source position, very small. Low-intensity contours somewhat widened, due to extensions of medium brightness (φ_o = 0°.4 × 0°.5). It is clear that IC 4706, 7 and NGC 6618 form one nebula, and are separated by a dark cloud. Highest values of *E* and *n* found in this survey, unreliable because of large optical depth.

39. No trace of emission, highly obscured region. E 45 is 0°.7 S.

40. Irregular nebula, medium brightness, in centre of dark cloud; some filamentary structure. The extension of contour 1 in this region corresponds to the Ophiuchus dark clouds.

41. No trace of emission at this position, or at the position of the maxima N and S. Some obscuration and a few very dark patches. At 85 Mc/s (MILLS *et al.* 1958) the source has a two to four times higher flux density; thus it is probably nonthermal.

42. Faint irregular emission region, with some structure, 0°.2 N of the source. SHARPLESS' position for E 53 is erroneous. It should be $\alpha = 18^h29^m.2$, $\delta = -7°43'$ (BD epoch).

43. Darkest parts of a dark foreground cloud, in which some faint emission patches. E 56 = SG 158 is 0°.5 W.

44. Nonthermal source. Very dark region. 2C 1607 (SHAKESHAFT *et al.* 1957).

45. Some obscuration, and a few very faint emission patches, of which E 58 is the brightest.

46, 48. No trace of emission, hardly any obscuration.

47, 49. Highly obscured region.

50. No trace of emission, some obscuration.

51. A roughly circular, very faint emission region, irregular structure, in a highly darkened region. If the identification is correct, it must be very heavily obscured.

52. No trace of emission, some obscuration. The size of this source is very uncertain.

53. No trace of emission, no obscuration.

54. Size and position of this maximum are very uncertain. Some obscuration.

55. Emission nebula of medium brightness with bright central patch of diameter 0°.15. Faint extensions to diameter 0°.9; extension to the N over 2°.5, containing E 66 and 67, is visible in the contours.

56. No trace of emission, no obscuration.

58. Faint emission region with some bright bits of diameter 0°.06 and 0°.03. It extends about 0°.4 to the S, and to the N it connects up with the large emission regions at No. 59.

59. Streaks of faint emission, extended in the α-direction, similar to the extension of the source.

60. The bulge in contour 1 around this position is partly due to NGC 6888, partly to some faint emission near α = 300°.3, δ = 38°. The radio diameter of NGC 6888 cannot be determined; it is an elliptical nebula of medium brightness.

61, 62, 63, 70, 73, 75. All assumed to be further away than the Cygnus Rift, at the same distance as the association VI Cyg, i.e. at r = 1500 pc. It is equally well possible that many of these nebulae are at the distance of the N America nebula, i.e. between 700 and 900 pc. A very good picture of the distribution of the optical nebulae in the Cygnus region is given in the mosaic photograph, composed of Palomar Schmidt red plates, by STRUVE (1957).

61. Emission nebula with bright, S-shaped central part. The ridge between it and No 63 is clearly visible in the photographs and extends a bit further to the S, although it seems to have no connection with No 62.

62. Bright triangular nebula, rather sharp edges. Extension to S is visible in the contours.

63. Source is 0°.6 S of bright bit in the emission wisps N of the Cyg complex. Some emission at the source position, but very faint. No proper identification. Are these wisps connected with VI Cyg? (MORGAN *et al.* 1955).

64. Faint nebula, elephant trunks? Probably very strong obscuration.

65, 66, 67, 69, 72, 73, 75. These sources are all within the contours of Cyg X, as observed with low resolving power. Adding up our flux densities, and making an estimate of the flux density of the background underlying these sources, we find for the total flux density of Cyg X the value S = 4900. This is in excellent agreement with the mean flux density S = 4700, derived from low-resolution observations at 7 different frequencies by DAVIES (1957). It is clear from our observations and observations with a beamwidth of 0°.75 by F. D. DRAKE (*private communication*) that the radio source Cyg X is not a single extended source, but consists of a large number of separate thermal sources.

65. Medium-brightness region in the string of faint nebulosity extending from No 67 to the SW over 3°. Brightest parts 0°.4 W of source. Obscuration at the source position. Assumed to be at same distance as N America nebula.

66. Strongest source of Cygnus group. Position of Cyg X is mainly determined by this source and No 67. It is 0°.13 NE of γ Cyg. Strong obscuration and no sign of bright nebula. DRAKE (*private communication*) assumes association with IC 1318b and/or γ Cyg. This seems highly unlikely, since DAVIES (1957) observes 21-cm line absorption at the position of Cyg X, and places it in the Perseus arm, at r = 6000 pc. Since most of the

other components of Cyg X are probably at $r < 1500$ pc, we assume that the absorption is due to No 66. Davies concludes from a comparison of surveys at many frequencies that the whole of Cyg X must be thermal, and finds $n = 5 - 8$ cm^{-3}. Taking into account the uncertainties involved, this is in fair agreement with our $n = 16$ cm^{-3}.

67. Bright irregular nebula with band of dark matter across it. Radio position is in the middle of this dark band, showing that the N and S halves are part of one nebula. It is the well-known γ Cyg nebulosity. With No 66 the strongest part of Cyg X. Assumed to be at same distance as N America nebula.
68. Ridge, running N and then NW, starting at No 67. String of nebulosity, interrupted by dark matter just N of No 67.
69. Situated at the SW end of the Cygnus Rift; 0°.5 W is centre of faint emission patch, about 0°.4 diameter, which is highly obscured, in particular on the side near No 69. Very faint emission at source position.
70. Irregular emission nebula of medium brightness, S part obscured. NW extremities also visible in contours.
71. Irregular nebula, medium brightness, probably some obscuration.
72. In centre of Cygnus Rift. Some very faint emission. Top in ridge No 74.
73. In centre of Cygnus Rift. Some nebulosity 0°.5 S and W.
74. Ridge following the centre of the Cygnus Rift from S to N. Contains sources Nos 70, 72 and 73, and some nebulosity S of No 73. Might indicate the presence of ionized hydrogen inside, or just behind the Rift. Placing the ridge arbitrarily in the middle of the Rift at $r = 350$ pc and assuming a thickness $l = 50$ pc, we find $n = 10$ cm^{-3}. Taking into account the large uncertainties, we may place the value of n between 3 and 20 cm^{-3}.
75. Highly obscured nebulosity in centre of Cygnus Rift, about 0°.25 W of the source. Might very well extend to the position of the source. Only very faint emission there. Second brightest source of Cyg X, causes the elongation of Cyg X to the ENE. At bulge of contours to NE only dark cloud.
76. Faint, roughly circular nebula, at the edge of the Cygnus Rift, 0°.2 N of the source.
77. Faint irregular patch of nebulosity embedded in dark clouds. Forms, together with No 79, a S extension of the N America and Pelican nebulae, No 80.
78. In W part of Network nebula, near 52 Cyg. At position of source an irregular, faint, roughly circular emission patch, with many small patches around. It does not have filamentary structure and is brighter on red plates, unlike most of the Network nebula.

   Hanbury Brown and Walsh (1955), at 92.5 Mc/s, find a source more in the centre of the whole nebula. If this source is nonthermal, it would be far below our limit of sensitivity. Our source is probably a region of strong Hα-emission in an otherwise nonthermal source.
79. Brighter part of the faint ridge connecting No 77 with No 80.
80. The double maximum is probably due to a zero-line error. The position given is that of the brightest point. The centre of the whole source, which is rather flat, is approximately at $\alpha = 313°.5$, $\delta = 44°.2$ (1957). Contour 1 just about defines the boundary of the emission region formed by the N America nebula and Pelican nebula. Optical separation of these two is due to a dark band from S to N. Brightest part probably behind this band. The whole nebula is bright and irregular.
82. The Moon was observed on only one night, Sep 21.0, 1956, near full moon. The brightness temperature of the disk is $T_d = 270$ °K ± 60.

d. *Source statistics*

In this section we shall discuss why a number of sources have not been identified, and draw some conclusions regarding the physical parameters of all the sources.

Excluding the Andromeda nebula and the Coma cluster, which were below the limit of detection, and the moon, the extended regions Nos 26, 36 and 45 and the ridges 68 and 74, we have a total of 74 discrete sources. Of these, 11 have a nonthermal

Table 7

Thermal sources in various regions of the sky

l ($\lvert b \rvert < 5°$)	Identified	Identification uncertain	Unidentified	Total
320°–330°	3		1	4
330°–340°	2	1	1	4
340 –350	4	1		5
350 –360	1	2	1	4
0 – 10			4	4
10 – 20		1	1	2
20 – 30	1			1
30 – 40	2		1	3
40 – 50	9	2	4	15
Rest of sky	13		1	14
Total	35	7	14	56

spectrum. In the present investigation we wish to confine ourselves to thermal sources only, and therefore shall not discuss those which are nonthermal. Seven sources are probably zero-line errors or are uncertain maxima in the contours, so that 56 discrete sources may be classified as thermal. In Table 7 these are divided into three groups: identified, identification uncertain, and unidentified. They are arranged according to galactic longitude in the survey regions S, A and C.

The list of 42 well-established discrete sources between $l = 320°$ and $l = 50°$ in the neighbourhood of the galactic plane, contains 20 sources which are unidentified or have an uncertain identification. In Figure 11, their number in 10° intervals along the galactic equator is plotted versus longitude together with the number of identified sources. The relative emptiness of a large region around $l = 20°$ is well known, both from the optical data on emission nebulae and from the observations of the galactic background radiation at radio frequencies. Both the numbers of identified and unidentified sources have a minimum in this region. The large number of unidentified sources between $l = 350°$ and $l = 40°$ is very striking. It is clear from the 21-cm line investigations (SCHMIDT 1957, WESTERHOUT 1957) that the region between $l = 20°$ and $l = 35°$ is an empty region. It is situated between the Orion and the Sagittarius spiral arms, where scarcely any neutral hydrogen is present over about 6 kpc. Possibly the thermal radio sources found in this region are in the Orion arm beyond $r = 6$ kpc. In the region $l = 350°$ to $l = 20°$ the line of sight passes through high-density regions in the Sagittarius arm and the Orion arm between $r = 6$ and 14 kpc. Between $l = 5°$ and 15°, where the number of unidentified sources is relatively large, there is indeed a high-density region at $r = 9$ kpc. In the region between $l = 40°$ and 50° most of the unidentified sources are at the position of the wellknown Cygnus Rift. It may be concluded that the unidentified sources must all be situated behind dark clouds; in the region $l < 40°$ many are at great distances from the sun.

Many of the small nebulae found by SHAJN and GAZE, SHARPLESS and others were not found in the main survey of regions S, A, C and O; neither were any planetary nebulae. The radio brightness of all these objects is apparently below our limit of detection. For an extended region ($\varphi > 0°.5$) this limit is about $E = 2 \times 10^3$, while for a nebula with $\varphi > 0°.5$, the limit of detection is given by $E\varphi^2 = 850$. It must therefore be concluded that the unobserved diffuse nebulae, many of which have diameters of the order of 0°.5, have $E < 3 \times 10^3$. On or near the galactic ridge some nebulae with $E > 3 \times 10^3$ may have escaped attention.

The expression for the limit of detection may also be written as $n^2\varphi^3 r > 5 \times 10^4$. Excluding the giants, the average large-size planetary nebula has $\varphi = 0°.01$. All those with $n > 7 \times 10^3$ cm^{-3} at $r = 1000$ pc, or $n > 3.5 \times 10^3$ cm^{-3} at $r = 4000$ pc would therefore have been detected. The optical depth of a planetary nebula at these values of n, r and φ happens to be around unity, so that nebulae with higher densities have the same surface brightness and remain at the limit of detection. Since the electron density in planetary nebulae is estimated to be between 10^3 and 10^4 cm^{-3}, the large-size planetaries are just below our

FIGURE 11

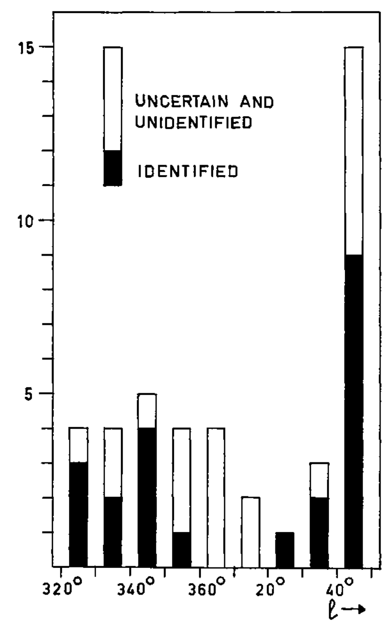

Number of sources, identified and unidentified or with uncertain identification, in 10-degree intervals in l.

limit of detection. None of the giant planetaries fall within the boundaries of our main survey. In the rapid survey for discrete sources, the limit is about a factor of 5 higher. It is safe to assume that all extended nebulae ($\varphi > 0°.5$) with $E > 10^4$ have been found; the giant planetary NGC 7293, which has $\varphi = 0°.25$, $r = 200$ pc, and which was not found, must have $n < 300$ cm^{-3}. Optical determinations of the average density over the whole nebula also give values well below 300 cm^{-3} (D. KOELBLOED, *private communication*).

In view of the scarcity of optical data on emission nebulae available at the present moment, we do not feel justified in making detailed comparisons of optical and radio measurements of physical parameters. New optical determinations of distances, emission measures, densities and masses are at present being made at various observatories. On the radio side, ours seems to be the most extensive list published so far. In a future comparison with optical observations, the low resolving power of the radio telescope, as compared to that of optical telescopes, will have to be taken into account. The most reliable method of comparing optical and radio observations is to smooth out the optical values of E over the gaussian antenna pattern (width at half-power points $0^\circ.57$) and from this smoothed-out value to compute the expected top intensity I at 1390 Mc/s. This value of I may then be compared with the observed radio value. In this way, all arbitrariness will be avoided in the assumptions of the diameter of a nebula, required for the computation of the radio value of E. Such a comparison of the optical and radio intensities will give a reasonable estimate of the total interstellar absorption in front of the nebula, including the dark clouds associated with the nebula.

A very rough comparison of the brightness of the individual nebulae with our value of E shows that a bright nebula has $E > 30 \times 10^3$, a nebula of medium brightness has $10 \times 10^3 < E < 30 \times 10^3$, and a faint nebula has $E < 10 \times 10^3$. Of the 51 nebulae for which E could be determined, 10 are in the first class, 20 in the second, and 21 in the third. Since the many nebulae which were not detected in our survey belong to the third class, we may conclude that the majority of emission nebulae have $E < 10 \times 10^3$. It is clear that only the brightest nebulae of this group were found. According to STRÖMGREN (1949) the average extended region optically detected has $E = 0.8 \times 10^3$, whilst the faintest extended emission region measured has $E = 0.4 \times 10^3$. It will be shown in Chapter 7d that the thermal part of the background radiation underlying the discrete sources is compatible with a model in which the radiation is due to a large number of such faint nebulae.

The average size of a nebula is a figure of considerable interest in a study of the distribution of ionized hydrogen throughout the Galactic System. Such a study is made in Chapter 7d. In Figure 12 the size $l = r\varphi/57.3$ of a nebula is plotted versus its density n; the values of r, φ and n are taken from Table 6. The line marked $r = 500$ denotes the limit of detection for small sources, with $\varphi < 0^\circ.5$ and $r > 500$ pc; the line marked $E = 2000$ denotes the limit of detection for extended sources with $\varphi > 0^\circ.5$. Values of n and l which are greater than 160 cm^{-3} and 40 pc, respectively, are indicated by arrows.

Two conclusions may be drawn from this figure:
a) Nebulae with $n > 40$ cm^{-3} have $l = 8$ pc ± 4.
b) Nebulae with $l > 20$ pc have $n < 20$ cm^{-3}.
As is well known, the diameter of an ionized hydrogen region is either the total size of the gas cloud, or is dependent on the gas density, the temperature and the radius of the exciting star. For an O5-star, the relation between the density and the diameter of the surrounding ionized region is $n^{2/3}\, l = 140$ (STRÖMGREN 1948). The relation $n^{2/3}\, l = 155$ fits the observed points with $l > 15$ pc very well. It is clear that, because of the proximity of the limit of detection, this is not an average value but an upper limit. Thus, for $l = 30$ pc, the density n is smaller than 12 cm^{-3}; the larger the nebula, the smaller the density. It follows that in the larger nebulae the number of exciting stars cannot be great. One O5-star or six B0-stars is about the maximum number. This observation may be of interest for the theory of stellar evolution. Apparently, groups of hot stars do not exist in large-size clouds of low density.

FIGURE 12

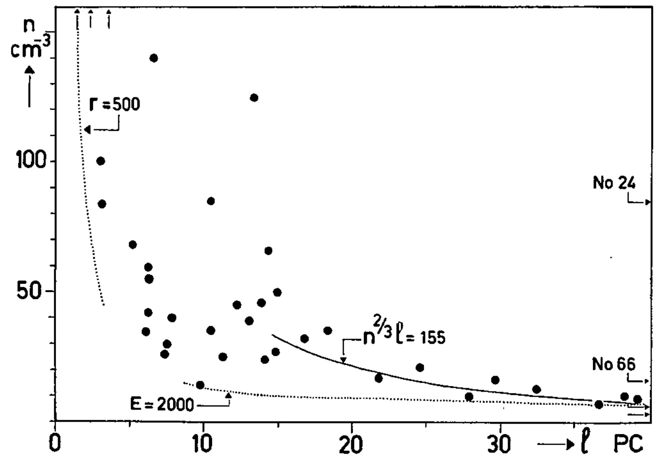

Density n of emission nebulae as a function of diameter l. Region to the left of and below the dotted lines is below the limit of detection.

The observed diameters of the denser nebulae do not surpass a value of 15 pc. It is likely, although not proven, that the less dense nebulae which are below the limit of detection, also have small diameters. The points in Figure 12 show a tendency to cluster at the low-density, small-diameter limits. About one half of the nebulae have densities below 50 and diameters below 15. The data on the high-density nebulae are very uncertain.

The masses given in Table 6 are even more uncertain than the densities. Very few mass determinations, based on optical observations, have yet been made. ALLER (1956) mentions masses of four nebulae, determined by BOGGESS, ranging from 120 to 1000 $M_\odot$. SHAJN and GAZE (1952) determined masses of emission nebulae in M 31 and M 33, ranging from 3×10^3 to 4×10^5 $M_\odot$ and masses of three galactic nebulae between 260 and 5800 $M_\odot$. They state that such massive nebulae are probably very rare, and that most nebulae will have masses well below 100 $M_\odot$.

Two thirds of the masses determined in the present investigation are greater than 1000 $M_{\odot}$. It is clear that objects of low mass can only be detected if the density, and hence the emission measure, is very high. The large proportion of massive nebulae may therefore be due to our limited sensitivity. It should be pointed out however, that owing to the low resolving power of the radio telescope, the faint outer parts of the nebulae are often included in the total intensity, and thus in the determination of the total mass. In optical determinations, usually only the mass of the bright central part is measured.

7. *Comparison with* MILLS' 85 *Mc/s survey*

a. *Thermal and nonthermal background radiation*

In this chapter we shall discuss the background radiation in the galactic ridge. Background radiation is defined as all the radiation which remains after subtraction of the observed discrete sources. It may be considered as the radiation from a continuous medium, or as the integrated radiation of many discrete sources, either thermal or nonthermal, over a solid angle considerably greater than that subtended by the antenna beam. The background radiation along the galactic ridge may be determined from a curve such as Figure 7, where the maximum intensity along the ridge is plotted versus galactic longitude. The discrete sources are subtracted by drawing the lower envelope of such a curve.

It was already evident from the early investigations by JANSKY that the intensity of the background radiation at low frequencies ($\nu < 30$ Mc/s) is far in excess of the intensity of the thermal radiation from ionized hydrogen. From later observations at high frequencies, as used in the present survey, it was clear that a large proportion of the high-frequency background intensity may be explained by thermal radiation. This was shown by computations based on optical observations of emission nebulae (e.g. WESTERHOUT and OORT 1951) and from a rough extrapolation of the low-frequency spectrum of the background radiation to high frequencies (e.g. HANBURY BROWN and HAZARD 1953). According to common usage, we shall call *nonthermal* the component which is strongest at low frequencies and which cannot be explained by a thermal emission mechanism. In this, we shall include the so-called isotropic component of the radiation, the origin of which is not clear, but which must have about the same spectrum as the rest of the nonthermal radiation.

Various attempts have been made to separate the thermal and nonthermal components of the background radiation, and in particular to derive a model of the distribution of the nonthermal sources.

This was relatively easy, because all attempts were based on observations at frequencies lower than 600 Mc/s, where the thermal component is only a small fraction of the total radiation. The intensity and absorption effects of the thermal radiation were derived from models of the distribution of the thermal component. WESTERHOUT and OORT (1951) were the first to suggest such a model.

Their analysis of the distribution of the nonthermal radiation, as were the analyses by BOLTON and WESTFOLD (1951) and BALDWIN (1955), was based on surveys with very wide beams (halfwidths of 17°, 17° and 2° × 15° respectively). It could not, therefore, give any definite conclusion regarding the distribution in the neighbourhood of the galactic plane. In fact, MILLS' (1958) results show that this distribution is completely different from that suggested by those surveys. The most comprehensive work was that of HANBURY BROWN and HAZARD (1953), who used the WESTERHOUT and OORT model for the thermal radiation, a number of low-frequency surveys and a few observations at 1200 and 3000 Mc/s to derive the distribution of the nonthermal radiation. Their analysis was based mainly on REBER's (1948) survey at 480 Mc/s, made with a 4°.5 beam, and on the above-mentioned model. The data were chosen so as to fit the observations with wide beams at the lower frequencies as well as possible. The results come very close to those obtained hereafter.

An estimate of the percentage of thermal radiation at 85 Mc/s was made by MILLS (1955). He compared intensities in the neighbourhood of the galactic centre in a rather crude measurement by PIDDINGTON and MINNETT (1951) at 1200 Mc/s, in a survey by MCGEE *et al.* (1955) at 400 Mc/s, which was later shown (PIDDINGTON and TRENT 1956) to have a wrong absolute intensity scale, and in his own 85 Mc/s results, which also had a wrong intensity scale (MILLS *et al.* 1958). As is shown in section f, the centre region is rather complicated and cannot be used as a reference region. This estimate therefore was of little value. PIDDINGTON and TRENT (1956) compared observations of the intensity at $\delta = -25°.5$ on the galactic ridge at 242, 400 and 600 Mc/s and concluded that at those frequencies the greater part of the radiation, or at any rate 50%, is thermal in origin. The intensity scales of both the 400 and the 600 Mc/s survey are too uncertain, however, to warrant this conclusion, in particular since the frequency range is rather small.

Recently, MILLS *et al.* (1958) made a survey at a frequency of 85 Mc/s with a beamwidth of 0°.9 at half-power. His resolving power is far greater than that so far attained at the low frequencies, and is comparable to ours. Since at his frequency the major

1958BAN....14..215W

component of the radiation is nonthermal, while at ours a large part must be thermal in origin, a comparison of his survey and ours may provide a reliable separation of the two components. The present survey is the first fairly complete one at a high frequency. No attempts have yet been made to find the intensity and the distribution of the thermal component from observational data. Our prime aim in this chapter is to obtain an estimate of this from our data, in conjunction with MILLS'.

We assume that the sources of thermal and nonthermal radiation are well mixed in the neighbourhood of the galactic plane.

The equation of transfer along the line of sight is

$$\frac{dI}{d\tau} = -I(\tau) + B(T) + \frac{j_n(\tau)}{\varkappa}, \qquad (24)$$

where $d\tau = \varkappa ds$ and $\varkappa$ is the absorption coefficient per unit length through the ionized hydrogen, given in (10). We have assumed that the nonthermal mechanism cannot give any absorption; thus, the optical depth τ depends only on the thermal component. $B(T)$ is the Rayleigh-Jeans brightness,

$$B(T) = \frac{2\nu^2}{c^2} kT, \qquad (25)$$

with $T = T(\tau) = T_e$, the electron temperature of the ionized gas, while $j_n(\tau)$ is the emissivity per unit volume of nonthermal radiation (index n). All these quantities vary with the distance $s = \int \frac{d\tau}{\varkappa}$. Equation (24) has the integral

$$I(\tau) = \int_0^\tau B(T)\, e^{-\tau} d\tau + \int_0^\tau \frac{j_n(\tau)}{\varkappa} e^{-\tau} d\tau. \qquad (26)$$

The second term at the right-hand side may also be written $\int_0^s j_n(\tau) e^{-\tau} ds$. It represents the nonthermal component of the total radiation. In the absence of absorption the total nonthermal radiation intensity along the line of sight would be $J = \int j_n\, ds$. HANBURY BROWN and HAZARD (1953) derived a similar equation for a mixture of hydrogen clouds and nonthermal discrete sources. Their equation (4) (appendix) reduces to our equation (26) if the optical depth of one cloud is $\ll 1$. For a medium where $T(\tau)$ and $j(\tau)$ are constant, i.e. where the electron temperature T_e of the ionized gas is everywhere constant, and the density distribution of the gas and of the sources of nonthermal radiation has the same form, (26) becomes

$$I(\tau) = [B(T_e) + J/\tau]\,(1 - e^{-\tau}), \qquad (27)$$

or, converting intensities into brightness temperatures,

$$T_b = (T_e + T_n/\tau)\,(1 - e^{-\tau}). \qquad (28)$$

Here, T_b is the total brightness temperature observed in a certain direction, T_n is the brightness temperature of the nonthermal radiation in the absence of absorption, and τ is the total optical depth of the ionized gas.

It may be shown that this formula is still approximately correct if the sources of thermal and nonthermal radiation do not have the same distribution, as long as it does not differ too much from a smooth one (factors of 5 in density along the line of sight being allowable) and τ does not surpass 0.5.

For $\tau \ll 1$, (28) reduces to

$$T_b = \tau . T_e + T_n, \qquad (29)$$

which holds for any distribution.

At 1390 Mc/s the observed brightness temperature may be represented by (29), at 85 Mc/s by (28). To separate the thermal and nonthermal radiation components with the aid of the observations at these two frequencies, we have to solve in any direction four unknowns from the two equations, namely the optical depths and the nonthermal brightness temperatures at 85 and 1390 Mc/s.

To solve these unknowns, we therefore require two further equations. These are found in the ratios of τ and T_n, respectively, at the two frequencies, i.e., in the spectrum of the two components. The problem is then reduced to the solution of two unknowns, τ and T_n at one frequency. The variation of τ with frequency is well known. It is given with sufficient accuracy by $\tau \propto \nu^{-2}$ (see equation (13)). In the next section we shall try to find the variation of T_n with frequency.

b. *The spectrum of the nonthermal radiation*

When consulting the literature of the last few years one finds that many authors have tried to determine the spectrum of the nonthermal radiation by comparing observations made with different equipment at different frequencies. Various authors find a different spectrum from the same data, depending on the corrections for beamwidth, intensity scale and zero level which they applied to surveys by others.

We define the spectral index α as the index in the relation $T_b \propto \nu^{-\alpha}$. Most authors have assumed that α is constant for $\nu > 20$ Mc/s; in view of the large uncertainties existing in the various surveys this

TABLE 8

Values of the spectral index α, derived by various authors

Region	Components	Frequency range	Beam	α	Weight	Author
Whole sky	i, n, t	25; 110 Mc/s	90°	2.41	2	HERBSTREIT and JOHLER (1948)
$l = 330°, b = -2°$	n, t	60-1000	2.8-40	2.51	2	PIDDINGTON (1951)
$l = 180°, b = 0°$	n	60-1000	2.8-40	2.73*	2	
$l = 200°, b = -30°$	i	60-1000	2.8-40	3.08*	1	
Galactic centre	n, t	18.3-1200	2.8-40	2.8	4	HANBURY BROWN and HAZARD (1953)
Coldest parts of sky	i	18.3-1200	2.8-40	2.5*	2	
$l = 210°, b = -90°/+30°$	i, n	18.3; 100	17	2.84*	2	SHAIN (1954)
$l = 310°, b = -20°, +40°$	i, n	18.3; 100	17	2.77*	2	
N galactic pole	i	9.15; 18.3; 100	30	2.8*	4	HIGGINS and SHAIN (1954)
Whole sky	i, n, t	100; 200	17	2.35	4	DRÖGE and PRIESTER (1956)
Whole sky	i, n, t	200; 400	17; 2	2.61	4	
Coldest parts of sky	i	80-400	2.8-40	2.68*	4	PIDDINGTON and TRENT (1956)
$\delta \approx -20°, \lvert b \rvert = 90°$-$20°$	i, n	38; 81.5; 175	20 × 70	2.50*	4	ADGIE and SMITH (1957)
Hottest parts of sky	n, t	60-900	3.5-20	2.36	4	KRAUS and KO (1957)
Coldest parts of sky	i	60-900	3.5-20	2.65*	4	

assumption can still be maintained. In Table 8 a number of determinations of the spectral index are listed. The radiation is usually divided into three components, a nonthermal isotropic component i, a nonthermal galactic component n and a thermal component t. From the data available so far there is no reason to assume that the spectra of i and n are different. The regions used to determine α are given in the first column of Table 8, while in the second column the components of the radiation to which α refers are tabulated. We have tried to assign weights to the various determinations. They are based mainly on a subjective estimate of their correctness, taking also into consideration the frequency range and the absolute intensity scales. The values of the beam-widths used in the surveys which were compared are given in the fourth column.

The weighted average of all values of α is 2.61. The weighted average of the values determined from the isotropic and nonthermal components only (*) is $\alpha = 2.70$. Considering the uncertainties in the basic data and the corrections, we conclude that the uncertainty of α cannot be much smaller than 0.10.

What really interests us in the present connection is the ratio of the intensities of the nonthermal radiation at 85 Mc/s and 1390 Mc/s. If we could compare these intensities at positions where only the nonthermal component contributes to the radiation, we could determine this ratio directly. The observations of the 21-cm line (SCHMIDT 1957) show that the neutral hydrogen in the Galactic System is concentrated in a layer of only 220 pc thickness around the galactic plane. Optical observations of emission nebulae, as well as the observations of emission nebulae at 1390 Mc/s described in this paper, show that the great majority of these are likewise strongly concentrated towards the galactic plane. The galactic ridge, observed at 1390 Mc/s (Figure 9) has a sharp top, about 3° to 4° wide, and smoothes out towards higher latitudes. Hence it seems safe to assume that the thermal component of the emission does not extend further than 4° in latitude at either side of the galactic ridge. The width of the layer of ionized hydrogen, derived from the separation of the two components (Figure 14), gives more weight to this assumption. It may be shown that a different assumption, for example a thermal component of 1 °K at 4° from the galactic ridge does not seriously influence this width, or the distribution of ionized hydrogen given in Table 14. On the basis of this distribution and a layer thickness of 200 pc, we expect a thermal brightness temperature of 0.5 °K at 4° from the ridge. Optical observations show that the layer of ionized hydrogen near the sun is probably thinner, thus decreasing this figure somewhat. In view of the uncertainties involved in the following derivation, it seems reasonable to neglect this small value. Accordingly we may use a comparison of the intensities at 85 and 1390 Mc/s at $b = -6°$ and $+4°$ to derive the ratio of the nonthermal radiation. At those latitudes, which form the limits of MILLS' published map, the intensities at 85 Mc/s are known,

TABLE 9

Determination of the zero level of the present survey from 900 Mc/s observations, and determination of the ratio of the 85 and 1390 Mc/s nonthermal brightness temperatures

Position			900 Mc/s		1390 Mc/s						85 Mc/s	ratio	zero level, adopted in separation
No.	l	b	I	T_b (obs)	T_b (extr)	I	T_b (obs)	T_b (extr)-T_b (obs) (zero level)	average zero level	T_b (obs+av.zero)	T_b (obs)	$\frac{T_b^{85}\text{(obs)}}{T_b^{1390}\text{(obs+zero)}}$	
			units	°K	°K	units	°K	°K	°K	°K	°K		°K
1	330°	−6°	5.5	14 -17	4.3-5.3	5	3.2	1.1-2.1		4.4-5.4	6000	1360-1110	
2	330	+4	3.8	9.5-12.5	2.9-3.9	2	1.3	1.6-2.6		2.5-3.5	5800	2320-1660	
3	325	−6	6.0	15 -18	4.6-5.6	3	2.0	2.6-3.6		3.2-4.2	5500	1720-1310	
4	325	+4	4.0	10 -13	3.1-4.1	5	3.2	−0.1-0.9		4.4-5.4	4700	1070- 870	
5	335	−6	6.5	16 -19	4.9-5.9	6	3.9	1.0-2.0	1.2-2.2	5.1-6.1	7800	1530-1280	1.5
6	335	+4	3.2	8 -11	2.5-3.5	4	2.6	−0.1-0.9		3.8-4.8	4000	1050- 840	
7	320	+4	4.0	10 -13	3.1-4.1	3	2.0	1.1-2.1		3.2-4.2	4400	1370-1050	
8	350	−6	3.9	10 -13	3.1-4.1	2	1.3	1.8-2.8		2.5-3.5	5500	2200-1570	
9	350	+4	4.1	10 -13	3.1-4.1	2	1.0	2.1-3.1		2.2-3.2	4800	2180-1500	
10	5	−6	4.4	11 -14	3.3-4.3	0	0.0	3.3-4.3		2.2-3.2	5000	2270-1560	2.9
11	5	+4	4.0	10 -13	3.1-4.1	0	0.0	3.1-4.1	2.2-3.2	2.2-3.2	3500	1600-1100	
12	19	−5	2.8	7 -10	2.1-3.1	2	1.3	0.8-1.8		3.5-4.5			
13	16	+3	3.0	7.5-10.5	2.3-3.3	1	0.7	1.6-2.6		2.9-3.9			
14	38	−4	2.7	7 -10	2.1-3.1	2	1.3	0.8-1.8		2.6-3.6			1.5
15	33	+2	0.5:	1.5-4.5:	0.5-1.5:	0	0.0	0.5-1.5:		1.3-2.3:			
16	49	−4	3.9	10 -13	3.1-4.1	1	0.7	2.4-3.4	1.3-2.3	2.0-3.0			
17	55	−1	3.2	8 -11	2.5-3.5	1	0.7	1.8-2.8		2.0-3.0			
18	51	+4	3.3	8 -11	2.5-3.5	2	1.3	1.2-2.2		2.6-3.6			

whereas at 1390 Mc/s the intensities above an unknown zero level are given.

The only way to obtain an estimate of the zero level is by extrapolation from surveys at lower frequencies. The nearest complete survey in which the zero level is well known is that by KRAUS and KO (1957) at 242 Mc/s. MCGEE *et al.* (1955) at 400 Mc/s have also estimated the zero level of their survey. Some doubt has been expressed about the correctness of this estimate (SEEGER *et al.* 1956) and there seems to be considerable error in their absolute intensities. Besides, they have only observed a small region around the galactic centre. An extrapolation from 242 to 1390 Mc/s requires an accurate knowledge of the spectral index; an uncertainty of 0.10 in α causes an error of about 17% in the derived brightness temperature. DENISSE *et al.* (1955, 1957) made a survey at a frequency of 900 Mc/s. An extrapolation from their data would be much safer. Their zero level is unknown, but they state that it is certainly below 3 °K. Since they used a careful technique, this figure, as well as their absolute temperature scale, seems to be rather trustworthy. We used their survey in the determination of our zero level. We have read the brightness temperature T_b from the 900 Mc/s map for a number of points well away from the galactic ridge. Since the zero level lies somewhere between 0 and 3 °K, the absolute temperature in those points must be between T_b and $T_b + 3$. For the extrapolation from 900 to 1390 Mc/s we used a spectral index $\alpha = 2.70 \pm 0.10$. The ratio between the brightness temperatures at the two frequencies is then 0.31 with an accuracy of 4%. This uncertainty is small compared to the uncertainty of 3 °K in the zero level and that of the temperature scale.

Subtraction of the observed brightness temperatures at 1390 Mc/s from the extrapolated temperatures then yielded a value for the temperature of the zero level in every point (Table 9). The zero levels in region A ($0° < l < 30°$) were expected to be higher than in regions S and C (Section 5a). Average zero levels therefore were determined for each of the three regions separately. An extrapolation from the 242 Mc/s data gave about the same result.

The absolute brightness temperatures are now known between limits differing 1 °K, disregarding the accuracy of the temperature scale (20%). The ratio of the 85 and the 1390 Mc/s absolute brightness temperatures was determined from 11 points, common to both surveys (columns 10, 11 and 12 of Table 9). The average ratio of $T_b^{85}(\text{obs})/T_b^{1390}$ (obs + zero) for these points, which should be identical with T_n^{85}/T_n^{1390}, lies between 1700 ± 150 and 1260 ± 150. These ratios correspond to spectral indices of 2.66 ± .04 and 2.55 ± .04. In all of these results the first and the second value refer to the assumption that the 900 Mc/s zero level is 0 °K and 3 °K, respectively. In the further computations we have adopted a ratio of the observed nonthermal temperatures at 85 and 1390 Mc/s of 1430. This ratio corresponds to $\alpha = 2.60$, which is lower than the average spectral index determined from Table 8. It might be increased to agree with $\alpha = 2.70$ if we assume that either the 85 Mc/s or the 1390 Mc/s survey, or both, have an incorrect temperature scale. At the high-frequency end, the 900 and 1390 Mc/s temperatures would both

TABLE 10

Narrow-beam surveys

Frequency Mc/s	Beamwidth	Author	Remarks
19.7	1°.4	SHAIN (1957)	
38	2.2 × 7.4	BLYTHE (1957)	Beamwidth at $\delta = -20°$
85	0.9	MILLS (1958)	
242	1.2 × 8	KRAUS and KO (1957)	
400	2	MCGEE *et al.* (1955)	T multiplied by 1.5 (PIDDINGTON and TRENT 1956)
600	3.3	PIDDINGTON and TRENT (1956)	Zero level between 3 and 13 °K
900	3 × 4	DENISSE *et al.* (1955, 1957)	Zero level between 0 and 3 °K

have to be wrong by about the same amount. A decrease of the 1390 Mc/s temperatures by a factor of about 0.75 would increase α from 2.60 to 2.70. Inclusion of a correction for a possible non-zero value of the thermal brightness temperature at 4° from the galactic ridge would have increased α from 2.60 to about 2.64. It is difficult to assess the correctness of the zero and the temperature scale of the 900 and 1390 Mc/s surveys.

At the low-frequency end, a slightly better possibility exists for checking the 85 Mc/s temperature scale, since several narrow-beam surveys have been made at both higher and lower frequencies. Most of these were not used in the previous determinations of the spectral index. We shall now investigate how well the 85 Mc/s temperatures fit into the series of temperatures measured at surrounding frequencies.

We have determined the temperature at the points given in Table 9 from the surveys listed in Table 10. We assumed that because of the narrow beams these temperatures are not influenced by the nearness of the galactic ridge. Therefore no correction was applied for the antenna pattern. At 38 and 19.7 Mc/s, the optical depth of the ionized hydrogen at these points is still negligible.

Using $\alpha = 2.60$, we computed the temperatures at 85 Mc/s from those at the other frequencies. We compared these with the observed 85 Mc/s temperatures by determining the ratio $T_b^{85}(\text{comp})/T_b^{85}(\text{obs})$ averaged over the points common to the 85 Mc/s survey and to each of the other surveys.

TABLE 11

Temperature ratios of different surveys and the 85 Mc/s survey, for two values of α

	$\alpha = 2.60$	$\alpha = 2.70$
f (Mc/s)	$T_b^{85}(\text{comp})/T_b^{85}(\text{obs})$	$T_b^{85}(\text{comp})/1.32\ T_b^{85}(\text{obs})$
19.7	1.30	0.84
38	3.32	2.18
242	1.24	1.06
400	1.32	1.15
600	1.86-2.18	1.72-2.02
900	0.99-1.26	0.95-1.22

These ratios are given in the second column of Table 11. It is clear that $T_b^{85}(\text{obs})$ is too low in comparison with the other surveys. On the other hand, it seems more likely that $\alpha = 2.70$ (Table 8). This would give $T_n^{85}/T_n^{1390} = 1890$, which is a factor of 1.32 higher than the ratio of 1430 obtained from a direct comparison of the 85 and 1390 Mc/s surveys. We obtain a consistent set of data if we assume that the temperature scale of the 85 Mc/s survey is a factor of 1.32 too low and $\alpha = 2.70$. On those assumptions, the third column of Table 11 was computed. With the exception of the ratios determined from the 38 and the 600 Mc/s survey, the values of $T_b^{85}(\text{comp})/1.32\ T_b^{85}(\text{obs})$ are in good agreement. From both comparisons it is clear that the temperature scales of the 38 and the 600 Mc/s surveys are considerably in error.

We may summarize the results of this section as follows:

1) The ratio of the observed brightness temperatures of the nonthermal radiation at 85 and 1390 Mc/s is 1430 ±200 (estimated error).

2) If the temperature scales at both frequencies, and the derivation of the 1390 Mc/s zero level, are correct, this ratio corresponds to a spectral index of 2.60 ±.05.

3) The spectral index of the nonthermal radiation, averaged over a number of determinations by different authors, is 2.70 ±.10.

4) Assuming that the 1390 Mc/s temperature scale is correct, we may choose between two alternatives: a) The temperature scale of the 85 Mc/s survey has to be multiplied by a factor of 1.32, and $\alpha = 2.70$; the nonthermal temperature ratio is 1890, the ratio of the observed nonthermal temperatures is 1430. b) The scale of the 85 Mc/s survey is correct, and $\alpha = 2.60$. The first alternative seems the more probable.

c. *Separation of the thermal and nonthermal components*

Before we can proceed with the separation of the observed radiation into thermal and nonthermal components, we shall have to make an assumption

TABLE 12

Results of the separation of the background radiation

Position		Observed			Computed			
		85 Mc/s	1390 Mc/s		1390 Mc/s		85 Mc/s	
l	b	$10^{-4}T_b^{85}$	I	T_b^{1390} + zero	$10^4\tau = T_t^{1390}$	T_n^{1390}	T_t^{85}	$10^{-4}T_n^{85}$
		°K	units	°K	°K	°K	°K	°K
322°	top	1.56	28	19.5	8.9	10.6	2120	1.52
325		2.30	37	25.5	9.1	16.4	2160	2.34
330		2.58	40	27.5	8.9	18.6	2120	2.66
332		1.91	33	23.0	9.6	13.4	2260	1.92
335.5		1.65	32	22.5	11.3	11.2	2610	1.60
340		1.63	29	20.5	9.3	11.2	2200	1.60
345		1.36	29.5	20.5	11.7	8.8	2680	1.26
348.5		1.37	32	22.5	13.6	8.9	3040	1.27
355.5		1.17	31	21.5	14.3	7.2	3170	1.03
0		1.06	22	16.0	9.3	6.7	2200	0.96
4.5		1.05	18.5	14.9	8.3	6.6	1990	0.94
10		0.90	13	11.4	5.7	5.7	1410	0.82
5	+0.2°	0.70	5	6.1	1.5	4.6	390	0.66
	−0.6	0.88	10	9.4	3.6	5.8	910	0.83
	−1.0	0.97	15	12.6	6.5	6.1	1600	0.87
	−1.55	1.05	18.5	14.9	8.3	6.6	1990	0.94
	−1.95	0.95	15	12.6	6.6	6.0	1610	0.86
	−2.2	0.86	10	9.4	3.8	5.6	960	0.80
	−2.9	0.67	5	6.1	1.7	4.6	440	0.66
354	+3.7	0.45	5	4.7	1.7	3.0	440	0.43
	+0.1	0.79	10	8.0	2.7	5.3	690	0.76
	−0.5	0.95	15	11.2	5.1	6.1	1270	0.87
	−1.0	1.12	25	17.8	10.8	7.0	2500	1.00
	−1.5	1.17	31	21.7	14.5	7.2	3210	1.03
	−2.0	1.10	25	17.8	11.0	6.8	2550	0.97
	−2.6	0.96	15	11.2	5.0	6.2	1250	0.89
	−3.4	0.81	10	8.0	2.6	5.4	670	0.77
	−5.2	0.63	5	4.7	0.4	4.3	110	0.61
339	+2.0	0.59	5	4.7	0.7	4.0	190	0.57
	+0.5	1.01	10	8.0	1.1	6.9	290	0.99
	−0.2	1.27	15	11.2	2.5	8.7	650	1.24
	−1.1	1.66	25	17.8	6.4	11.4	1570	1.63
	−1.6	1.64	29	20.3	9.1	11.2	2160	1.60
	−2.0	1.36	25	17.8	8.7	9.1	2070	1.30
	−2.85	1.00	15	11.2	4.7	6.5	1170	0.93
	−3.6	0.83	10	8.0	2.4	5.6	690	0.80
332	+2.1	0.81	5	4.7	− 1.2	4.7	− 330	0.67
	+0.8	1.14	10	8.0	0	8.0	000	1.14
	0.0	1.43	15	11.2	+ 1.5	9.7	+ 390	1.39
	−0.85	1.69	25	17.8	6.2	11.6	1530	1.66
	−1.2	1.84	30	21.0	8.2	12.8	1970	1.83
	−1.45	1.91	33	23.0	9.6	13.4	2260	1.92
	−1.65	1.91	30	21.0	7.7	13.3	1860	1.90
	−2.2	1.80	25	17.8	5.3	12.5	1320	1.79
	−3.0	1.30	15	11.2	2.2	9.0	570	1.29
	−4.0	0.95	10	8.0	1.6	6.4	420	0.92
	−6.0	0.64	5	4.7	0.3	4.4	80	0.63

TABLE 12 (*continued*)

Position		Observed			Computed			
		85 Mc/s	1390 Mc/s		1390 Mc/s		85 Mc/s	
l	b	$10^{-4}T_b^{85}$	I	T_b^{1390} + zero	$10^4\tau = T_t^{1390}$	T_n^{1390}	T_t^{85}	$10^{-4}T_n^{85}$
		°K	units	°K	°K	°K	°K	°K
323°.5	+3°.2	0.74	5	4.7	− 0.6	4.7	− 160	0.67
	+1.6	0.97	10	8.0	+ 1.4	6.6	+ 360	0.94
	+0.5	1.28	15	11.2	2.4	8.8	620	1.26
	−0.4	1.66	25	17.8	6.4	11.4	1570	1.63
	−1.1	1.78	35	24.2	12.0	12.2	2740	1.74
	−1.25	1.73	37	25.5	13.5	12.0	3020	1.72
	−1.5	1.57	35	24.2	13.7	10.5	3060	1.50
	−2.0	1.36	25	17.8	8.8	9.0	2090	1.29
	−2.25	1.26	20	14.5	6.1	8.4	1500	1.20
	−2.8	1.00	15	11.2	4.7	6.5	1170	0.93
	−3.8	0.81	10	8.0	2.6	5.4	670	0.77
	−4.8	0.68	5	4.7	0	4.7	0	0.67

regarding the zero level of the present survey. We could have used the average value of the limits to the zero levels determined from the 900 Mc/s survey. But in comparing the 85 and 1390 Mc/s surveys, we preferred to compute the zero level from the 85 Mc/s survey. We divided the observed temperatures given in Table 9 by 1430 and compared these with the 1390 Mc/s temperatures. The average zero levels used in the further reductions are given in the last column of Table 9. The zero level for $l > 10°$ was computed from the 242 Mc/s survey, taking $\alpha = 2.70$. For $l < 10°$ the comparison with the 242 Mc/s value shows excellent agreement. All values are within the limits set by the 900 Mc/s survey.

To avoid the extra multiplication of the 85 Mc/s temperatures by 1.32 we formulated the reductions so that the second of the two alternatives for the nonthermal temperature ratio is correct. Outside the gas disk, both alternatives give the same conversion factors from 85 to 1390 Mc/s. With the first alternative, inside the disk, where a fraction of the radiation is thermal, only part of the 32% increase in the value of T_b^{85} is compensated by the increase in the nonthermal temperature ratio in the conversion. If we did not simultaneously decrease the thermal component, the resulting values of T_b^{1390} would be too high. Tests showed that this decrease amounts to 5% at the most, so that the difference between the two alternatives has a negligible influence on the results.

The two equations supplementing equations (28) and (29) now are:

$$T_n^{85}/T_n^{1390} = 1430 \qquad (30)$$

and

$$\tau_{85}/\tau_{1390} = (85/1390)^{-2} = 267\,. \qquad (31)$$

Substitution of these values and $T_e = 10^4$ °K in (28) gives

$$T_b^{85}(\text{obs}) = (10^4 + 1430\, T_n^{1390}/267\,\tau_{1390})\,(1 - e^{-267\tau_{1390}})\,. \qquad (32)$$

From (29), $T_n^{1390} = T_b^{1390} - 10^4\,\tau_{1390}$, which gives

$$10^{-4}\,T_b^{85}(\text{obs}) = T_b^{1390}a(\tau) - b(\tau)\,, \qquad (33)$$

$$a(\tau) = \frac{5.356}{\tau_{1390} \times 10^4}\,(1 - e^{-267\tau_{1390}})\,, \qquad (34)$$

$$b(\tau) = 4.356\,(1 - e^{-267\tau_{1390}})\,. \qquad (35)$$

In (32), T_b^{1390} represents T_b^{1390}(obs + zero). We tabulated the functions $a(\tau)$ and $b(\tau)$. With the aid of this table, the value of τ was solved from equation (33) for each point where both T_b^{85}(obs) and T_b^{1390} were known. The values of T_b^{85}(obs) were taken from a detailed contour map by MILLS *et al.*, a simplified version of which has been published in their (1958) article. The values of T_b^{1390} were obtained by multiplying our intensity in units by 0.65 and then adding the value assumed for the zero level, as given in Table 9.

The separation into thermal and nonthermal components was made for 59 points where the influence of bright sources is small. For 12 points on the galactic ridge, the best possible value of the background temperature was obtained by drawing a lower envelope of the curve of top intensities. For the 1390 Mc/s measurements this curve is given in Figure 7. The intensities in 47 points on five cross-sections

FIGURE 13

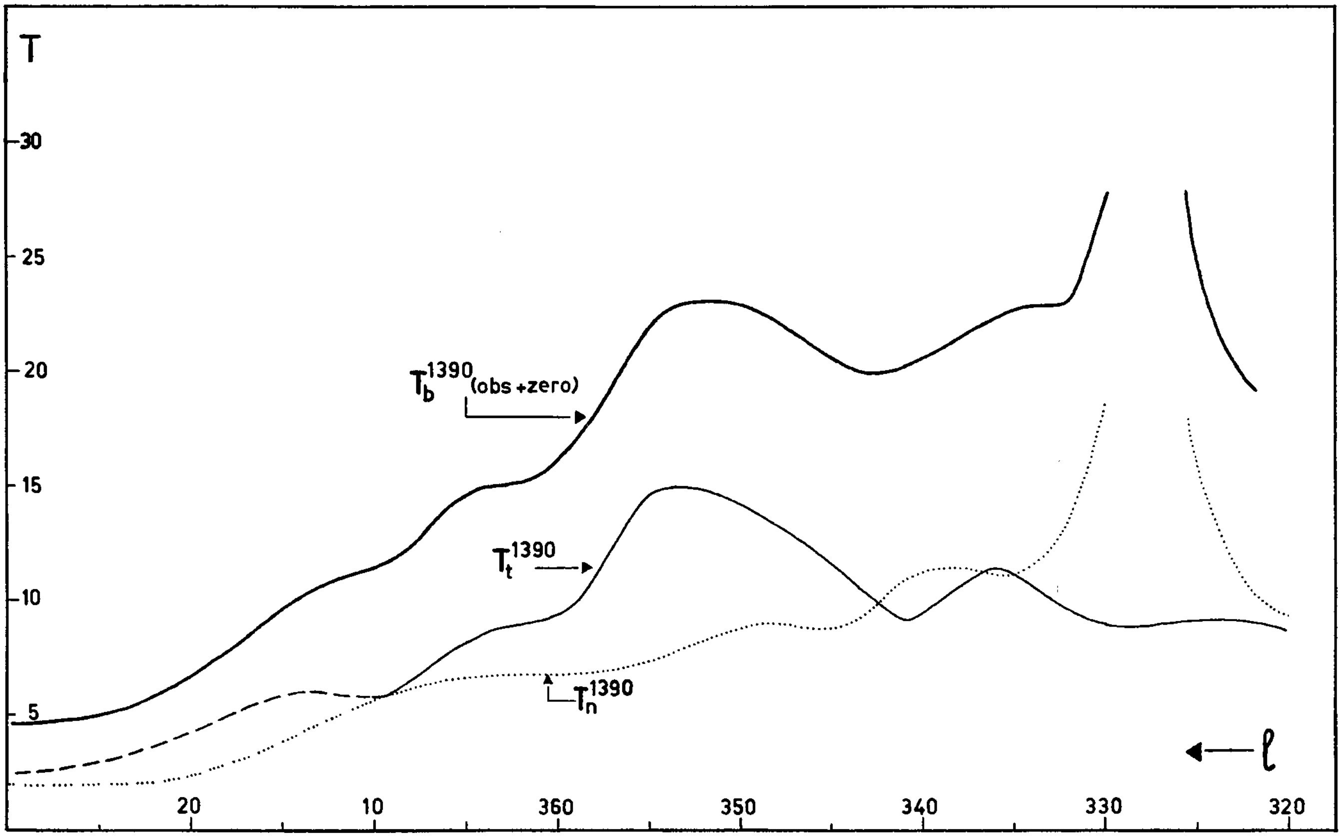

Total, thermal and nonthermal brightness temperatures along the galactic ridge, at 1390 Mc/s.

perpendicular to the galactic plane were obtained by averaging the contours over the longitude intervals 4°-6°, 353°-355°, 338°-340°, 331°.5-332°.5 and 323°-324°, respectively.

The observed temperatures and the computed thermal and nonthermal brightness temperatures at 1390 and 85 Mc/s are given in Table 12.

The results are illustrated in Figures 13 and 14. The curves in Figure 13 give the distribution of the total brightness temperature T_b^{1390} and of the nonthermal and thermal components T_n^{1390} and T_t^{1390} along the galactic ridge. The computations could only be made up to $l = 10°$, since MILLS' survey does not extend any further. We made a tentative extrapolation of the curves to $l = 30°$. It appears that the fairly constant value of the observed background temperature between $l = 330°$ and $l = 355°$ is due to the combined effect of an increase of T_t and a decrease of T_n with increasing l. As was noted by MILLS *et al.*, T_n increases towards the galactic centre in steps, the positions of which roughly correspond to the positions where the line of sight passes tangentially along a spiral arm. A similar effect, although less pronounced, is visible in the distribution of T_t. A discussion of the space distribution of the nonthermal radiation will be given in a forthcoming paper by MILLS' group.

The distribution of the radiation in latitude may be found in the separation of the cross-sections, Figure 14. The widths at half intensity of the curves in Figure 14 are given in Table 13.

The nonthermal distribution smoothes out considerably at a distance of approximately 4° in latitude from the top of the ridge. For this reason various authors separated the nonthermal radiation into two components. The isotropic component has a half-width of 60° or 70° (MILLS 1955) and a top temperature of about 4000 °K. The values of the halfwidth, given in Table 13, refer to the other component measured above the 4000 °K level. This part of the

TABLE 13

Halfwidths of the thermal and nonthermal brightness distributions, perpendicular to the galactic plane

l	thermal	nonthermal
°	°	°
5	1.5	4.1
354	1.5	4.8
339	1.9	3.0
332	1.6	4.0
323.5	1.6	5.0

FIGURE 14

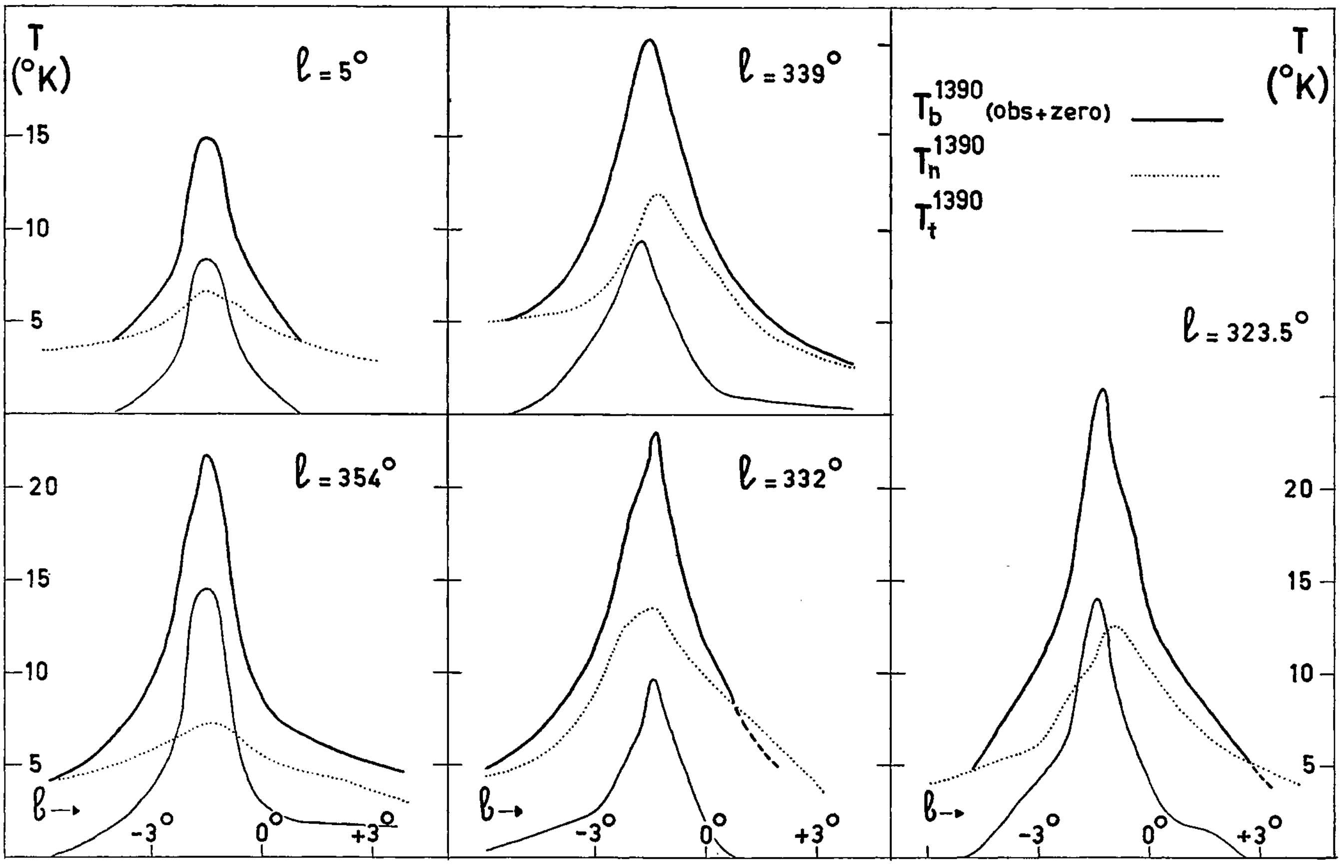

Total, thermal and nonthermal brightness temperatures in cross-sections perpendicular to the galactic plane, at 1390 Mc/s.

nonthermal component, which is often called the disk component, has an average halfwidth of 4°.2. The average width of the thermal component is 1°.6. This figure, which is only slightly dependent on the assumed zero level, supports the assumption made in Chapter 7b, that the thermal radiation at a distance of 4° from the galactic ridge is negligible.

d. *Space distribution of ionized hydrogen*

We shall now endeavour to determine the space distribution of the ionized hydrogen which causes the distribution of the thermal radiation observed on the sky.

The intensity of the thermal radiation has a maximum at $l = 353°$ and decreases towards the longitude of the galactic centre. We immediately infer from this fact that the density close to the galactic centre must be much lower than that further out. Since the largest contribution to the observed radiation at $l = 353°$ must come from hydrogen between roughly $R = 3$ and 4 kpc, we may expect a high gas density at that distance from the centre.

In deriving the model we assumed axial symmetry. This assumption is strengthened by the observations of PIDDINGTON and TRENT (1956) at 600 Mc/s. Theirs is the only survey at higher frequencies which covers regions at both sides of the galactic centre. Thermal radiation is responsible for only one quarter of the ridge temperature at that frequency. Nevertheless a feature such as the maximum around $l = 352°$, which we find to be thermal in origin, is visible in their survey; a similar feature, around $l = 305°$, is symmetrically placed with respect to the galactic centre.

The model consists of a number of rings around the centre, in which we have adjusted the optical

FIGURE 15

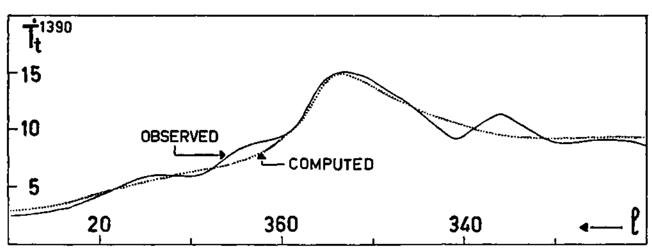

Observed and computed brightness temperatures of the thermal radiation along the galactic ridge.

TABLE 14

Distribution of ionized hydrogen as a function of R; n = total average space density, N = density inside a cloud, α = fraction of space occupied by ionized clouds

R	$10^4\tau$/kpc	nN	$n(N = 5)$	$\alpha(N = 5)$	$n(N = 10)$	$\alpha(N = 10)$
kpc		cm^{-6}	cm^{-3}	%	cm^{-3}	%
0 –2	0	0	0	0	0	0
2 –3	0.28	0.15	0.03	0.6	0.015	0.15
3 –3.5	1.12	0.60	0.12	2.4	0.060	0.60
3.5–4	1.96	1.05	0.21	4.2	0.105	1.05
4 –4.5	1.40	0.75	0.15	3.0	0.075	0.75
4.5–5	0.84	0.45	0.09	1.8	0.045	0.45
5 –7	0.56	0.31	0.06	1.2	0.031	0.31
7 –10	0.28	0.15	0.03	0.6	0.015	0.15
>10	0	0	0	0	0	0

depth per unit length (or density of sources of thermal radiation) so that the integral along the line of sight for every direction between $l = 327^\circ.5$ and $l = 30^\circ$ is roughly equal to the measured value. The optical depth per kiloparsec adopted in the model is given for the various rings in the second column of Table 14, and the resulting distribution of thermal radiation with galactic longitude as compared to the observations is illustrated in Figure 15. In our model the emptiness of the region $R < 3$ kpc is very striking. In this respect it is of interest to note that BAADE (1958) has been unable to observe any blue supergiants and HII regions in the Andromeda nebula within 3 kpc from the centre.

The model was made to agree with the observations between $l = 320^\circ$ and 10°. For $l > 30^\circ$, with the exception of the Cygnus region, the observations were either incomplete or showed no radiation above the limit of detection. Some further remarks on these regions will be made below.

FIGURE 16

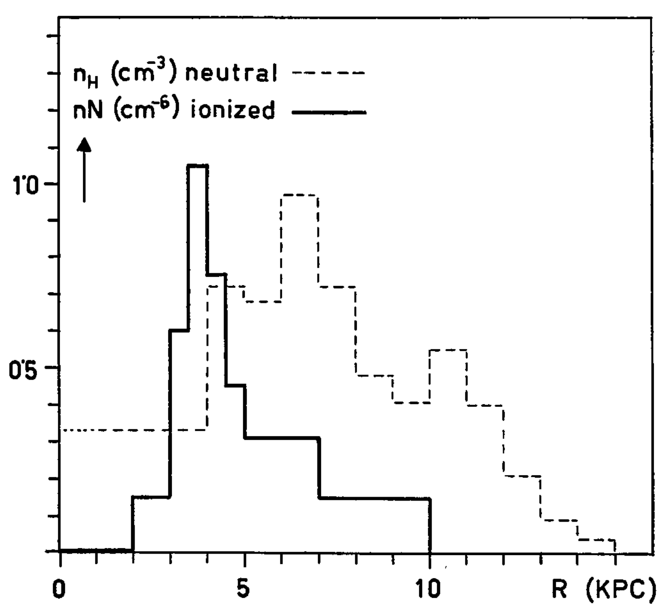

Density distribution of ionized and neutral hydrogen in the Galactic System. n = average space density, N = average density inside one cloud, assumed to be between 5 and 10 cm^{-3}.

It was shown in Chapter 6a that on the assumption of an electron temperature $T_e = 10^4$ °K throughout, the brightness temperature T_b and the emission measure E are related to the optical depth τ by $T_b = 10^4\,\tau$ and $E = 538.10^4\,\tau$. The model thus gives the distribution of the emission measure throughout the Galactic System. The values of

$$\int_0^{1000\,\mathrm{pc}} N^2 ds$$

are equal to $538.10^4\,\tau$/kpc. If the gas were homogeneously distributed in space this integral would become $n^2.10^3$, where n is the space density.

It is well known, however, that the gas is distributed in clouds. If a fraction α of space is occupied by ionized clouds, with a density of N per cm^3 inside each cloud, the average space density in a unit volume $n = \alpha.N$, and

$$\int_0^{1000\,\mathrm{pc}} N^2 ds = \overline{N^2} \times 10^3 = 10^3\alpha\left(\frac{n}{\alpha}\right)^2 = 10^3 nN \qquad (36)$$

$$= 538.10^4\,(\tau/\mathrm{kpc})\,.$$

From inspection of photographs it is clear that most of the faint emission regions have a fairly constant brightness over their entire surface, with only minor bright knots, and therefore an almost constant value of N throughout the nebula. Only the brighter nebulae consist of several regions of high density embedded in a low-density medium. Thus, the assumption made in the first equation in (36), that the ionized clouds have a homogeneous density, must be mainly correct.

In Chapter 6d it was shown that most emission regions have values of N below 10 cm^{-3}. Neutral hydrogen clouds seem to have densities of the order of 5 cm^{-3}. Optical observations indicate that the faint emission regions have values of E around 400 cm^{-6} pc, and diameters of the order of 10 pc, which leads to $N = 6$ cm^{-3}. We shall assume that the greater part of the thermal background emission is due to a large number of such clouds. The values of n and α, computed from the observed values of nN with $N = 5$ and $N = 10$ cm^{-3} are given in Table 14.

In Figure 16 the distribution of nN and the distribution of the space density of neutral hydrogen n_H (WESTERHOUT 1957, Table 8), are plotted versus R.

The density ratio of the ionized and the neutral hydrogen as a function of the distance to the galactic centre is given in Table 15. It is determined from a comparison with the 21-cm line data. The density ratio near the sun (average of $R = 6 - 10$ kpc), 0.06 for $N = 5$ or 0.03 for $N = 10$, happens to be the same as the total mass ratio (Table 16). This density ratio is well in accordance with the optical estimates.

Due to the sharp increase in the density of ionized hydrogen, the ratio reaches a maximum value between $R = 3.5$ and 4 kpc, which is ten times higher than that near the sun.

It is difficult to determine the value of α from optical data (OORT 1955, discussion). In Table 14 we find that in the neighbourhood of the sun 0.6 to 0.15% of space is filled with ionized clouds. As was already mentioned in Chapter 6d, STRÖMGREN estimates the emission measure of an average emission region at 800 cm^{-6} pc. With $N = 5$, such an emission region must have a diameter of about 30 pc. With $\alpha = 0.6\%$, we find that within 2000 pc of the sun there are only 27 such regions; with $\alpha = 0.15\%$ and $N = 10$, the diameter of an emission region is 8 pc and there are 94 such regions within $r = 2000$ pc. The latter figure seems more realistic on the basis of the very uncertain optical data. Smaller values of the average emission measure would give larger values of the total number of emission regions. The faintest emission regions which were optically detected have $E = 400$. We conclude that the optical and the radio data agree if we assume that the majority of emission regions have emission measures between 400 and 800, densities between 5 and 10 and diameters between 5 and 30 pc.

If the average value of the density in a cloud could be determined with greater accuracy, the data derived in this investigation would give a much better estimate of the distribution of ionized hydrogen than hitherto available. Our present knowledge already puts fairly narrow limits to the density.

It will be shown in a subsequent note (WESTERHOUT 1958) that if a considerable part of the background temperature is due to bright emisson nebulae ($E > 10^4$), the densities given in Table 14 might be lower by a factor of two or more.

The value for the density near the sun, given by the model, is an average over the whole ring between $R = 7$ and 10 kpc, and does not include local high-density regions. For example, the higher intensities in the Cygnus region were not taken into account in deriving the model. In this region the line of sight passes lengthwise through the Orion arm. Assuming arbitrarily that half of the radiation has a thermal origin, and excluding the bright source No 66, which is the brightest component of Cyg X and is presumably situated in the Perseus arm at $r = 6$ kpc (DAVIES 1957), the average optical depth over the region is of the order of 6×10^{-4}, which leads to an emission measure $E = 3200$ cm^{-6} pc. Assuming that the line of sight passes through 5 kpc of Orion arm, we have $nN = 0.6$. This is about four times higher than the value found from our simplified model, and thus far in excess of the average density in the Orion arm, although still 0.6 times smaller than the average value around $R = 4$ kpc. It is clear that the high density is due to a local concentration of ionized hydrogen, and not to a high-density ring or spiral arm. We have been able to identify a number of features in this region with bright emission nebulae having much greater densities than those of the average faint emission regions. In fact, the concentration of nearby bright nebulae seems to be unusually large in the Cygnus region. No concentrations with comparable intensity are found in other parts of the Milky Way.

In the region between $l = 165°$ and $195°$ (Orion region) no traces were found of a galactic ridge; the upper limit of the ridge temperature was found to be 2.5 °K. The surveys at 242, 600 and 900 Mc/s give ridge temperatures of 35, 10 and 3 °K, respectively. If all radiation at those frequencies were due to ionized hydrogen, the temperature of the ridge would be 1.1 °K, while if the radiation were partly nonthermal this value would be considerably lower. If we take

TABLE 15

Density ratio of ionized and neutral hydrogen as a function of distance to the galactic centre

R	n(ionized)/n(neutral)	
kpc	$N = 5$ cm^{-3}	$N = 10$ cm^{-3}
0 −2	0	0
2 −3	0.09	0.05
3 −3.5	0.36	0.18
3.5−4	0.64	0.32
4 −4.5	0.21	0.10
4.5−5	0.13	0.06
5 −6	0.09	0.05
6 −7	0.06	0.03
7 −8	0.04	0.02
8 −9	0.06	0.03
9 −10	0.07	0.04
>10	0	0

1 °K as the upper limit of the thermal radiation, then $\tau = 10^{-4}$ and $E < 540$; assuming that the line of sight in this direction passes through 2.5 kpc of interstellar matter, we find $nN < 0.2$. This is in accordance with our model, in which we found $nN = 0.15$.

So far we have not mentioned the thickness of the layer of ionized hydrogen. The average width in latitude at half intensity of the observed brightness distribution of the thermal component is 1°.6. Inspection of Figure 9 shows that the five cross-sections from which this average is determined are a fair sample of the general distribution. We made the simple assumption that the layer is homogeneous in a direction perpendicular to the galactic plane, while the density outside it is zero. Assuming a thickness of 200 pc, and using the density distribution given in Table 14, we find a distribution of the brightness temperature in latitude at different longitudes which resembles reasonably well the observed distribution with halfwidth 1°.6. The actual space distribution will certainly be less extreme, showing a smooth decrease of density in the direction perpendicular to the galactic plane. In view of the uncertainties involved we did not feel justified at this stage in deriving more sophisticated models. The thickness of 200 pc is in satisfactory agreement with the thickness of the layer of neutral hydrogen, determined by Schmidt (1957) from observations of the 21-cm line. He found a layer with almost gaussian cross-section and a thickness at half-density of 220 pc.

In the neighbourhood of the sun, the layer of OB stars and optically observed emission nebulae is somewhat thinner, having a thickness at half-density of the order of 150 pc. Except for the cross-section at $l = 5°$, the halfwidth of the layer derived in the present investigation is mainly determined by the high-density region between $R = 3$ and 5 kpc. Schmidt's results refer to the region between $R = 3$ and 7 kpc. It seems quite possible that the smaller value of the layer thickness near the sun is a local phenomenon. Since our estimate of the layer thickness has a large uncertainty ($\pm 30\%$ being quite possible) no definite conclusions can be drawn.

Integration of the value of nN over the model gives the total mass of ionized hydrogen

$$M/M_{\odot} = \frac{42}{N} \times 10^{7} . \qquad (37)$$

The total mass of the Galactic System, derived by Schmidt (1956) is $M/M_{\odot} = 7 \times 10^{10}$. The total mass of neutral hydrogen has been derived from the 21-cm line data (Westerhout 1957, Kerr and Hindman 1957). The results of the mass determination are summarized in Table 16.

One of the main assumptions used in the separation of thermal and nonthermal radiation was the ratio of the observed nonthermal brightness temperatures at 85 and 1390 Mc/s. The amount of thermal radiation at 1390 Mc/s increases more or less proportionally to this ratio. This was also shown in a preliminary separation, in which the ratio was taken to be 1100 instead of the 1430 finally adopted. The total mass derived from the results of this preliminary separation was $M/M_{\odot} = \frac{33}{N} \times 10^{7}$. Therefore, with an estimated uncertainty of 15% in the temperature ratio, the uncertainty in the total mass is also 15%; this figure is smaller than that arising from the uncertainty in N and in the derived space distribution. Taking the average of the two values of the mass given in Table 15, we find for the total mass of the ionized hydrogen in the Galactic System $M/M_{\odot} = 6.3 \times 10^{7}$ $\pm 40\%$, where the uncertainty is a very rough estimate.

Table 16

Total mass and mass ratios of ionized and neutral hydrogen in the Galactic System

	ionized		neutral
	$N = 5$	$N = 10$	
$M/M_{\odot}$	8.4×10^{7}	4.2×10^{7}	1.4×10^{9}
M/M_{total}	0.0012	0.0006	0.02
$M_{ionized}/M_{neutral}$	0.06	0.03	

e. *Ionized hydrogen and expanding arms*

The density of ionized hydrogen in the region $R < 3$ kpc, excluding the source Sgr A in the nucleus, must be very small. In the same region the neutral hydrogen has very high velocities and expanding motion, while the density of ionized hydrogen shows a very sharp maximum just outside it. It is interesting to speculate about a possible connection between these three phenomena.

Radial velocities up to 200 km/sec have been observed in the neutral hydrogen in the region $R < 3$ kpc (Kwee, Muller and Westerhout 1954). These velocities were at first believed to be due to a state of strong turbulence, possibly caused by the high gradient in the angular velocity of rotation in that region. Subsequent observations by van Woerden *et al.* (1957) showed that a secondary maximum observed in the 21-cm line in the direction of the centre must be caused by a concentration of neutral hydrogen moving radially outward. On the basis of these observations and of observations made by F. J. Kerr and J. V. Hindman (*personal communication*), it seems probable that the maximum which is visible in the 21-cm line profiles between $l = 334°$ and $l = 305°$ is due to a spiral arm at a distance of 3 kpc from the centre expanding with a velocity of

50 km/sec. It is not clear whether the arm really has a spiral shape or whether it is more or less circular. Recent 21-cm line observations by G. W. Rougoor (*personal communication*) with the 25-m telescope in Dwingeloo showed that not only this spiral arm, but also a large part, if not all, of the high-velocity neutral hydrogen in the centre region is expanding, with velocities up to 200 km/sec.

The average density of the neutral hydrogen within $R = 3$ kpc is 0.4 cm^{-3} (Kwee, Muller and Westerhout 1954, substantiated by recent observations made by G. W. Rougoor). With a layer thickness of 200 pc, the mass of neutral hydrogen which is observed in expansion is 5.5×10^7 $M_{\odot}$. If we take the average velocity of expansion at 100 km/sec, the gas requires 3×10^7 years to reach the boundary of the region at $R = 3$ kpc. If the expansion process is continuous, it follows that every 3×10^7 years the gas mass has to be renewed, so that the total amount of gas which was ejected from the nucleus during the lifetime of the Galactic System, 5×10^9 years, is 9×10^9 $M_{\odot}$. This is about one eighth of the total mass of the Galactic System and six times the total mass of interstellar gas; it seems unlikely that such a large mass could be concentrated in the nucleus at one time, since this is probably very small.

According to Baade (1958) the nucleus of the Andromeda nebula is a bright disk with dimensions $2''.5 \times 1''.5$. At a distance of 6×10^5 pc this corresponds to a diameter of 6 pc. Estimates of the diameters of bright nuclei in other extragalactic nebulae give values of the order of 20 pc. If a mass of 9×10^9 $M_{\odot}$ were concentrated in a sphere with a diameter of 20 pc, the average density would be 15×10^{-17} grams/cm^3 or 9×10^7 protons/cm^3. This is certainly not a correct model for the galactic nucleus, since it would give an intensity at the high radiofrequencies which would be at least an order of magnitude greater than that observed. It seems more likely that the nucleus consists of a very massive cloud of ionized hydrogen with a high concentration towards the centre. Possibly accretion of matter from all sides by the nucleus provides it with the mass necessary for the continuous ejection of hydrogen in the galactic plane.

It seems likely that the high concentration of ionized gas between $R = 3$ and 4 kpc is due to an unusually large number of newly formed hot stars. If the expanding spiral arm at $R = 3$ kpc is actually a ring, we have the following situation: a) Between $R = 0$ and $R = 3$ kpc an expanding mass of gas with velocities of expansion up to 200 km/sec. Scarcely any ionized hydrogen is present in this region. b) At $R = 3$ kpc, a concentration of neutral hydrogen expanding with a velocity of 50 km/sec, and taking part in the galactic rotation. The rotational velocity at $R = 3$ kpc is of the order of 200 km/sec. c) At $R = 3.5$ kpc, a high concentration of hot stars causing strong ionization.

The following tentative explanation may be suggested:

a) While the neutral hydrogen is expanding, the conditions for star formation are unfavourable.

b) During its outward motion, the gas either obtains or retains an angular momentum which leads to a rotational velocity of about 200 km/sec at $R = 3$ kpc. It seems probable that magnetic forces are responsible for both the expansion and the rotation.

c) At $R = 3$ kpc a concentration is formed in the expanding gas. This may be due to a combination of factors, such as the influence of the gravitational field of the Galactic System, the shape of the magnetic force field which governs the expansion, and perhaps other braking mechanisms.

d) In this concentration conditions for star formation become very favourable, so that after 10^7 years, the time necessary for the matter in the expanding ring to travel from $R = 3$ to $R = 3.5$ kpc with a velocity of 50 km/sec, a large number of new stars are formed, causing strong ionization. The uncertain points in this explanation are the origin of the expanding gas, and the mechanism whereby the expansion velocity decreases at $R = 3$ kpc.

f. *The source at the galactic centre*

The observations of the bright source No 24 in the direction of the galactic centre are of considerable interest. The intensity given in Table 6 was obtained by subtracting the galactic ridge as measured well away from the source (top intensity 31 units = 20 °K, total width between half-intensity points 2°.6). The source is elongated, and has a sharp central peak. The widths in galactic longitude and latitude between half-intensity points are $\Delta l \times \Delta b = 0°.83 \times 0°.64$; the widths between the points where the intensity is one-tenth the top intensity are $2°.60 \times 1°.44$. Its shape might be explained by adopting a source having a gaussian shape with halfwidths of about $0°.55 \times 0°.25$ and a maximum brightness temperature of 500 °K, on top of a more extended source with halfwidths of approximately $2° \times 1°$ and a maximum brightness temperature of approximately 25 °K. A small source with a halfwidth of 0°.25 in declination, i.e. with $\Delta b \approx 0°.2$, was observed by Haddock and McCullough (1955) at a frequency of 9500 Mc/s. The small source is at exactly the same position as the broad one; it seems very likely that they are physically connected.

Various authors have discussed the spectrum of the source (Priester 1955, Davies and Williams 1955, Smith *et al.* 1956). They concluded that there must be two sources at this position, a nonthermal one which gives rise to the high brightness temperatures observed at the low frequencies, and a thermal one which is observed at the high frequencies. We will show in the following that the broad source with a top brightness temperature of 25 °K at 1390 Mc/s is nonthermal, whilst the narrow source with a top temperature of 500 °K is thermal.

DAVIES and WILLIAMS (1955) and MCCLAIN (1955) observed 21-cm line absorption at the position of the source. They tried to obtain an estimate of its distance. The result of this very uncertain estimate was a distance of 3 kpc. They suggest identification of the thermal component with an HII region, caused by an association of O and B-stars at $r = 3$ kpc. The chance that an HII region of a brightness comparable to that of the brightest HII regions found in this survey is situated exactly in the direction of the galactic centre, but at only 3 kpc from the sun, seems very small.

Observations by VAN WOERDEN *et al.* (1957) of 21-cm line absorption in the expanding spiral arm at $R = 3$ kpc placed the source at a distance of less than 3 kpc from the centre. Later observations of absorption by the expanding medium showed that it is, in all probability, at the centre of expansion, and thus in the nucleus of the Galactic System (G. W. ROUGOOR, *personal communication*).

The existence of a thermal and a nonthermal source at the same position is most clearly demonstrated in the high-resolution survey at 85 Mc/s. A detailed contour map of the region around the galactic centre at this frequency is given by MILLS (1956). The values of the brightness temperature given in that paper have to be multiplied by a factor of 2 (MILLS *et al.* 1958). A broad source with approximately the same position and dimensions as the extended source observed at 1390 Mc/s, has two maxima about 1°.9 apart. The position and the width of the minimum, which is situated in the centre of the source at 85 Mc/s, agree excellently with that of the thermal source, which is the major component at 1390 Mc/s. In Figure 17 a comparison is made of cross-sections in l and b through the source, at 85 and 1390 Mc/s. It is quite clear from the observed brightness temperatures that the broad source is the nonthermal component. This component, which is very conspicuous in all low-frequency surveys, is quite clearly associated with the centre of the Galactic System. The thermal component, which seems to be embedded in the nonthermal one, causes strong absorption of the nonthermal radiation at 85 Mc/s.

We shall investigate whether the observations at 1390 and 85 Mc/s are in quantitative agreement. We adopt a model in which the broad source has widths at half intensity of approximately 2° × 1°, and a top brightness temperature of 25 °K at 1390 Mc/s and 36000 °K at 85 Mc/s. We have assumed that the ratio of these brightness temperatures is the same as that of the nonthermal background temperature, i.e. 1430. The thermal source is assumed to have halfwidths of 0°.55 × 0°.25, and a top temperature of 500 °K at 1390 Mc/s and 10000 °K at 85 Mc/s. The optical depths are $\tau = 0.05$ and $\tau = 267 \times 0.05 = 13$, respectively. At 85 Mc/s, optical depth unity is reached at 0°.25 in latitude and 0°.55 in longitude away from the centre. The thermal source will thus absorb practically all the radiation originating behind it over a region of 0°.50 × 1°.10. If we suppose that the thermal source is exactly at the centre of the nonthermal source, this means that we observe only half the top intensity of the nonthermal source, i.e. 18000 °K. The intensity of the thermal source itself is 10000 °K, giving a total of 28000 °K. This is the temperature which would be observed if no background radiation were present.

The background temperature underlying the source has been separated into a thermal component of 9°.3 and a nonthermal component of 11° top temperature at 1390 Mc/s (Chapter 7c, Figure 13). The thermal component at 85 Mc/s then has an optical depth of 0.25 and a top temperature of 2200 °K, whilst the nonthermal component has a top temperature of (1430 × 11°) × 0.22/0.25 = 13800 °K (equation (28)). The total value of 16000 °K is in reasonable agreement with the 85 Mc/s observations. Half this background radiation may be assumed to originate behind the galactic centre, and hence will be completely absorbed; the total background temperature at the position of the source is thus 1200° + (1430 × 5°.5) 0.12/0.125 = 8700 °K.

Part of the radiation from the galactic centre is absorbed by the ionized hydrogen between the centre and the sun. The optical depth of this layer is $\tau = 0.12$ and it will decrease the intensity of the source by a factor of $e^{-\tau} = 0.88$. The total expected temperature at 85 Mc/s is thus 0.88 × 28000 + 8700 = 33300 °K. The temperature observed at this position at 85 Mc/s is 31700 °K; our derived value is in excellent agreement with this.

A good illustration of the absorbing effect of the thermal source on the 85 Mc/s temperatures is obtained by reducing the observed 85 Mc/s temperatures to 1390 Mc/s, assuming that the thermal source is absent. Such an illustration is given in Figure 17, where the observed 1390 Mc/s temperatures are also given. The background temperature as determined from neighbouring longitudes was subtracted from the observed 85 Mc/s temperatures, leaving only the source temperature. This was corrected for the absorbing effect of the layer of ionized hydrogen by multiplying by a factor $e^{0.5\tau}$ where τ is the total optical depth at 85 Mc/s. The resulting temperatures were then divided by 1430 to obtain the nonthermal

FIGURE 17

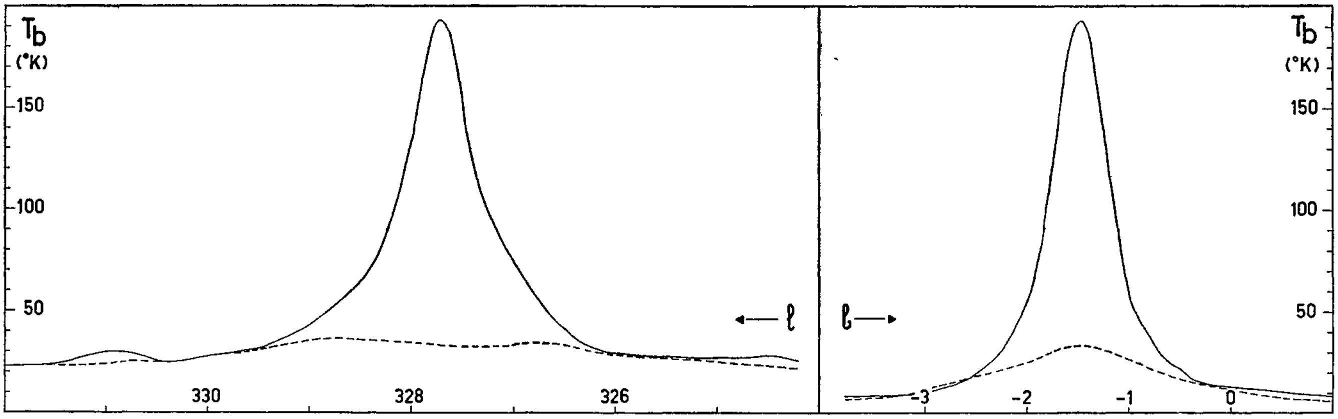

Cross-sections through the position of the galactic nucleus in l and b showing absorption at 85 Mc/s.
——— Brightness temperatures at 1390 Mc/s. - - - - - Brightness temperatures at 85 Mc/s, reduced to 1390 Mc/s:
$T(85) = [T_b^{85}(\text{obs}) - T_b^{85}(\text{background})]\, e^{0.5\tau}/1430 + T_b^{1390}$ (background).

temperature at 1390 Mc/s, and the background temperature at 1390 Mc/s was added. The temperatures thus obtained are comparable to the observed 1390 Mc/s temperatures away from the thermal source.

For an exact comparison, we would have to apply corrections for the smoothing effect of the antenna pattern of the 85 Mc/s survey. In view of the large uncertainties which are already present in this order-of-magnitude calculation, this was considered unnecessary. The antenna pattern tends to fill in the minimum, so that the expected temperature would come out somewhat higher. The top temperature of 36000 °K adopted for the nonthermal source must therefore be considered a maximum value.

In our model, the absorption is negligible further than 0°.7 in longitude from the centre. Inspection of Figure 17 shows that there is still some absorption at 1° from the centre. We made the assumption that the broad source is entirely nonthermal. It is clear that the thermal source is not entirely gaussian but has low-intensity wings out to more than 1° from the centre. This is confirmed by SHAIN's observations (1957) with a 1.4 degree beam, which show strong absorption by the thermal source at a frequency of 19.7 Mc/s. The ratio of the optical depths at 19.7 and 1390 Mc/s is 5000; therefore, a thermal brightness temperature of 2 °K at 1390 Mc/s is equivalent to optical depth unity at 19.7 Mc/s. The halfwidth of the absorbed region at 19.7 Mc/s is 2°.4. Apparently the low-intensity wings of the thermal source extend considerably further than 1° from the centre. The possibility that part of this is due to ionized hydrogen regions between the centre and the sun cannot be excluded. It is clear, however, that most of the thermal radiation from the direction of the galactic centre is concentrated in the narrow source. Thus the situation in the galactic centre is as follows. The centre contains a source of nonthermal radiation of dimensions 2° × 1°, or 300 × 150 pc, and a top brightness temperature of approximately 25 °K at 1390 Mc/s, i.e. 36000 °K at 85 Mc/s. An ionized hydrogen region is situated in the centre of this source, very close to or around the nucleus of the Galactic System. It has dimensions of 0°.55 × 0°.25, or 80 × 35 pc, a mass of $2.5 \times 10^5\, M_\odot$ and a density of 85 cm^{-3}.

The author wishes to express his sincere thanks to Professor H. C. VAN DE HULST and Professor J. H. OORT for their constructive criticism during the various stages of this investigation, to Messrs E. RAIMOND and J. PONSEN for their large share in the calibration measurements; and to Messrs T. HOEKEMA and P. H. KIEL, who carried out most of the reductions.

The work described in this paper was made possible by the financial support from the Netherlands Organization for Pure Research (Z.W.O.).

REFERENCES

L. H. ALLER 1956, "Gaseous nebulae", p. 286, Wiley, New York.
W. BAADE 1958, "Large scale structure of the Galactic System", *I.A.U. Symp.* No. 5, p. 1, Cambridge University Press.
J. E. BALDWIN 1955, *M.N.* **115**, 690.
J. E. BALDWIN and D. W. DEWHIRST 1954, *Nature* **173**, 164.
J. H. BLYTHE 1957, *M.N.* **117**, 652.
J. G. BOLTON and K. C. WESTFOLD 1951, *Austr. J. Sci. Res.* A4, 476.
S. CEDERBLAD 1946, *Lund. Medd.* II, No. 119.
R. D. DAVIES, 1957, *M.N.* **117**, 663.
R. D. DAVIES and D. R. W. WILLIAMS 1955, *Nature* **175**, 1079.
J.-F. DENISSE, E. LEROUX and J.-L. STEINBERG 1955, *Comptes Rendus* **240**, 278.

J.-F. DENISSE, J. LEQUEUX and E. LEROUX 1957, *Comptes Rendus* **244**, 3030.
C. S. GUM 1955, *Mem. R.A.S.* **67**, 155.
F. T. HADDOCK, C. H. MAYER and R. M. SLOANAKER 1954, *Nature* **174**, 176.
F. T. HADDOCK and T. P. MCCULLOUGH 1955, *A.J.* **60**, 161.
J. P. HAGEN, E. F. MCCLAIN and N. HEPBURN 1954, *Proc. I.R.E.* **42**, 1811.
R. HANBURY BROWN and C. HAZARD 1953, *Phil. Mag.* **44**, 939.
R. HANBURY BROWN and D. WALSH 1955, *Nature* **175**, 808.
B. G. HOOGHOUDT 1959, *B.A.N.*, in preparation.
H. C. VAN DE HULST, B. G. HOOGHOUDT, R. J. SCHOR, W. HUISMAN, B. B. SCHIERBEEK and G. H. JÖBSIS 1957, *De Ingenieur* **69**, O. 1.
I.A.U. 1958, *Report of Commission* 33b.
H. L. JOHNSON and W. W. MORGAN 1954, *Ap.J.* **119**, 344.
H. M. JOHNSON 1953, *Ap.J.* **118**, 370.
H. M. JOHNSON 1955, *Ap.J.* **121**, 604.
H. M. JOHNSON 1956, *Ap.J.* **124**, 90.
F. J. KERR and J. V. HINDMAN 1957, *P.A.S.P.* **69**, 558.
J. D. KRAUS, H. C. KO and S. MATT 1954, *A.J.* **59**, 439.
J. D. KRAUS and H. C. KO 1957, "Celestial radio radiation", R.F. Project 73, *Sci. Rep.* No. 1, Ohio.
K. K. KWEE, C. A. MULLER and G. WESTERHOUT 1954, *B.A.N.* **12**, 211 (No. 458).
B. Y. MILLS 1955, *Austr. J. Phys.* **8**, 368.
B. Y. MILLS 1956, *Observatory* **76**, 891.
B. Y. MILLS, A. G. LITTLE and K. V. SHERIDAN 1956, *Austr. J. Phys.* **9**, 218.
B. Y. MILLS, E. R. HILL and O. B. SLEE 1958, *Observatory* **78**, 116.
R. MINKOWSKI 1949, *P.A.S.P.* **61**, 151.
R. MINKOWSKI 1955, "Gas dynamics of cosmic clouds", *I.A.U. Symp.* No. 2, p. 3, North Holland Publishing Company, Amsterdam.
W. W. MORGAN, S. SHARPLESS and D. OSTERBROCK 1952, *Sky and Telescope* **11**, 138.
W. W. MORGAN, A. E. WHITFORD and A. D. CODE 1953, *Ap.J.* **118**, 318.
W. W. MORGAN, B. STRÖMGREN and H. M. JOHNSON 1955, *Ap.J.* **121**, 611.
C. A. MULLER 1956, *Philips Technical Review* **74**, 305 and 351.
C. A. MULLER and G. WESTERHOUT 1957, *B.A.N.* **13**, 151 (No. 475).
E. F. MCCLAIN 1955, *Ap.J.* **122**, 376.
R. X. MCGEE, O. B. SLEE and G. J. STANLEY 1955, *Austr. J.Phys.* **8**, 347.
J. OHLSSON, A. REIZ and I. TORGÅRD 1956, *Lund Observatory Tables*, The Observatory, Lund.
J. H. OORT 1955, "Gas dynamics of cosmic clouds", *I.A.U. Symp.* No. 2, p. 226 (discussion), North Holland Publishing Company, Amsterdam.
D. OSTERBROCK 1955, *Ap.J.* **122**, 235.
D. OSTERBROCK and M. J. SEATON 1957, *Ap.J.* **125**, 66.
J. L. PAWSEY 1955, *Ap.J.* **121**, 1.
J. H. PIDDINGTON 1951, *M.N.* **111**, 45.
J. H. PIDDINGTON and H. C. MINNETT 1951, *Austr. J. Sci. Res.* A4, 459.
J. H. PIDDINGTON and G. H. TRENT 1956, *Austr. J. Phys.* **9**, 481.
W. PRIESTER 1955, *Zs.f. Ap.* **38**, 73.
G. REBER 1948, *Proc. I.R.E.* **36**, 1215.
M. SCHMIDT 1956, *B.A.N.* **13**, 15 (No. 468).
M. SCHMIDT 1957, *B.A.N.* **13**, 247 (No. 475).
E. SCHOENBERG 1929, *Handbuch der Astrophysik* II, 1, p. 268, Springer, Berlin.
CH. L. SEEGER 1956, *B.A.N.* **13**, 100 (No. 472).
CH. L. SEEGER 1957, U.R.S.I. *Report of sub-commission* Vd.
CH. L. SEEGER, G. WESTERHOUT and H. C. VAN DE HULST 1956, *B.A.N.* **13**, 89 (No. 472).
C. A. SHAIN 1957, *Austr. J. Phys.* **10**, 195.
G. A. SHAJN and V. T. GAZE 1952, *Publ. Crimean Obs.* **8**, 80.
G. A. SHAJN and V. T. GAZE 1952, *Publ. Crimean Obs.* **9**, 13.
G. A. SHAJN and V. T. GAZE 1955, *Publ. Crimean Obs.* **15**, 11.
J. R. SHAKESHAFT, M. RYLE, J. E. BALDWIN, B. ELSMORE and J. H. THOMSON 1955, *Mem. R.A.S.* **67**, 106.
S. SHARPLESS 1953, *Ap.J.* **118**, 362.
S. SHARPLESS 1954, *Ap.J.* **119**, 334.
S. SHARPLESS and D. OSTERBROCK 1952, *Ap.J.* **115**, 89.
S. F. SMERD and K. C. WESTFOLD 1949, *Phil. Mag.*, Ser. 7, Vol. XI, 831.
F. G. SMITH, P. A. O'BRIEN and J. E. BALDWIN 1956, *M.N.* **116**, 282.
B. STRÖMGREN 1948, *Ap.J.* **108**, 242.
B. STRÖMGREN 1949, "Problems of cosmical aerodynamics", p. 7, CADO, Dayton, Ohio.
O. STRUVE 1957, *Sky and Telescope* **16**, 118.
G. WESTERHOUT 1956, *B.A.N.* **13**, 105 (No. 472).
G. WESTERHOUT 1957, *B.A.N.* **13**, 201 (No. 475).
G. WESTERHOUT 1957, *Comptes Rendus* **245**, 35.
G. WESTERHOUT 1958, *B.A.N.* **14**, 261 (No. 488).
G. WESTERHOUT and J. H. OORT 1951, *B.A.N.* **11**, 323 (No. 426).
G. R. WHITFIELD 1957, *M.N.* **117**, 680.
H. VAN WOERDEN, G. W. ROUGOOR and J. H. OORT 1957, *Comptes Rendus* **244**, 1691.

TABLE OF CONTENTS

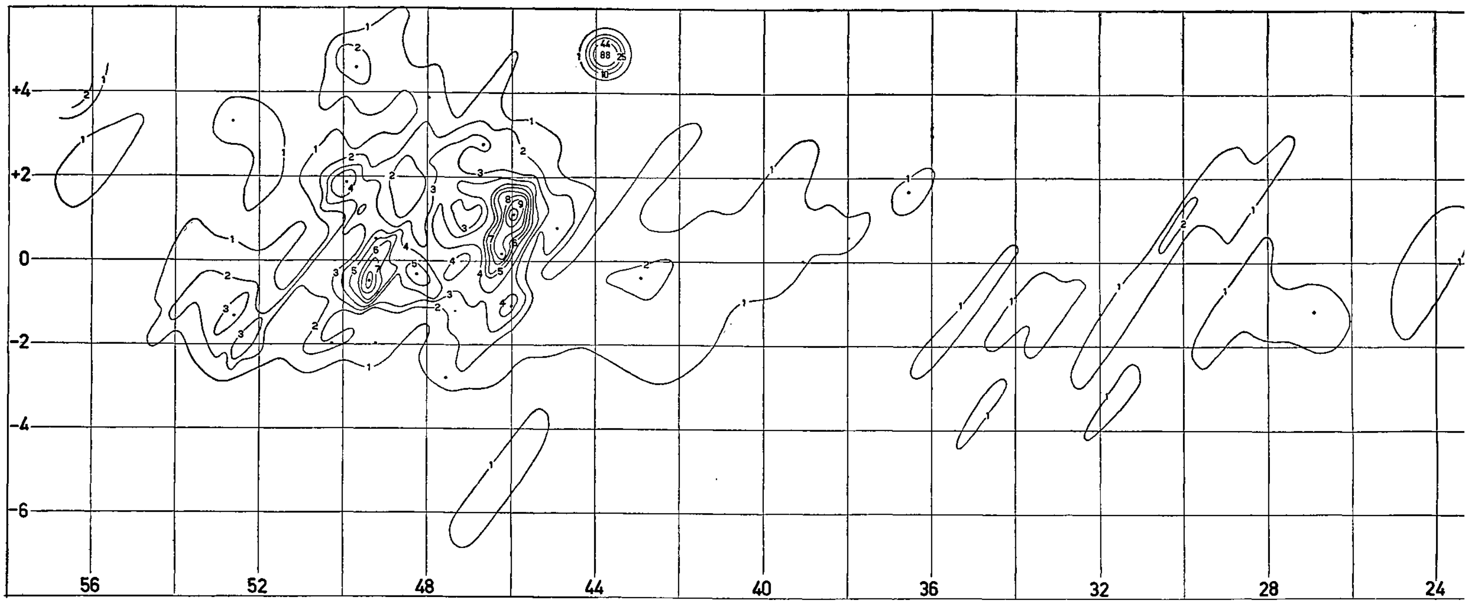

+4
+2
0
-2
-4
-6
56
52
48
44
40
36
32
28
24

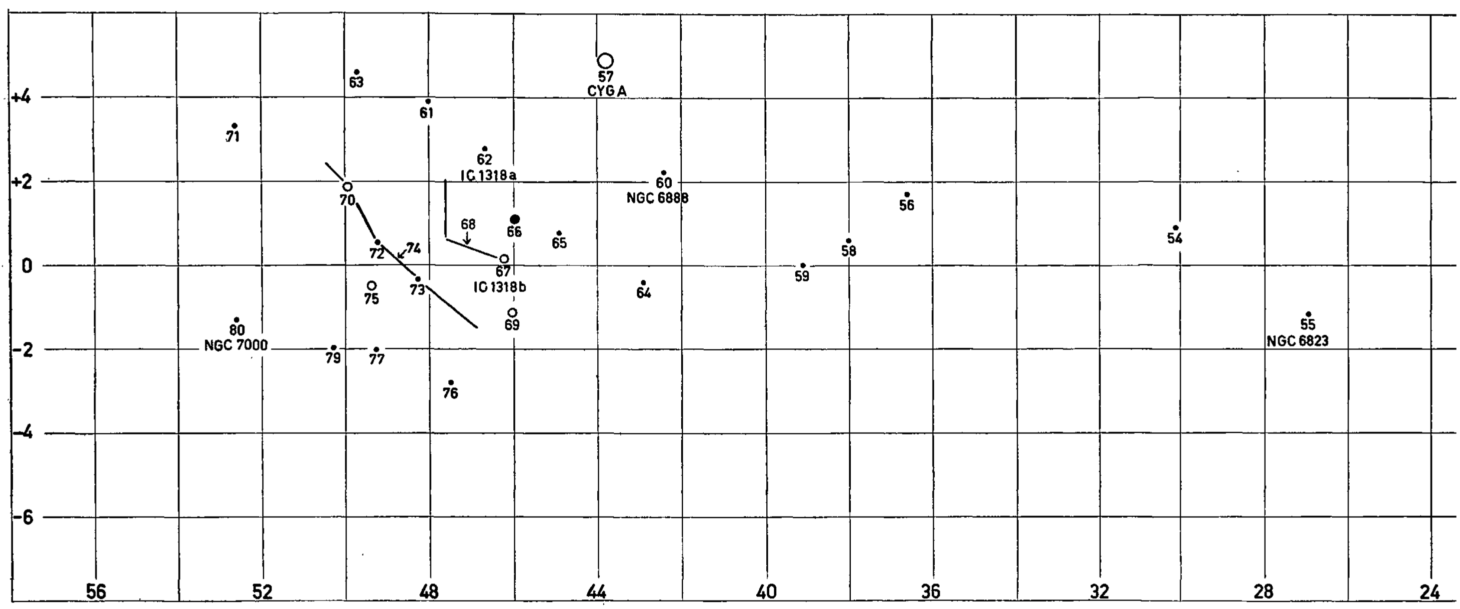

+4
+2
0
-2
-4
-6
56
52
48
44
40
36
32
28
24
57
CYG A
63
61
71
62
IC 1318a
60
NGC 6888
70
68
66
65
72
74
56
58
54
67
IC 1318b
75
73
59
64
69
80
NGC 7000
79
77
55
NGC 6823
76

FIGURE 9

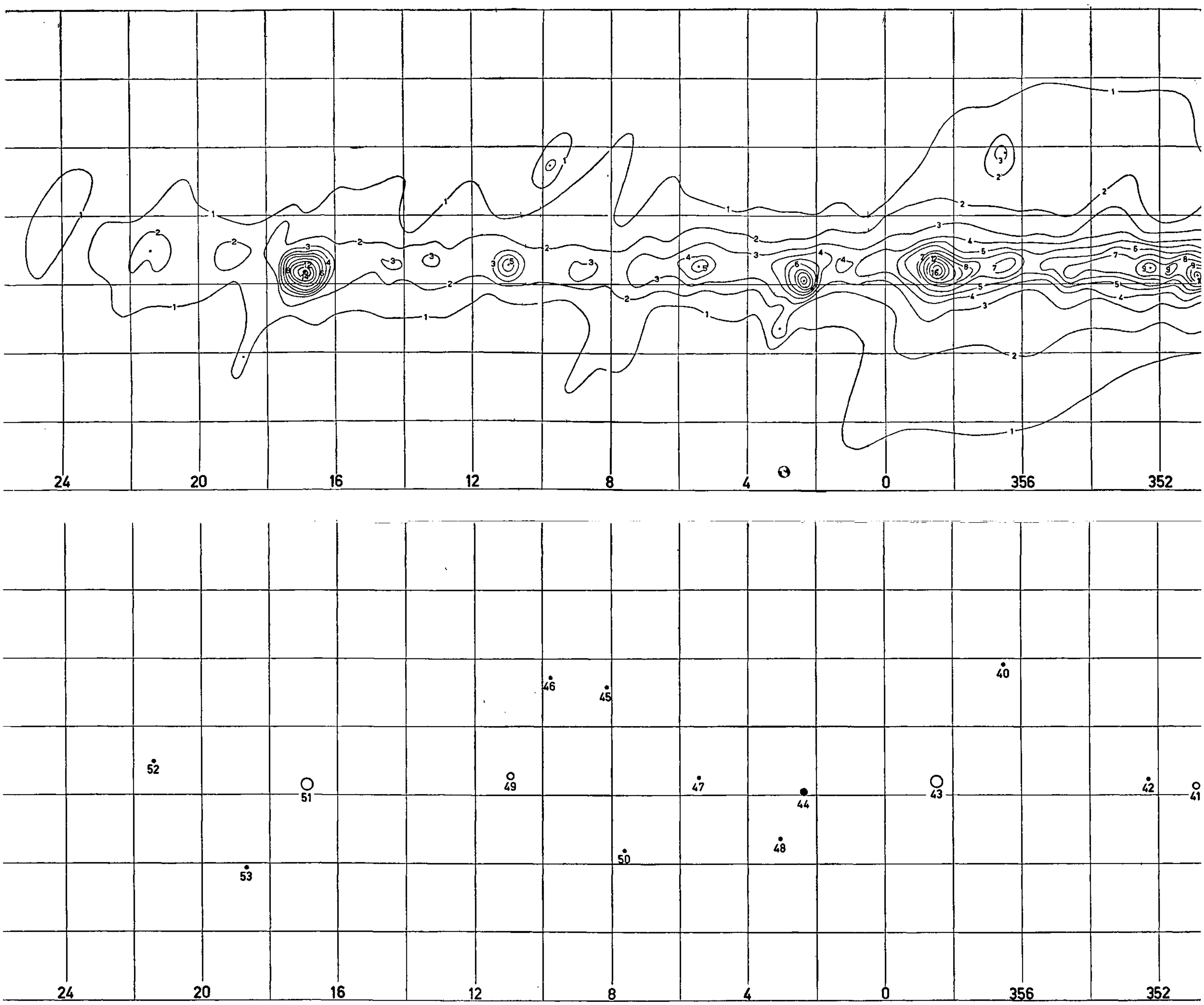

Map of the galactic ridge, with identification of the discrete sources. Contour intervals are 5 units (3.25 °K in T_b). Small dots, $I \leq 15$ units, small circles, $15 < I \leq 30$, big dots $30 < I \leq 45$, big circles $I > 45$.

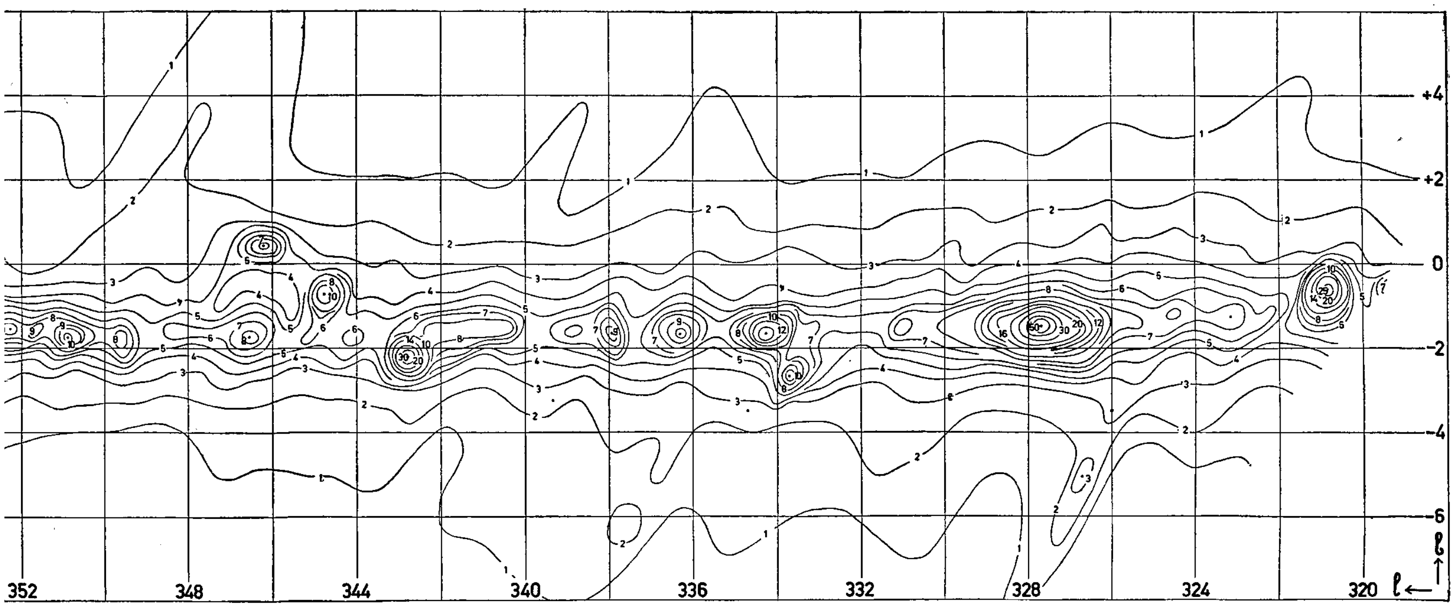
352
348
344
340
336
332
328
324
320
+4
+2
0
-2
-4
-6

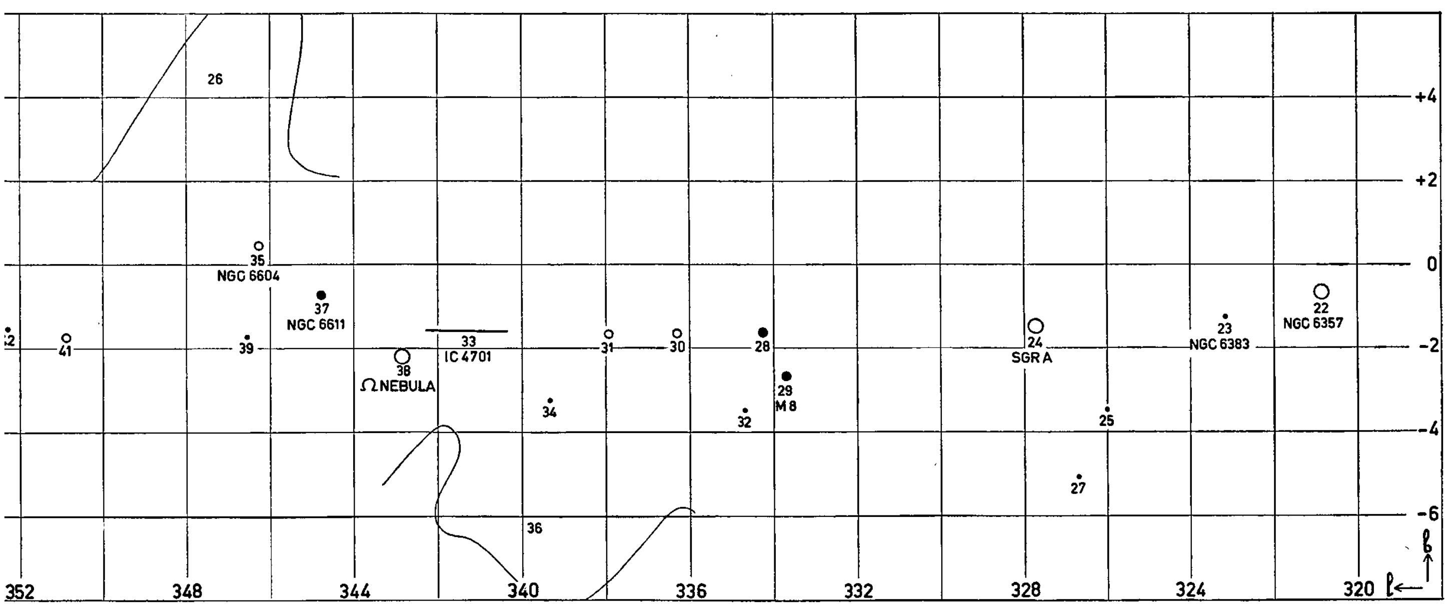
26
35
NGC 6604
37
NGC 6611
41
39
33
IC 4701
38
Ω NEBULA
31
30
28
29
M 8
34
32
36
24
SGR A
25
27
23
NGC 6383
22
NGC 6357
352
348
344
340
336
332
328
324
320
+4
+2
0
-2
-4
-6